

DEVELOPMENT AND SCREENING OF CHALCONES
AGAINST CANCER PROTEIN TARGETS USING IN
SILICO AND IN VITRO TECHNIQUES

Miss Kanyani Sangpheak



A Dissertation Submitted in Partial Fulfillment of the Requirements
for the Degree of Doctor of Philosophy in Biotechnology
Common Course
Faculty of Science
Chulalongkorn University
Academic Year 2018
Copyright of Chulalongkorn University

การพัฒนาและคัดกรองสารชาลโคนเพื่อยับยั้งโปรตีนเป้าหมายของเซลล์มะเร็งโดยใช้เทคนิค
ทางคอมพิวเตอร์และในระดับหลอดทดลอง



วิทยานิพนธ์นี้เป็นส่วนหนึ่งของการศึกษาตามหลักสูตรปริญญาวิทยาศาสตรดุษฎีบัณฑิต
สาขาวิชาเทคโนโลยีชีวภาพ ไม่สังกัดภาควิชา/เทียบเท่า
คณะวิทยาศาสตร์ จุฬาลงกรณ์มหาวิทยาลัย
ปีการศึกษา 2561
ลิขสิทธิ์ของจุฬาลงกรณ์มหาวิทยาลัย

Thesis Title
By Miss Kanyani Sangpheak
Field of Study Biotechnology
Thesis Advisor Assistant Professor Thanyada Rungrotmongkol
Thesis Co Advisor Dr. Chompoonut Rungnim

Accepted by the Faculty of Science, Chulalongkorn University in Partial
Fulfillment of the Requirement for the Doctor of Philosophy

..... Dean of the Faculty of Science
(Professor POLKIT SANGVANICH)

DISSERTATION COMMITTEE

..... Chairman
(Assistant Professor Dr. Kanoktip Packdibamrung)
..... Thesis Advisor
(Assistant Professor Thanyada Rungrotmongkol)
..... Thesis Co-Advisor
(Dr. Chompoonut Rungnim)
..... Examiner
(Assistant Professor Dr. Kuakarun Krusong)
..... Examiner
(Assistant Professor Dr. Warinthorn Chavasiri)
..... External Examiner
(Assistant Professor Nadtanet Nanthaboot)


จุฬาลงกรณ์มหาวิทยาลัย
CHULALONGKORN UNIVERSITY

กานต์ญาณี สังเคือก : การพัฒนาและคัดกรองสารชาโลนเพื่อยับยั้งโปรตีนเป้าหมายของเซลล์มะเร็งโดยการใช้นิเทศนิตทางคอมพิวเตอร์และในระดับหลอดทดลอง. (DEVELOPMENT AND SCREENING OF CHALCONES AGAINST CANCER PROTEIN TARGETS USING IN SILICO AND IN VITRO TECHNIQUES) อ.ที่ปริกษาหลัก : ผศ. ดร.ธัญญดา รุ่งโรจน์มั่งกล, อ.ที่ปริกษาร่วม : ดร.ชมพูนุช รุ่งนั่ม

การรักษาระบบจำเพาะเจาะจงต่อเซลล์มะเร็ง หรือ **targeted therapy** เป็นการรักษาระบบใหม่ที่มีประสิทธิภาพในการรักษาระบบมะเร็งได้อย่างตรงจุด ซึ่งทำให้เซลล์ปกติจะได้รับผลกระทบจากการรักษาน้อย โทโปไอโซเมอร์เรส $\text{II}\alpha$ (hTopoII α) และ Epidermal growth factor receptor (EGFR) เป็นโปรตีนซึ่งได้รับความสนใจมากที่สุดกลุ่มหนึ่งในการวิจัยและพัฒนาายาต้านมะเร็ง เนื่องจากเป็นเป้าหมายที่มีศักยภาพสูง ซึ่งโทโปไอโซเมอร์เรส $\text{II}\alpha$ (hTopoII α) ทำหน้าที่เกี่ยวข้องกับการคลายเกลียวดีเอ็นเอ ขณะที่เกิดการ replication ขณะที่ EGFR จะมีหน้าที่เกี่ยวข้องกับการส่งสัญญาณระดับเซลล์ สารชาโลน หรือ 1,3-diphenyl-2-propene-1-one เป็นสารกลุ่มโพลีฟีนอลชนิดหนึ่งสามารถพบได้ในพืชหลายชนิด สามารถสังเคราะห์ขึ้นได้ง่าย โดยให้มีหมู่แทนที่ได้ที่ตำแหน่งต่างๆ กันหลายตำแหน่ง ส่งผลให้สามารถสร้างสารอนุพันธ์ได้หลากหลาย เนื่องด้วยหลากหลายทางโครงสร้างนี้จึงทำให้สารชาโลนสังเคราะห์นั้นมีความหลากหลายทางฤทธิ์ชีวภาพซึ่งพบว่าสามารถยับยั้งโทโปไอโซเมอร์เรส $\text{II}\alpha$ (hTopoII α) และ Epidermal growth factor receptor tyrosine kinase (EGFR-TK) ได้ สารประกอบอนุพันธ์ของกลุ่มชาโลนที่มีการดัดแปลงโครงสร้าง 47 สารถูกนำมาทดสอบการใช้เทคนิคทางคอมพิวเตอร์ในการคำนวณ และการทดสอบในหลอดทดลอง พบว่าสารชาโลน 3d มีฤทธิ์ฆ่าเซลล์มะเร็งกระเพาะปัสสาวะ, ปากมดลูกและ เต้านม ได้ดีที่สุดในกลุ่มที่มีค่า IC_{50} 10.8, 3.2 and 21.1 μM ตามลำดับ ในขณะที่ชาโลน 1c, 2a, 3e, 4e และ 4t สามารถยับยั้งเซลล์มะเร็งผิวหนัง (A431) ด้วย IC_{50} values < 10 μM ทำการทดสอบยืนยันการยับยั้งการทำงานของสารประกอบชาโลนกับโปรตีนเป้าหมายทั้งสองชนิด พบว่าชาโลน 3d สามารถยับยั้งโทโปไอโซเมอร์เรส $\text{II}\alpha$ ได้ดีกว่า salvicine ซึ่งใช้เป็นสารเทียบ นอกจากนี้ยังพบว่าชาโลน 1c, 2a และ 3e ยับยั้งเอนไซม์ EGFR-TK ได้มากกว่า 50% ซึ่งใกล้เคียงกับยา erlotinib ต่อมาการศึกษาแบบแผนในการเข้าจับกัน (binding pattern) และสมบัติต่างๆ ของสารออกฤทธิ์ประสิทธิภาพสูงกับโปรตีนทั้งสองชนิดโดยระเบียบวิธีทางโมเลกุลาร์ไดนามิกซิมูเลชัน จากผลการศึกษาพบว่าชาโลน 3d เกิดอันตรกิริยากับโทโปไอโซเมอร์เรส $\text{II}\alpha$ ได้ดีกว่า salvicine ขณะที่ 1c, 2a และ 3e จับได้ดีกับกรดอะมิโนชนิดไฮโดรโฟบิก 7 ตัว ซึ่ง M793 เป็นอะมิโนแอซิดที่สำคัญต่อการเข้าจับกับทั้งสามชาโลน หลังจากนั้นจึงนำมาศึกษาเภสัชจลนศาสตร์ใน 4 ขั้นตอนคือ การดูดซึม การกระจายตัว การเผาผลาญ และการขับถ่ายของสารชาโลนทั้ง 6 สาร พบว่าสารชาโลนทั้ง 6 สารสามารถนำไปพัฒนาเป็นยาต่อไปได้ หลังจากนั้นจึงทำการศึกษาความสัมพันธ์ระหว่างสารชาโลนจำนวน 23 สารกับฤทธิ์การยับยั้งเซลล์มะเร็งผิวหนัง A431 โดยวิธี 2D-QSAR ซึ่งสมการที่ดีที่สุดในการอธิบายความสัมพันธ์โดยใช้วิธี Multiple linear regression (MLR) ให้ค่า $R^2 = 0.968$ ซึ่งจากผลการศึกษาที่ได้นั้นเป็นข้อมูลที่มีประโยชน์อย่างมากต่อการออกแบบสารชาโลนยับยั้งเซลล์มะเร็งที่มีประสิทธิภาพสูงต่อไปในอนาคตได้

สาขาวิชา เทคโนโลยีชีวภาพ
ปีการศึกษา 2561

ลายมือชื่อนิสิต
ลายมือชื่อ อ.ที่ปริกษาหลัก
ลายมือชื่อ อ.ที่ปริกษาร่วม

5772885023 : MAJOR BIOTECHNOLOGY

KEYWORD Chalcone Human topoisomerase II α EGFR Anticancer MTT assay
D: Enzyme assay Molecular dynamics simulation

Kanyani Sangpheak : DEVELOPMENT AND SCREENING OF
CHALCONES AGAINST CANCER PROTEIN TARGETS USING IN
SILICO AND IN VITRO TECHNIQUES. Advisor: Asst. Prof. Dr.
Thanyada Rungrotmongkol Co-advisor: Dr. Chompoonut Rungrim

Targeted cancer therapy has become one of high potential cancer treatments. Human topoisomerase II α (hTopoII α) and Epidermal growth factor receptor tyrosine kinase (EGFR-TK) are proteins that play important roles on cell cycle. The hTopoII α catalyzes the cleavage and rejoining of double-stranded DNA while EGFR function on cell signaling. Thus, the two proteins have been suggested as molecular target for the development of novel cancer therapeutics. A series of 47 chalcone derivatives was screened against hTopoII α and EGFR-TK by *in silico* and *in vitro* techniques. Chalcone 3d showed a high cytotoxicity with IC₅₀ values of 10.8, 3.2 and 21.1 μ M against the HT-1376, HeLa and MCF-7 cancer cell lines, respectively, while 1c, 2a, 3e, 4e and 4t exhibited potent compounds against A431 with IC₅₀ values < 10 μ M. To confirm the result the inhibition of those chalcone on enzyme assay was obtained. The 3d showed an inhibitory activity against hTopoII α that was better than the known inhibitor, salvicine. Only three chalcones (1c, 2a and 3e) had an inhibitory activity against EGFR-TK with relative inhibition percentages closed to the approved drug, erlotinib. The binding interaction of potent chalcones complex with hTopoII α and EGFR-TK were studied using molecular dynamics simulation. The observed 3d/hTopoII α interactions affirmed that 3d strongly interacts with the ATP binding pocket residues while 1c, 2a and 3e/EGFR-TK were well occupied within the ATP binding site and strongly interacted with the 7 hydrophobic residues including the important hinge region residue M793. From ADMET properties, all six chalcones could be served as a lead compounds for development of hTopoII α and EGFR-TK inhibitors. The information of drug development can be obtained by quantitative structure-activity relationship (QSAR) techniques. A series of chalcone derivatives against A431 were subjected to QSAR analyses. The MLR equation indicated a good correlation between observed and predicted values with $R^2 = 0.968$. The understanding of the relationship between structures and pharmacological effects and the ligand-protein binding pattern leads to important information for the design of high potential anti-cancer drugs.

Field of Study: Biotechnology

Student's Signature

Academic Year: 2018

.....
Advisor's Signature

Year:

.....
Co-advisor's Signature

.....

ACKNOWLEDGEMENTS

Many people have contributed to the development of this study, which I am very appreciated for their kind cooperation and their advice. I would like to express my greatest gratitude to my advisor, Assistant Professor Dr. Thanyada Rungrotmongkol, and my co-advisor Dr. Chompoonut Rungnim for her invaluable advice, guidance, support, and encouragement throughout this thesis. Without their kindness and cheerfulness, this work could not be accomplished. My appreciation is also expressed to Assistant Professor Dr. Warinthron Chavasiri for synthesized compounds used in this work and his valuable comments. Sincere thanks are also extended to Assistant Professor Dr. Kanoktip Packdibamrun, Associate Professor Dr. Kuakarun Krusong and Assistant Professor Dr. Nadtanet Nunthaboot who serve as the members of my Doctoral committees for spending their time, comments and suggestion. Special thanks to my collaborators, Associate Professor Dr. Kiattawee Choowongkomon at Department of Biochemistry, Faculty of Science, Kasetsart University, Professor Dr. Peter Wolschann and Dr. Monika Mueller at Department of Pharmaceutical Chemistry, University of Vienna, Austria for all facilities and instrument used in cell testing and enzyme assay and also their technical advice and training. My gratitude is also extended to Associate Professor Phornphimon Maitarad at Research Center of Nano Science and Technology, Shanghai University, China for her generous advice and guidance about the QSAR technique. My thanks are also expressed to all member not only in the Biosim laboratory but also other laboratory members; Dr. Supaporn Seetaha and Lueacha Tabtimmai for their help, kindness and support. Finally, the gratitude was dedicated to my parents, Dr. Kowit Hengphasatporn, and my partner in crime Jaturapat Kittikarnchanaporn for their understanding, encouragement, and everything giving in my life. I thanks the Thailand Graduate Institute of Science and Technology [TGIST Grant No. TG550958052D], the 90th Anniversary of Chulalongkorn University Fund (Ratchadaphiseksomphot Endowment Fund), and the Overseas Research Experience Scholarship for Graduate school and Faculty of Science, Chulalongkorn University.

Kanyani Sangpheak

TABLE OF CONTENTS

	Page
.....	iii
ABSTRACT (THAI)	iii
.....	iv
ABSTRACT (ENGLISH)	iv
ACKNOWLEDGEMENTS	v
TABLE OF CONTENTS	vi
LIST OF TABLES	x
LIST OF FIGURES	xii
LIST OF ABBREVIATIONS	xv
INTRODUCTION	1
1.1 Cancer	1
1.2 Cancer Statistics	1
1.3 Cancer treatments	4
1.3.1 Surgery	4
1.3.2 Radiation therapy	4
1.3.3 Chemotherapy	5
1.3.4 Immunotherapy	7
1.3.5 Targeted therapy	8
1.4 Topoisomerase	11
1.5 Epidermal Growth Factor Receptor (EGFR)	17
1.6 Chalcones	21
1.7 Objective of the present work	22
CHAPTER II	23
THEORY AND BACKGROUND	23
2.1 Molecular docking	23

2.2	Molecular dynamics simulation	24
2.3	Quantitative structure-activity relationship (QSAR).....	27
2.3.1	Molecular descriptor [171].....	27
2.3.2	Regression Analysis for QSAR studies.....	27
2.3.2.1	Multiple Linear Regression (MLR).....	27
2.3.2.2	Partial Least Squares (PLS).....	28
2.3.3	Evaluation of the Models [176].....	28
2.4	ADMET properties of a drug molecule.....	29
2.5	ADP-Glo Kinase assay	32
CHAPTER III		34
MATERIALS AND METHODS.....		34
3.1	Equipment.....	34
3.2	Chemicals	34
3.3	Cancer cell lines, Enzyme and Bacterial strains.....	36
Part I Computational approach		37
3.4	Topoisomerase II (hTopoII α)	37
3.4.1	Molecular docking of hTopoII α	37
3.4.2	MD simulation of hTopoII α	37
3.5	Epidermal Growth factor receptor tyrosine kinase domain (EGFR-TK)	38
3.5.1	MD simulation of EGFR-TK	38
Part II Experimental methods		40
3.6	Topoisomerase II (hTopoII α)	40
3.6.1	Synthesis of chalcone derivatives.....	40
3.6.2	Cell culture and sample preparation.....	40
3.6.3	Cytotoxicity assay	40
3.6.4	Expression and enrichment of the recombinant human Topoisomerase II α ATPase domain	41
3.6.5	ATPase assay.....	41
3.7	Epidermal Growth Factor Receptor tyrosine kinase domain (EGFR-TK).....	42

3.7.1 Cell culture and cell viability assay (MTT assay)	42
3.7.2 Purification of intracellular domain of EGFR transfected Hela cell	43
3.7.3 Tyrosine kinase inhibition assay	43
Part III QSAR and ADMET	44
3.8 Quantitative structure–activity relationship	44
3.9 ADME and toxicity prediction	45
CHAPTER IV	46
RESULTS AND DISCUSSION	46
Part I Computational screening of chalcones acting against topoisomerase II α and their cytotoxicity towards cancer cell lines	46
4.1 Molecular docking studies	46
4.2 Cytotoxicity towards cancer cell lines	48
4.3 Inhibition of the hTopoII α ATPase domain	50
4.4 MD simulations	51
Part II Biological evaluation and molecular dynamics simulation of chalcone derivatives as EGFR-tyrosine kinase inhibitors	54
4.5 Cytotoxicity effect against A431 and A549 cell lines	54
4.6 Inhibition of rEGFR tyrosine kinase activity by chalcones	57
4.7 Molecular binding and interaction of potent chalcones	59
Part III Quantitative structure–activity relationship and ADMET	64
4.9 Physicochemical properties of potent chalcones	71
Part IV Design new compounds for topoisomerase II α and EGFR-TK inhibitor ...	76
4.10 Topoisomerase	76
4.10.1 Design the new compound for topoisomerase II α inhibitors	76
4.11 Design the new compound for EGFR-TK inhibitors	80
CHAPTER V	83
CONCLUSION	83
5.1 Computational screening of chalcones acting against topoisomerase II α and their cytotoxicity towards cancer cell lines	83

5.2 Biological evaluation and molecular dynamics simulation of chalcone derivatives as EGFR-tyrosine kinase inhibitors	83
5.3 QSAR model	84
5.4 Physic properties of potent chalcones	84
5.5 Design of the new compounds	85
REFERENCES	86
APPENDICES	101
APPENDIX 1: Chemical structure of the 47 designed chalcones from six different groups.	102
APPENDIX 2: RMSD plots during 80 ns MD for the simulated systems of chalcone 3d/hTopoII α	103
APPENDIX 3: The percent survival rate of the 47 chalcones against human embryonic fibroblast compare with approved anticancer drug	104
VITA.....	105

LIST OF TABLES

	Page
Table 1. Examples of cancers treated with radiation therapy [8].	5
Table 2. Common class of cancer chemotherapy	7
Table 3. Therapeutic antibodies approved by the US FDA for cancer treatment.....	9
Table 4. Small molecules inhibitors approved by the US FDA for cancer treatment [56].....	10
Table 5. Current topoisomerase inhibitors.....	15
Table 6. Current specific/selective tyrosine kinase inhibitors (TKIs) targeting receptor tyrosine kinases (RTKs) [10, 59].....	20
Table 7. Molecular docking software [166].....	23
Table 8 Contact residues of the hTopoII α ATPase domain for the binding of salvicine and three chalcones (3c, 3d and 3f). The residues in bold format stabilize the ligand binding via H-bond interaction, while the conserved residues between each chalcone and salvicine are shown in underlined format.	48
Table 9. In vitro IC ₅₀ values of the three chalcone compounds and salvicine against the HT-1376, HeLa and MCF-7 cancer-derived cell lines and the rhTopoII α ATPase domain.....	50
Table 10. IC ₅₀ values of potent chalcones against two cancer cell lines A431 and A549 compared to erlotinib	56
Table 11. Calculated properties of chalcone derivatives using the Material studio software.....	65
Table 12. Correlation matrix of anticancer activity against A431 for 9 properties. High correlations ($\geq \pm 0.8$) are labelled in gray cells.	67
Table 13. Regression Statistic for the QSAR Models I-IV.....	68
Table 14. Residual values of training and test set obtained from Equation (IV) for A431 cancer cell lines.....	70
Table 15. Toxicity, ADME, drug likeness and pharmacokinetics of three potent chalcones and salvicine against Topoisomerase II.	72
Table 16. Toxicity, ADME, drug likeness and pharmacokinetics of three potent chalcones and erlotinib against EGFR.....	74

Table 17. Design of new compounds from 3d scaffold with CDOCKER interaction energy (kcal/mol) inhibit topoisomerase II α	77
---	----



LIST OF FIGURES

	Page
Figure 1. Normal cells become to malignant or invasive cancer. Before cancer cells form in tissues of the body, the cells go through abnormal cells and form a tumor.....	1
Figure 2. Ten Leading Cancer Types for the Estimated New Cancer Cases and Deaths of male and female, United States, 2018. [4].....	2
Figure 3. Breast, cervix, colorectal, liver and lung cancers combined had the highest age-standardized rates in 2012 and accounted for more than half of the incidence, prevalence and mortality in Thailand. *excluding non-melanoma skin cancer [6].....	3
Figure 4. National and subnational average annual percent change of each cancer from 2000-2012 for female and males. [6].	3
Figure 5. Comparison of the two genders on the basis of different side effects associated with chemotherapeutic drugs.....	6
Figure 6. Topoisomerase I (TopoI, left) and II (TopoII, right). Noncovalent binding of (A) TopoI and (D) TopoII to DNA. The arrow indicates the reversible ligation and cleavage reaction under normal condition (A, B for TopoI and D, E for TopoII). (C) Trapping the cleavage complexes of DNA topoisomerases by TopoI inhibitors and (F) TopoII inhibitors promotes DNA damages [77].....	11
Figure 7. Structure of eukaryotic topoisomerase II α a) Domain arrangement of TopoII α . Functional regions are colored and labeled. CTR, C-terminal region. (b) Model of the ternary complex. [95]	13
Figure 8. The mechanism of topoisomerase II [96].....	14
Figure 9. The hTopoII α structures used in the docking study. (A) The ATPase domain of hTopoII α with the 5'-adenylyl- β , γ -imidodiphosphate, AMP-PNP (space filling model), in the ATP binding pocket, where the GHKL and transducer domains are shown in green and pink (PDB code: 1ZXM). (B) The hTopoII α /DNA/etoposide ternary complex (PDB code: 3QX3) [41].....	15
Figure 10. Structural of EGFR in three domains including; extracellular receptor domain, membrane domain and intracellular domain with tyrosine kinase function. A. The extracellular region comprises 4 domains, the N-lobe of the kinase domain is in light blue and the C-lobe in darker blue. B. Representative cartoons of the domains of EGFR. Domains I and III adopt a β -helix fold. Domains II and IV adopt extended structures comprising a series of disulfide-bonded modules [138].	18

Figure 11. The scheme shows the mechanism of EGFR activation. The monomer to dimer transition in EGFR that is triggered by ligand binding. [138].	19
Figure 12. Epidermal growth factor receptor (EGFR) and its downstream signaling proteins. Arrows and perpendicular lines indicate activation/induction and inhibition/suppression, respectively [139].	19
Figure 13. Chemical structure of chalcone	22
Figure 14. Typical intramolecular interactions	25
Figure 15. The drug excretion's routes [183]	31
Figure 16. Principle of the ADP-Glo™ Kinase Assay.	33
Figure 17. CDOCKER interaction energies (kcal/mol) of the designed chalcone derivatives binding at two different sites relative to the known hTopoII α inhibitors, salvicine and etoposide.	47
Figure 18. Superimposed structures of the three most active chalcones 3c (green), 3d (cyan) and 3f (blue) from the docking study with that of salvicine in the ATP-binding pocket of the hTopoII α ATPase domain. Figure created by NGL viewer (http://nglviewer.org/ngl/).	47
Figure 19. (A) SDS-PAGE gel analysis of the enriched rhTopoII α ATPase domain. Lane M: molecular weight marker of standard protein; Lane 1: enriched rhTopoII α ATPase domain (45 kDa). (B, C) The IC ₅₀ curves of (B) salvicine and (C) 3d against the ATPase activity of rhTopoII α . Data are shown as the mean \pm 1 SD, derived from three independent experiments.	51
Figure 20. (A) Per-residue decomposition free energy of 3d/hTopoII α complex and (B) the binding orientation of 3d inside the ATP-binding pocket of ATPase domain, drawn from the last MD snapshot.	53
Figure 21. (Top) Per-residue decomposition free energy of the 10 key residues (black) and their contribution from backbone (dark grey) and side chain (light grey). (Bottom) The vdW (EvdW + Gnonpolar) and electrostatic (Eele + Gpolar) energy contributions are given in black and grey lines, respectively.	53
Figure 22. Hydrogen bond formation between chalcone 3d and the two residues in the ATP binding pocket of hTopoII α ATPase domain, where the percentage of H-bond occupation is also given.	54
Figure 23. Percent survival rate of the 47 chalcones and erlotinib against (A) human lung adenocarcinoma cell lines (A549) and (B) human epidermoid carcinoma cell lines (A431)	56

- Figure 24. (A) Representative SDS-PAGE gel analysis of the enrichment of the EGFR-TK ICD, loading 5 μg protein per track. Lane M: molecular weight marker of standard protein; Lane 1: supernatant, Lane 2: Flow through, Lane 3: 10% of buffer B, Lane 4: 45 kDa of EGFR-TK domain (B) The relative EGFR-TKI activity (%) of the five potent chalcone derivatives and erlotinib at 1 μM , as assayed using the ADP-glo kinase assay.....58
- Figure 25. (A) Per-residue decomposition free energy of three chalcone/EGFR-TK complexes and (B) their binding orientation inside the ATP-binding pocket of tyrosine kinase domain drawn from the last MD snapshot, where the energy contour of residue contribution for ligand binding was shaded.....61
- Figure 26. Time evolution of the number of intermolecular hydrogen bonds formed between the EGFR-TK residues and the three screened chalcones.62
- Figure 27. Time-dependent distance between the centers of mass of the residues L718 and G796 for apo and complex forms over the 500 ns of the trajectory.62
- Figure 28. Solvent-accessible surface area (SASA, \AA^2) of apo form and three chalcones complexes along the 500-ns simulation where the amino acids within a 7- \AA sphere of chalcone used for SASA calculations are also shown in the right-hand side.63
- Figure 29. Plot of multiple linear regression analysis which indicates linear relationship between experimental and predicted $\log\text{IC}_{50}$ with $r^2 = 0.93$ for human skin cancer cell lines.69

LIST OF ABBREVIATIONS

ALK	anaplastic lymphoma kinase
BSA	Bovine serum albumin
BRAF	Serine/threonine-protein kinase B-Raf.
CD20	B-lymphocyte antigen
EBRT	External beam radiation therapy
EGFR-TK	Epidermal growth factor receptor tyrosine kinase
HF	Hartee-Fock Method
HER2/neu	Human epidermal growth factor receptor 2
hTopoII α	Human topoisomerase II α
JAK	Janus family of protein kinases
mAbs	monoclonal antibodies
MLR	Multiple Linear Regression
MTT	3-(4,5-Dimethylthiazol-2-yl)-2,5-diphenyltetrazolium bromide
NSCLC	Non-small-cell lung carcinoma
PARP	Poly ADP ribose polymerase
PAGE	Polyacrylamide gel electrophoresis
PDGFR	Platelet Derived Growth Factor Receptor
PLS	Partial Least Square
PSA	polar surface area
QSAR	Quantitative Structural Activity Relationship
RAF	Rapidly Accelerated Fibrosarcoma.
SASA	Solvent accessible surface area
SDS	Sodium dodecyl sulfate
SMIs	Small molecule inhibitors

SSE	Sum of Squared Errors
VEGF	Vascular endothelial growth factor
vdW	van der Waals



INTRODUCTION

1.1 Cancer

Cancer is a group of diseases characterized by the uncontrolled growth and spread of abnormal cells. Normally, human cells grow and divide to form new cells as the body needs them. When cells grow old or damages, they die, and new cells take their place. When cancer cells develop, this process breaks down. As cells become more and more abnormal, old or damaged cells survive when they should die, and new cells form when they are not needed. These cancer cells can divide without stopping and may form growths called tumors (Fig. 1). A tumor can be benign or malignant. A benign tumor does not spread to other parts of the body so, this type of tumor is not cancer. Unlike benign tumors, malignant tumors can make up of cancerous cells, which can spread by spread into, or invade, nearby tissues. In addition, as these tumors grow, some cancer cells can break off and travel to distant places in the body through the blood or the lymph system and form new tumors far from the original tumor [1].

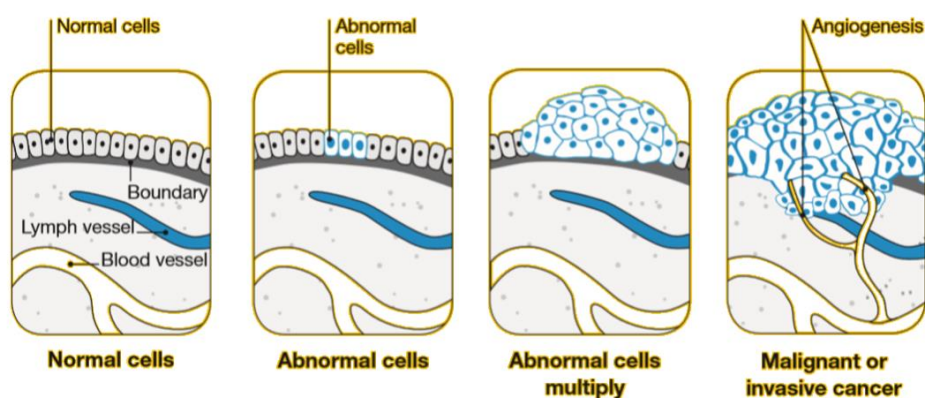


Figure 1. Normal cells become to malignant or invasive cancer. Before cancer cells form in tissues of the body, the cells go through abnormal cells and form a tumor.

1.2 Cancer Statistics

Nowadays, cancer is one of the most serious groups of diseases in the world. Cancer is a second leading causes of death worldwide next to heart diseases [2]. The

number of deaths attributed to cancers being about 9.6 million in 2018, accounting for about 1 in 6 deaths worldwide (World Health Organization, 2017) [3]. In 2018, the mortality data collected by the National Center for Health Statistics counted 1,735,350 new cancer cases and 609,640 cancer deaths in the United States. [4]. The most common causes of cancer death are cancers of the lung, prostate, and colorectal in men and the lung, breast, and colorectal in women (Fig. 2). These four cancers types account for 45% of all cancer deaths in United States while 60% of the cancer in Thailand is coming from five cancer types; breast, cervical, colorectal, liver and lung cancer (see also; Fig. 3) [5]. In female, incident of all cancer expressed to remain constant whereas, incident of all cancers seems to be declined from 2000 to 2012 in male because of the decreasing in lung cancer (Fig. 4). Virani S. and co-worker found that liver and lung cancers exhibit higher problems in the northeast and north regions, respectively. Liver cancers are predictable to increase in the northern and south males and females [6].

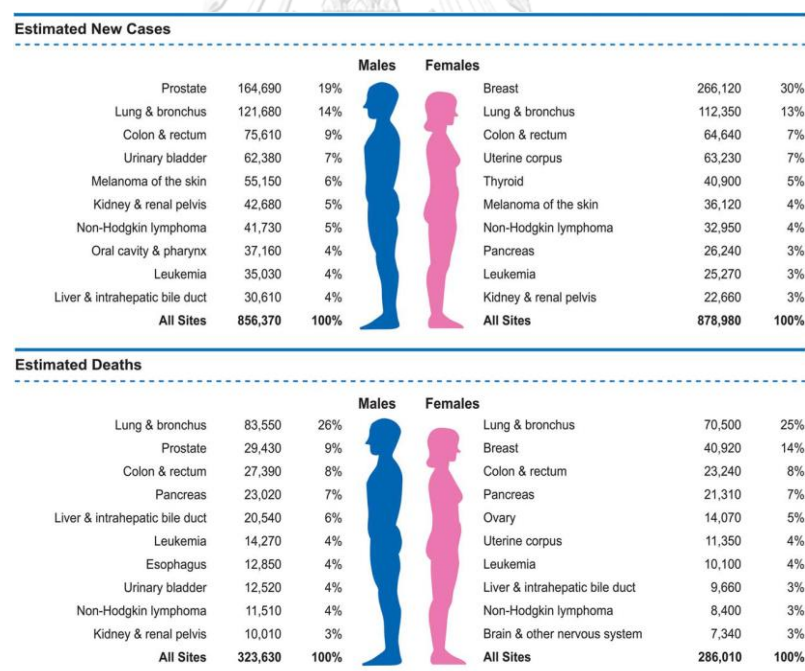


Figure 2. Ten Leading Cancer Types for the Estimated New Cancer Cases and Deaths of male and female, United States, 2018. [4].

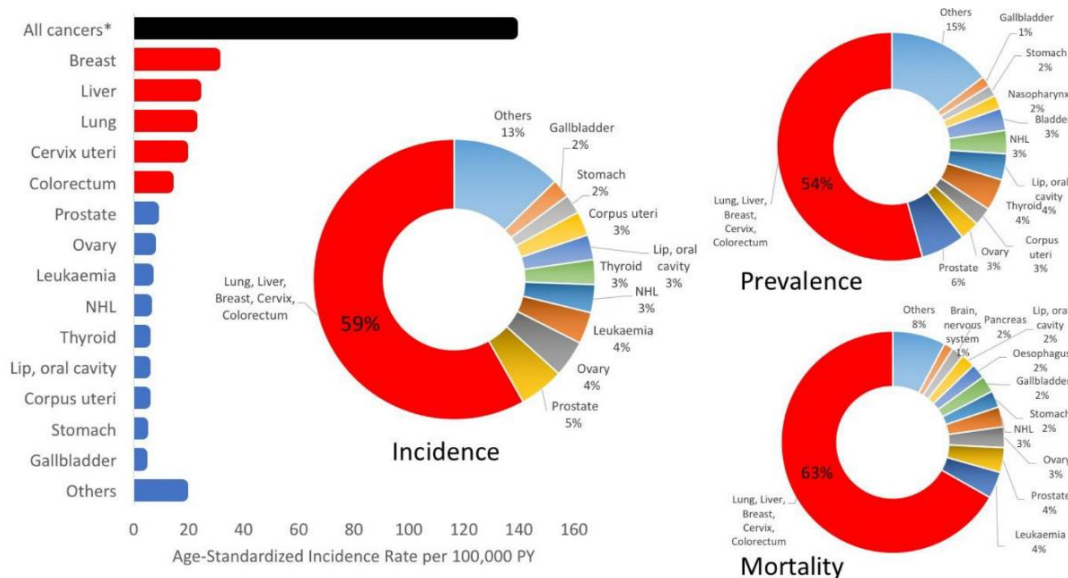


Figure 3. Breast, cervix, colorectal, liver and lung cancers combined had the highest age-standardized rates in 2012 and accounted for more than half of the incidence, prevalence and mortality in Thailand. *excluding non-melanoma skin cancer [6].

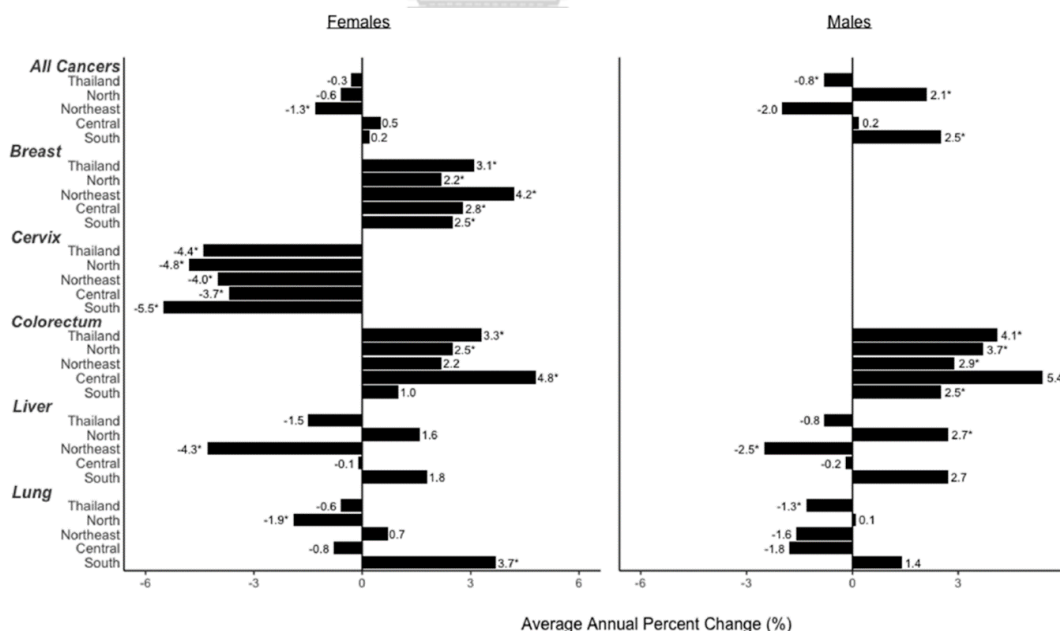


Figure 4. National and subnational average annual percent change of each cancer from 2000-2012 for female and males. [6].

1.3 Cancer treatments

Nowadays, there are many treatments for remission or cure cancer, that make the signs and symptoms of cancer reduce or disappear. Type of treatment will depend on several factors, including: (i) type of cancer, (ii) where the cancer began, (iii) whether the cancer has spread to other parts of your body. Several types of cancer treatments, such as surgery, radiation therapy, chemotherapy, as well as other therapeutic modalities (e.g. immunotherapy, hormone therapy, biological therapy, photodynamic therapy) and a combination of these (e.g. radiosurgery).

1.3.1 Surgery

Surgery treatment is suitable for the patient who has the cancer in one area (localized). It may be used to remove tissue that might contain cancer cells. Surgery is most successful when the tumor has not spread to other areas. Surgery offers the greatest chance of a cure for many types of cancer. However, this treatment has a risk to make some common side effect for example, pain is the common side effect of the operation or surgery can become infected and sometime while recovering from the surgery the patients are at an increased risk of developing a blood clot. In some cases, they may get loss of an organ function [7].

1.3.2 Radiation therapy

Radiation therapy uses high dose of radiation to kill cancer cells or cause genetic changes resulting in cancer cell death. There are two types of radiation therapy, External beam radiation therapy and Internal radiation therapy. For external beam radiation therapy, this type of radiation comes from a machine that aims radiation at cancer. It sends radiation to a part of body from many directions and treats a specific part of body. If the patients have cancer in lung, they will have radiation only to chest, not to whole body. This type of treatment is used to treat many types of cancer (Table 1). On the other hand, internal radiation therapy is a treatment in which a source of radiation is put inside the body. The radiation source can be solid or liquid. It is often used to treat cancers of the head and neck, breast, cervix, prostate, eye, and certain types of thyroid cancer. High doses of radiation therapy are good to

destroy cancer cells, but radiation not only kills or slows the growth of cancer cells, it can also affect nearby healthy cells. Damage to healthy cells can cause side effects [8].

Table 1. Examples of cancers treated with radiation therapy [8].

Early cancers curable with radiation therapy alone	Cancers curable with radiation therapy in combination with other modalities
<ul style="list-style-type: none"> ▪ Skin cancers (Squamous and Basel cell) 	<ul style="list-style-type: none"> ▪ Breast carcinomas
<ul style="list-style-type: none"> ▪ Prostate carcinomas 	<ul style="list-style-type: none"> ▪ Rectal and anal carcinomas
<ul style="list-style-type: none"> ▪ Lung carcinomas (non-small cell) 	<ul style="list-style-type: none"> ▪ Local advanced cervix carcinomas
<ul style="list-style-type: none"> ▪ Cervix carcinomas 	<ul style="list-style-type: none"> ▪ Locally advanced head and neck carcinomas
<ul style="list-style-type: none"> ▪ Lymphomas (Hodgkin's and low grade Non-Hodgkin's) 	<ul style="list-style-type: none"> ▪ Locally advanced lung carcinomas
<ul style="list-style-type: none"> ▪ Head and neck carcinomas 	<ul style="list-style-type: none"> ▪ Advanced lymphomas
	<ul style="list-style-type: none"> ▪ Bladder carcinomas
	<ul style="list-style-type: none"> ▪ Endometrial carcinomas
	<ul style="list-style-type: none"> ▪ CNS tumors
	<ul style="list-style-type: none"> ▪ Soft tissue sarcomas
	<ul style="list-style-type: none"> ▪ Pediatric tumors

1.3.3 Chemotherapy

Chemotherapy is the most effective and widely used treatment in most types of malignancies [9]. Chemotherapy is the application of chemicals or drugs to kill cancer cells or slow the growth of cancer cells. The chemical is called cytotoxic,

which means toxic to cells. There are several different classes of anticancer drugs based on their mechanisms of action, and they include the following: a) alkylating agents which damage DNA; b) anti-metabolites that replace the normal building blocks of RNA and DNA; c) antibiotics that interfere with the enzymes involved in DNA replication; d) topoisomerase inhibitors that inhibit either topoisomerase I or II, which are the enzymes involved in unwinding DNA during replication and transcription; e) mitotic inhibitors that inhibit mitosis and cell division; and f) corticosteroids, which are used for the treatment of cancer and to relieve the side effects of other drugs [10]. Chemotherapy works like a two-sided sword, because chemotherapy works on cells, that are dividing rapidly. Cancer cells divide rapidly, as do some healthy cells. These include cells in the blood, mouth, digestive system and hair follicles. The effect of the drugs was shown to reduce not only cancer but to destroy normal cells resulting in the chemotherapy dose dependent side effects such as fatigue, nausea, hair loss, vomiting, etc. and even death may also occur in severe cases (Fig. 5). [11-13]. There are 132 cancer chemotherapy drugs approved by the US Food and Drug Administration, of which 56 drugs have been reported to cause oxidative stress [14]. Table. 2 shows the most common chemotherapy drugs used up to now.

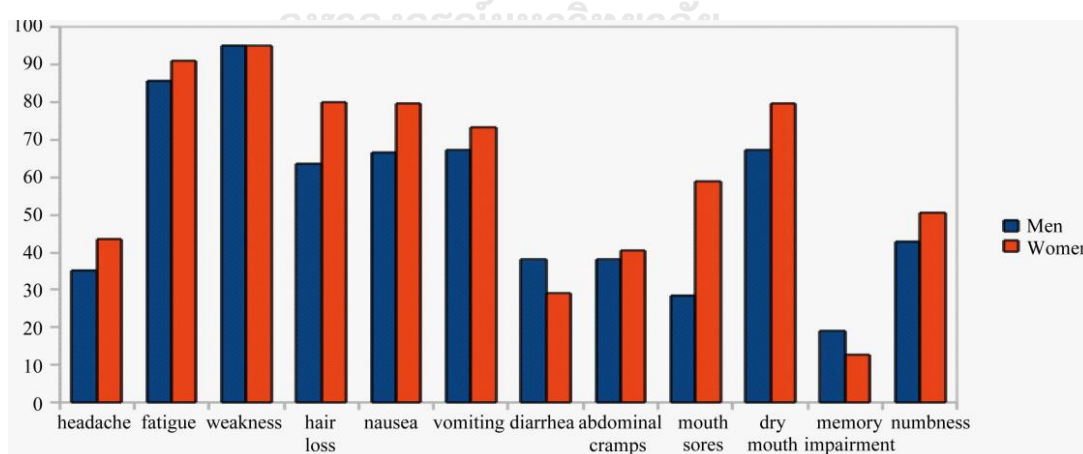


Figure 5. Comparison of the two genders on the basis of different side effects associated with chemotherapeutic drugs.

Table 2. Common class of cancer chemotherapy

Class of Chemotherapy	Mechanism of Action	Examples of Specific Drugs
Alkylating agents	Put chemical groups on DNA causing DNA break, pair abnormally, or cross link, so the cell cannot divide.	Busulfan [15], Cisplatin [16, 17] Cyclophosphamide [18], Melphalan [19]
Inhibition of DNA replication	Disrupt DNA replication, the cells cannot perform the functions.	Fluorouracil [20], Gemcitabine [21] Methotrexate [22, 23]
Mitotic inhibitor	Binding to proteins that is essential for cell division.	Docetaxel [24], Paclitaxel [25], Vinblastine [26], Vincristine [27]
Antitumor antibiotics	Prevent cell division by binding to DNA or inhibiting RNA	Doxorubicin [28], Epirubicin [29], Mitoxantrone [30], Bleomycin [17]
Topoisomerase inhibitors	Inhibit topoisomerase causing the cell stop division.	Topotecan [31-33], Irinotecan [31, 34-36], Salvicine [37-41], Etoposide [42, 43], novobiocin [44, 45]
EGFR tyrosine kinase	Inhibit cell proliferation which overexpresses EGFR by targeting the epidermal growth factor receptor tyrosine kinase.	Erlotinib [46-48], Cetuximab [49], Gefitinib [50, 51]

1.3.4 Immunotherapy

Normally, the immune system produces specialized disease-fighting cells that circulate throughout the body, continually seeking out and destroying “foreign” agents. Some cancer cells mutate and then escape the detection from the immune response because of their similarities to healthy tissues. Therefore, cancer immunotherapies override cancer’s evasive strategies to confirm that powerful, precise and adaptable immune attack is focuses on tumors anywhere in the body. They are various types of immunotherapy, including; a) cancer vaccines b) monoclonal antibodies (MABs) c) non-specific immunotherapies d) immune

checkpoint inhibitors e) cytokines (immune hormones) [52]. Immunotherapy is not widely used as surgery, chemotherapy and radiotherapy. Cancer immunotherapy is likely to benefit some people with some types of cancer. It can cause side effects such as inflammation in any of the organs in the body and common side effects include fatigue, skin rash and diarrhea because it acts on the immune system [53, 54].

1.3.5 Targeted therapy

Targeted cancer therapy, in which the drugs are used to specifically block cancer cell proliferation, promotes cell cycle regulation or induces apoptosis or autophagy and targeted delivery of toxic substances specifically to cancer cells to destroy them. This technique has become one of the high potent cancer treatments because they are delivering drugs to genes or proteins that are specific to cancer cells and less damage to normal cells [55]. A potent target for the targeted cancer therapy is required. Proteins that are present in cancer cells but not in normal cells or that are more abundant in cancer cells would be potential targets, especially if they are known to be involved in cell growth or survival [56-58]. For example, topoisomerase II α (hTopoII α), epidermal growth factor receptor (EGFR) have been focused as good targets because they are playing an important role in cell cycle process. There are two types of targeted therapy; monoclonal antibodies (mAbs) and small molecule inhibitors (SMIs). mAbs block a specific target on the outside of cancer cells or in the tissue surrounding it while small molecule can penetrate the cell membrane to interact with targets inside a cell. Small molecules are usually designed to interfere with the enzymatic activity of the target protein [59]. During the recent years, several mAbs and SMIs (Table 3 and 4) have been approved by authorities for cancer treatment.

Table 3. Therapeutic antibodies approved by the US FDA for cancer treatment

Monoclonal antibody	Target	indication	year	references
Rituximab	CD20	Low-grade B-cell non-Hodgkin lymphoma	1997	[60-62]
Trastuzumab	HER2/neu	Metastatic breast cancer	1998	[63, 64]
Gemtuzumab-ozogamicin	CD33	Acute myeloid leukemia	2000	[65, 66]
Alemtuzumab	CD52	Chronic lymphocytic leukemia	2001	[67, 68]
Ibritumomab-tiuxetan	CD20	Non-Hodgkin lymphoma	2002	[69]
Tositumomab	CD20	Non-Hodgkin lymphoma	2003	[70-72]
Cetuximab	EGFR	Metastatic colorectal cancer, head and neck cancer	2004	[73-75]
Bevacizumab	VEGF	Metastatic colorectal cancer, NSCLC	2004	[76]

Table 4. Small molecules inhibitors approved by the US FDA for cancer treatment [56]

Monoclonal antibody	Target	FDA-approved indication
Afatinib	EGFR and HER2	<ul style="list-style-type: none"> • Non-small cell lung cancer (with EGFR exon 19 deletions or exon 21 substitution (L858R) mutations)
Alectinib	ALK	<ul style="list-style-type: none"> • Non-small cell lung cancer (with ALK fusion)
Erlotinib	EGFR (HER1)	<ul style="list-style-type: none"> • Non-small cell lung cancer (with EGFR exon 19 deletions or exon 21 substitution (L858R) mutations) • Pancreatic cancer
Gefitinib	EGFR (HER1)	<ul style="list-style-type: none"> • Non-small cell lung cancer (with EGFR exon 19 deletions or exon 21 substitution (L858R) mutations)
Imatinib	KIT, PDGFR, ABL	<ul style="list-style-type: none"> • GI stromal tumor (KIT+) • Dermatofibrosarcoma protuberans
Pazopanib (Votrient)	VEGFR, PDGFR, KIT	Renal cell carcinoma
Sorafenib (Nexavar)	VEGFR, PDGFR, KIT, RAF	Hepatocellular carcinoma Renal cell carcinoma
Ruxolitinib (Jakafi)	JAK1/2	Myelofibrosis
Rucaparib (Rubraca)	PARP	Ovarian cancer (with BRCA mutation)
Vemurafenib (Zelboraf)	BRAF	Melanoma (with BRAF V600 mutation)

1.4 Topoisomerase

To maintain DNA compaction during the cell process, enzymes capable of managing superhelices tension and knots are necessarily required. Topoisomerases are enzymes that solve DNA topological problem that result from strand separation during replication and transcription [77-79]. They are classified into two categories by the number of DNA strands that they transiently break. Type I topoisomerases cause transient single-strand breaks during DNA replication, while type II removes knots and tangles by generating transient double-strand breaks in double helix (Fig. 6). Type I and type II act on both negative and positive supercoil DNA.

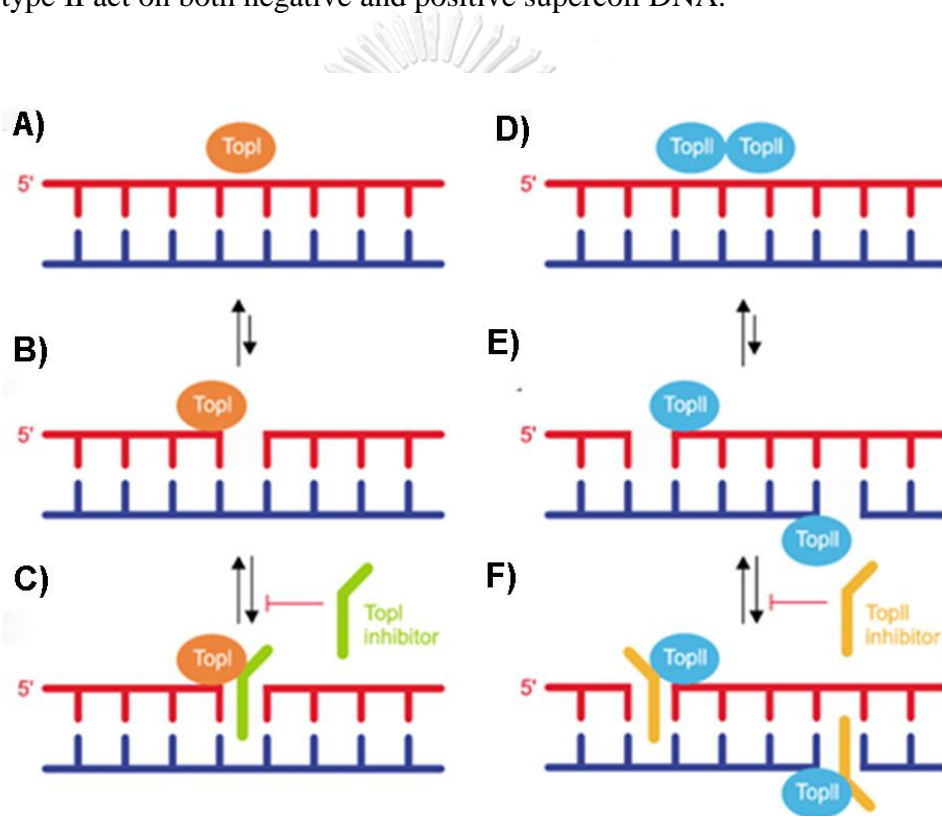


Figure 6. Topoisomerase I (TopoI, left) and II (TopoII, right). Noncovalent binding of (A) TopoI and (D) TopoII to DNA. The arrow indicates the reversible ligation and cleavage reaction under normal condition (A, B for TopoI and D, E for TopoII). (C) Trapping the cleavage complexes of DNA topoisomerases by TopoI inhibitors and (F) TopoII inhibitors promotes DNA damages [77].

Human topoisomerase II (hTopoII) (Fig. 7) is an enzyme which catalyzes the cleavage and rejoining the double-stranded DNA and so it is essential in several vital cell processes, such as replication, transcription, chromosome separation and segregation [32]. All known type II topoisomerases are adenosine triphosphate (ATP)-dependent. ATP binding and hydrolysis modulate conformational changes in a DNA-bound type II topoisomerase. These changes are involved in coupling the DNA-dependent ATPase activity of the enzyme to its transport of one duplex DNA segment, termed the T-segment, through the topoisomerase-mediated gate in another DNA segment, termed the G-segment (Fig. 8) [80]. Generally, hTopoII exists in two homologous structures but in different isoforms, hTopoII α and hTopoII β . The hTopoII α isoform shows a low expression level in the G cell cycle phase but an increased concentration in the S and G2/M phases compared to normal cells, whilst hTopoII β does not change its concentration during the cell cycle [81]. Since hTopoII α is highly overexpressed in proliferating cancer cells [82], it has gained attention from many researchers who are developing new anti-cancer drugs. There are two important motifs for drugs targeting hTopoII α , namely the ATPase domain (Fig. 9A) and the DNA-binding core (Fig. 9B) [83]. The hTopoII α inhibitors can be divided into two categories, hTopoII α poisons and hTopoII α catalytic inhibitors [32]. For hTopoII α poisons (etoposide, doxorubicin, anthracyclines and mitoxantrone), they are clinically active agents that generate a high level of hTopoII-DNA covalent complexes by stimulating cleavage of the G-segment and blocking relegation of DNA [84]. On the other hand, hTopoII α catalytic agents (ICRF-187, novobiocin, merbarone and salvicine) affect the catalytic cycle of hTopoII α by elimination of the enzymatic activity [85-87]. Although these different catalytic agents share the same effect, they interact with hTopoII α at different binding sites. For example, the ICRF-187 binding pocket is located in the middle of the primary dimer interface [85], while merbarone acts by blocking the DNA cleavage reaction of hTopoII α . The merbarone binding site possesses an interaction domain overlapping with that of etoposide [88-90]. Salvicine, a derivative of diterpenoid quinones isolated from the traditional Chinese medicinal plant *Salvia prionitis* [87, 91], targets the ATPase domain [92-94].

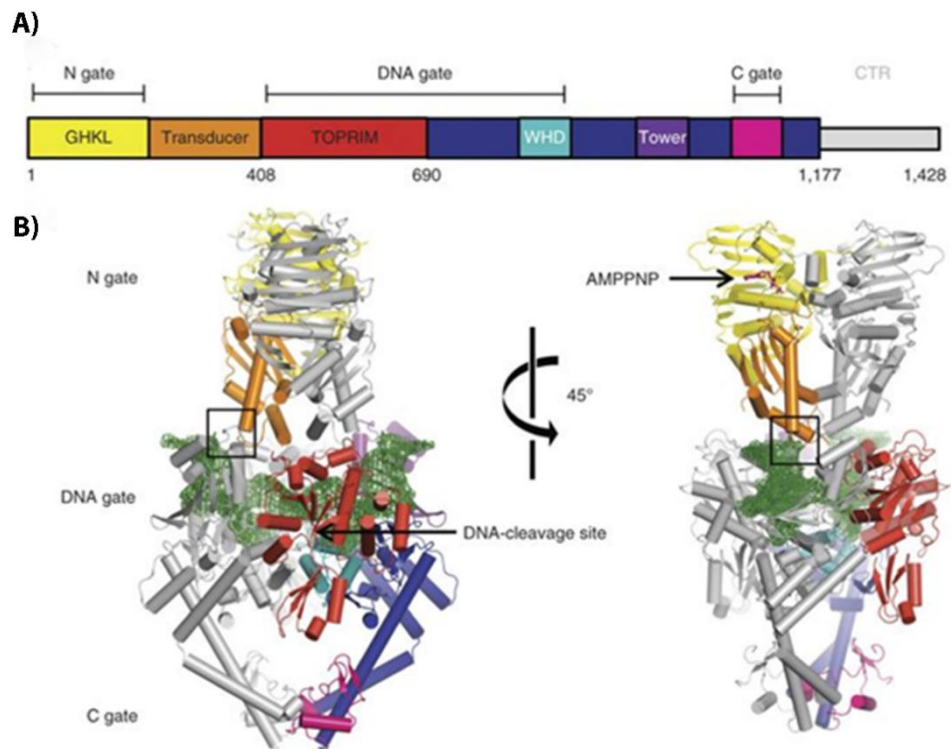


Figure 7. Structure of eukaryotic topoisomerase II α a) Domain arrangement of TopoII α . Functional regions are colored and labeled. CTR, C-terminal region. (b) Model of the ternary complex. [95]

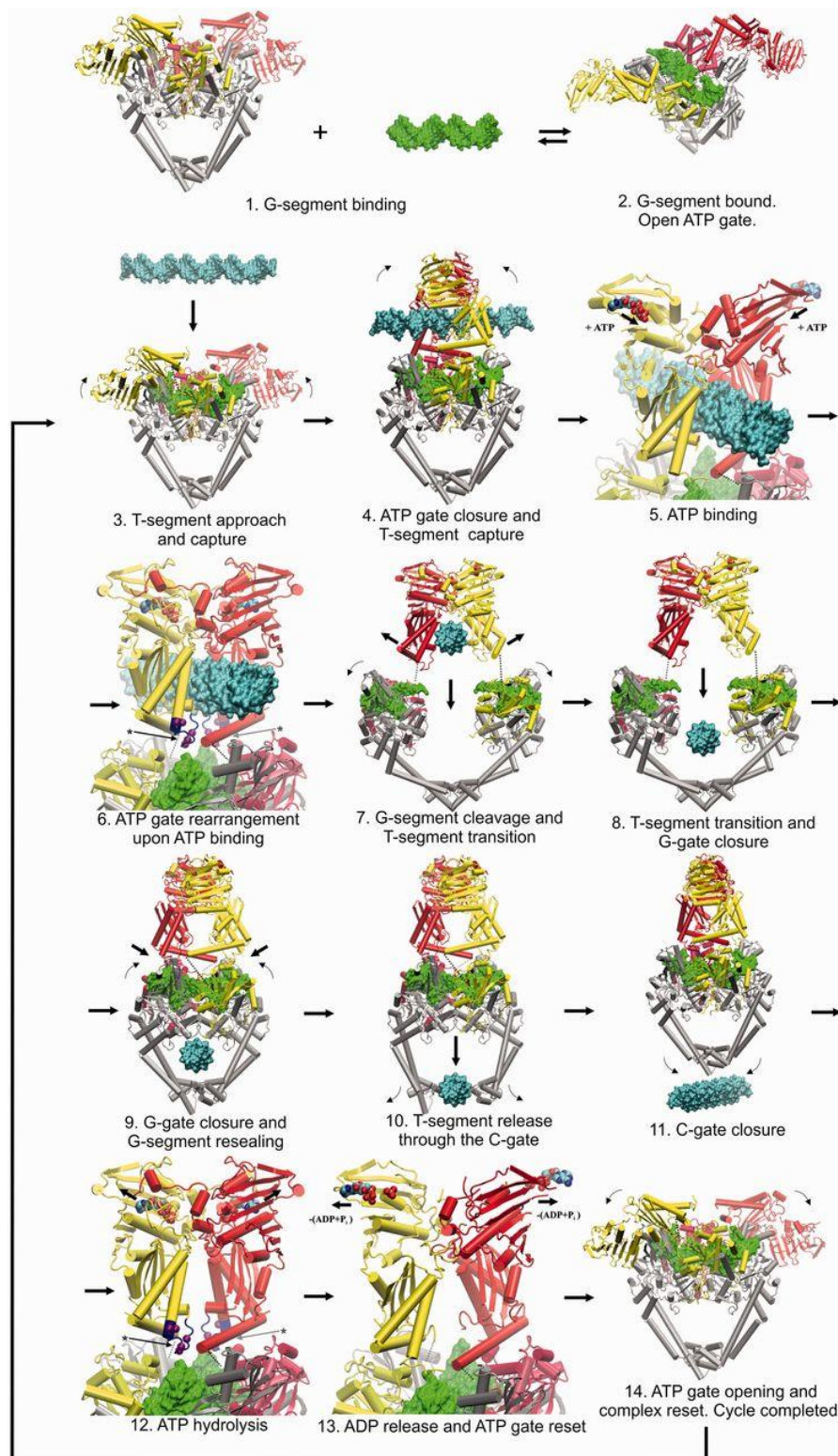


Figure 8. The mechanism of topoisomerase II [96]

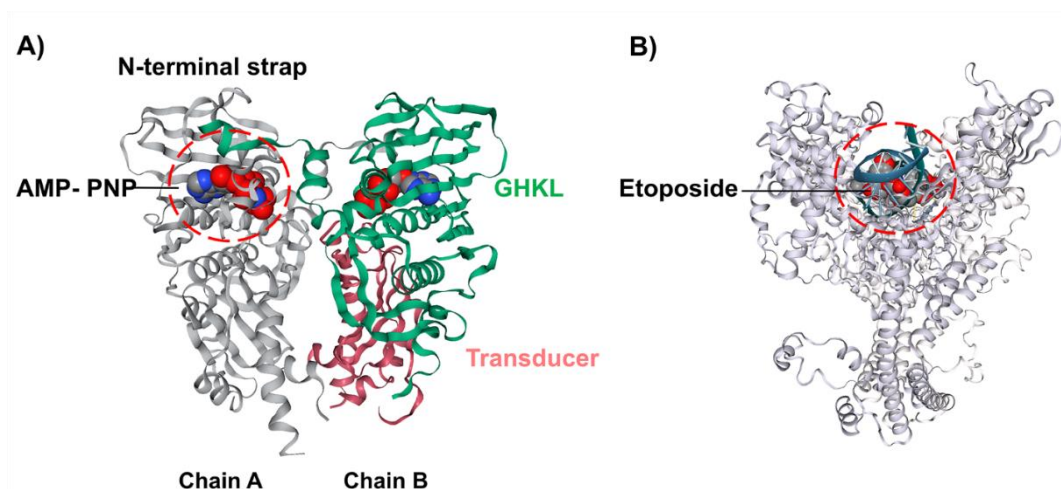


Figure 9. The hTopoII α structures used in the docking study. (A) The ATPase domain of hTopoII α with the 5'-adenylyl- β,γ -imidodiphosphate, AMP-PNP (space filling model), in the ATP binding pocket, where the GHKL and transducer domains are shown in green and pink (PDB code: 1ZXM). (B) The hTopoII α /DNA/etoposide ternary complex (PDB code: 3QX3) [41].

Table 5. Current topoisomerase inhibitors

Topoisomerase I inhibitors			
inhibitors	mechanism	toxicity	cancer
Topotecan [97-99]	It is forming a stable covalent complex with the DNA/topo I aggregate.	Hematological, granulocytopenia and thrombocytopenia	ovarian cancer [100], breast cancer [101]
Irinotecan [102, 103]	It interacts with cellular Topo I DNA complexes and has S-phase-specific cytotoxicity	Myelosuppression and diarrhea	colorectal cancer [104], small cell lung cancer [105]

Topoisomerase II inhibitors			
inhibitors	mechanism	toxicity	cancer
Etoposide [81, 106, 107]	Non-intercalating TopoII poison	Bone marrow suppression, nausea, vomiting and alopecia	skin cancers, Small cell lung [108], Non-lymphocytic leukemia [109], breast cancer [110]
Teniposide [81, 111]	Non-intercalating TopoII poison	Like those of etoposide	non-lymphocytic leukaemia [112]
Anthracyclines [81]	DNA intercalation	Myelosuppression, nausea, vomiting, alopecia and mucositis	breast cancer [113]
Mitoxantrone [81]	DNA intercalation	Myelosuppression, nausea, vomiting, alopecia and cardiotoxicity	breast cancer, acute promyelocytic or myelogenous leukemias, and androgen-independent prostate cancer [114].
Doxorubicin [115]	DNA intercalation	Nausea or vomiting and loss of appetite	non-Hodgkin's lymphoma, bladder cancer [116]
Salvicine [38, 39, 91]	Binding to ATPase domain and inhibiting topo-mediated DNA relegation and ATP hydrolysis.	Leukopenia, neutropenia, elevation of transminases, nausea, vomiting, mucositis [117]	Breast cancer [117], Non-small cell lung [118] and gastric cancer, leukemia cell lines, stomach cancer cells [119]

1.5 Epidermal Growth Factor Receptor (EGFR)

Epidermal growth factor receptor, EGFR or Erb1/HER-1 (Fig. 10) is one of four transmembrane proteins in a family of transforming growth factor (TGF) receptors. The other members of this group include ErbB2/HER-2, ErbB3/HER-3, and ErbB4/HER-4 [120]. EGFR consists of an extracellular receptor domain, a single hydrophobic transmembrane region and an intracellular domain with tyrosine kinase function [121]. It plays an important role in cell signaling, enhanced cell survival, proliferation and resistance to anti-cancer therapeutics. The binding of EGF to the extracellular receptor domain of EGFR leads to the phosphorylation of tyrosine residues on TK domain, resulting in the recruitment of many intracellular signaling molecules (see also Fig. 11 and 12). Accordingly, targeting EGFR proteins have been suggested as a high-powered strategy for targeted cancer therapy [122, 123]. EGFR is overexpressed in many human cancers, including non-small cell lung, breast, head and neck, bladder, and ovarian carcinoma [124]. Thus, EGFR is promising as a molecular target for cancer drug discovery [125], especially, in human epidermoid carcinoma A431 cells and human non-small lung cancer (NSCLC) [126-129]. Many therapeutic agents were developed for inhibiting EGFR including monoclonal antibody (mAbs) and small-molecule tyrosine kinase inhibitors (TKIs) [130]. mAbs acts directly against the extracellular receptor domain, while TKIs interrupt the intracellular EGFR tyrosine kinase activity. Both of these therapeutic agents inhibit cellular proliferation, facilitate apoptosis, and reduce survival signals, tumor metastasis, and angiogenesis [131]. Several tyrosine kinase inhibitors have been used in recent years are shown in Table 5. Gefitinib (IressaTM, AstraZeneca), an oral administration EGFR tyrosine kinase inhibitor was approved by the FDA for non-small-cell lung cancer (NSCLC) in 2003 [132] [133]. The mechanism of gefitinib is to compete with adenosine triphosphate at the binding site on the tyrosine kinase domain to prevent autophosphorylation of EGFR in human cancer cell lines. Erlotinib (TarcevaTM, OSI-Pharma/Genentech/Roche) works in the same way as Gefitinib. It has been used in a treatment for NSCLC and pancreatic cancer. [134], and lapatinib [135] and irreversible inhibitors afatinib [136] and dacomitinib [137].

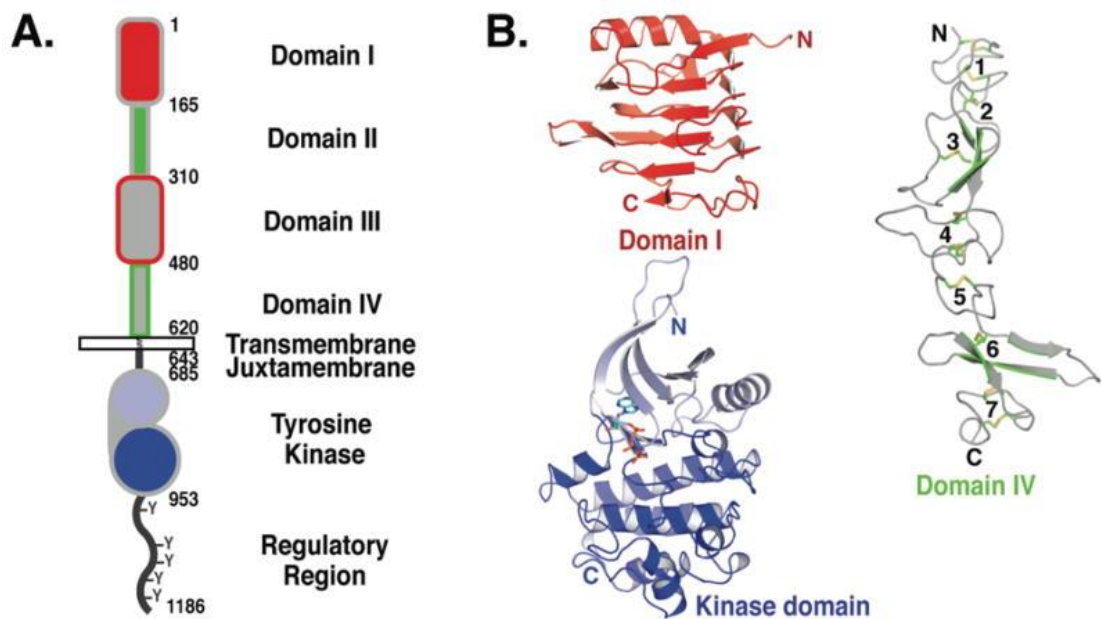


Figure 10. Structural of EGFR in three domains including; extracellular receptor domain, membrane domain and intracellular domain with tyrosine kinase function. A. The extracellular region comprises 4 domains, the N-lobe of the kinase domain is in light blue and the C-lobe in darker blue. B. Representative cartoons of the domains of EGFR. Domains I and III adopt a β -helix fold. Domains II and IV adopt extended structures comprising a series of disulfide-bonded modules [138].

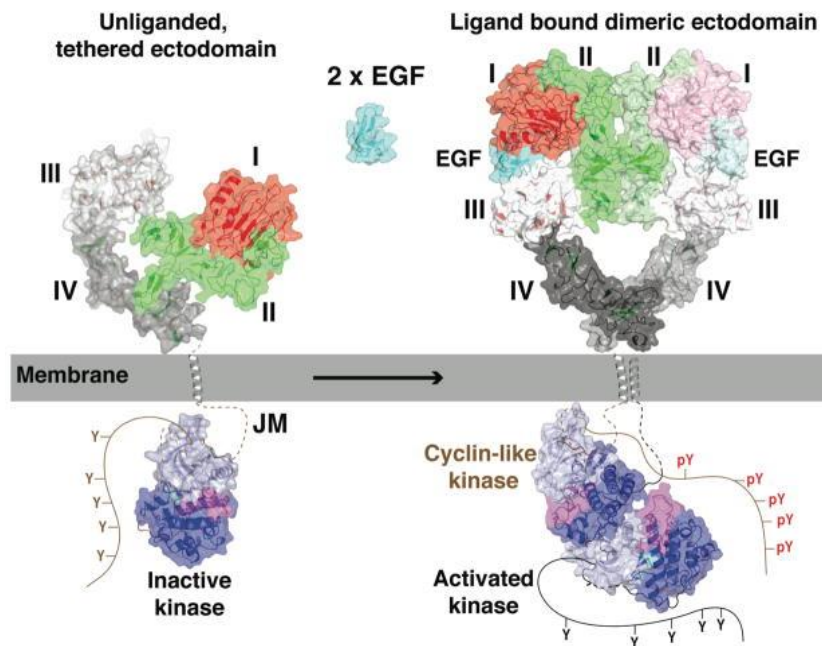


Figure 11. The scheme shows the mechanism of EGFR activation. The monomer to dimer transition in EGFR that is triggered by ligand binding. [138].

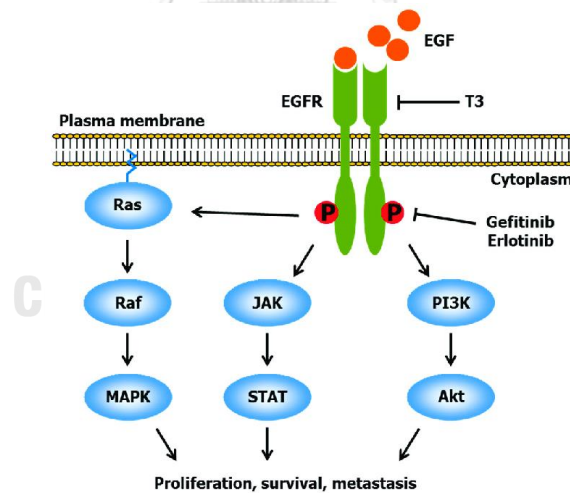


Figure 12. Epidermal growth factor receptor (EGFR) and its downstream signaling proteins. Arrows and perpendicular lines indicate activation/induction and inhibition/suppression, respectively [139].

Table 6. Current specific/selective tyrosine kinase inhibitors (TKIs) targeting receptor tyrosine kinases (RTKs) [10, 59].

Name	Selective Target	FDA Approved	Cancer
Afatinib	HER2, EGFR	+	NSCLC, head and neck, breast cancer
Canertinib	EGFR, HER2	-	NSCLC, head and neck, breast, ovarian cancer
Cediranib	VEGFRs	-	NSCLC, kidney and colorectal cancer
CP-673451	PDGFRs	-	NSCLC, colon carcinoma, glioblastoma
Crizotinib	MET	+	NSCLC, neuroblastoma
Crenolanib	MET, ALK, FLT3, PDGFR	-	AML, gastrointestinal stromal tumor, glioma
Dacomitinib	EGFR	-	NSCLC, gastric, head and neck cancer, glioma
Erlotinib	EGFR	+	NSCLC, pancreatic cancer
EMD1214063	MET	-	NSCLC
EMD1204831	MET	-	NSCLC
Gefitinib	EGFR	+	NSCLC, AML
Icotinib	EGFR	+	NSCLC
KW-2449	FLT3	-	AML
Lapatinib	HER2, EGFR	+	Breast cancer
Lenvatinib	VEGFR2,2	+	Approved for thyroid cancer in Japan

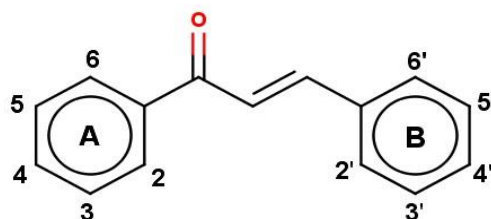
Name	Selective Target	FDA Approved	Cancer
LY2801653	Met, RON	-	NSCLC
Neratinib	DGFR, HER2	-	NSCLC, breast cancer
PD-173074	FGFRs	-	NSCLC, gastric carcinoma
Quizartinib	FLT3	-	AML
R428	AXL	-	AML, NSCLC, breast cancer
Tandutinib	FLT3	-	RCC, CML
Tivantinib	MET	-	RCC, breast cancer
Tivozanib	VEGFR1,2,3	-	RCC, breast cancer
Vatalanib	VEGFR2	-	NSCLC, DLBCL, colorectal adenocarcinoma

*HER; human epidermal growth factor receptor, EGFR; epidermal growth factor receptor; NSCLC; non-small cell lung cancer, VEGFR; vascular endothelial growth factor receptor, PDGFR; platelet-derived growth factor receptor, ALK; anaplastic lymphoma receptor tyrosine kinase, FLT3: Fms-like tyrosine kinase 3, AML: acute myeloid leukemia, CML: chronic myeloid leukemia, RCC: renal cell carcinoma, DLBCL: Diffused large B-cell lymphoma.

1.6 Chalcones

The polyphenolic compounds, chalcones or 1,3-diphenyl-2-propene-1-ones (Fig. 13), are precursors for flavonoids and isoflavonoids. They consist of two aromatic rings connected by an α,β -unsaturated carbon atom chain. Chalcones are naturally found in several plants, such as *Piper methysticum* [140] and members of the *Glycyrrhiza* [141] and *Angelica* [142]. Natural and synthetic derivatives of chalcones have been reported to exert several biological activities, including anti-fungal, anti-microbial, anti-protozoal, anti-viral, anti-malarial, anti-inflammatory and antioxidant effects [143-146]. In addition, they have been shown to have cytotoxic activities against various cancer cell lines, including breast (MCF7) [147-149], ovary (A2780)

[150], lung (A549) [149, 151], colon (SW480) [152], liver (HepG2) [153, 154] and cervical (HeLa) [155] cancer-derived cell lines. Chalcones have attracted attention because of their promising therapeutic effects, since they are able to target multiple cellular molecules, such as MDM2/p53, tubulin, proteasome, NF-kappa B, TRIAL/death receptors and mitochondria mediated apoptotic pathways, cell cycle, STAT3, AP-1, NRF2, AR, ER, PPAR- γ , β -catenin/Wnt [156] and especially hTopoII α [146, 157-159]. Moreover, epipodophyllotoxin-chalcone hybrids exhibited an enhanced *in vitro* cytotoxicity and higher topoisomerase II inhibitory efficiency than etoposide [160]. A series of chalcone-triazole derivatives presented a promising anticancer activity against the A-549 cell line and showed high binding affinities towards DNA topoisomerase II α and α -glucosidase targets [161]. Moreover, the novel bis-fluoroquinolone chalcone-like derivatives were found to inhibit both hTopoII α and tyrosine kinase [162]. Recently, a series of 2'- and 4'-aminochalcones were found to inhibit the growth of a canine malignant histiocytic cell line (DH82) and the transcription of the hTopoII α and TP53 genes [163].



CHULALONGKORN UNIVERSITY

Figure 13. Chemical structure of chalcone

1.7 Objective of the present work

- i) To search for potent chalcones against target cancer cells
- ii) To study the interaction of chalcones with cancer protein target
- iii) To design new compounds that with high potential.

CHAPTER II

THEORY AND BACKGROUND

2.1 Molecular docking

Molecular docking is a technique which predicts the binding mode of a ligand bound into a macromolecular target to form a stable complex. Information of the preferred orientation in turn may be used to predict how well the ligand can bind into the receptor. A variety of molecular docking software is available (Table 7). Docking methods have many algorithms, but in this study, we have employed CDOCKER algorithm in Accelrys Discovery Studio 3.0 (Accelrys, Inc.) program. A CDOCKER algorithm is a grid-based molecular docking method that generates randomly ligand conformations using CHARMM [164]. CDOCKER has been shown to give highly accurate docked poses [165]. The receptor is held fixed while the ligands are flexible during the refinement process. Ligand conformations are randomly generated from the initial ligand structure through high temperature molecular dynamics, followed by random rotations. The random conformations are refined by grid-based (GRID 1) simulated annealing and a final grid-based or full force field minimization.

Table 7. Molecular docking software [166]

Name	URL
Autodock	http://autodock.scripps.edu/
DOCK	http://dock.compbio.ucsf.edu/
FlexX	https://www.biosolveit.de/FlexX/
FITTED	http://fitted.ca/
FlipDock	http://flipdock.scripps.edu/
GOLD	http://www.ccdc.cam.ac.uk/solutions/csd-discovery/components/gold/
Glide	https://www.schrodinger.com/glide
ICM	http://www.molsoft.com/

2.2 Molecular dynamics simulation

Molecular dynamic (MD) simulation is defined as a computer simulation technique used to describe the time-dependent behavior of a biological system by integrating the Newton's laws of motion. Computer simulations act as a bridge between experiment and theory. This technique is widely used to calculate changes in the binding free energy of a drug candidate, or to observe the energies and the mechanism of the conformation change of a biological system such as protein in solution, membrane embedded protein, or large macromolecular complexes. The molecular dynamics simulation method is based on Newton's law equation (eq.1)

Newton's equation of motion is given by

$$F_i = m_i a_i = m_i \frac{dv_i}{dt} = m_i \frac{dr_i^2}{dt^2} \quad (\text{eq. 1})$$

where F_i is the force extent on particle i , m_i is the mass of particle i and a_i is the acceleration of particle i , v_i is the velocity of particle i .

The force F_i can also be expressed as the gradient of the potential energy (V)

$$F_i = -\nabla V_i(R) = \frac{dV_i}{dr_i} \quad (\text{eq. 2})$$

Combining these two equations (eq. 1 and eq. 2) lead to

$$F_i = m_i \frac{dr_i^2}{dt^2} = -\frac{dV_i}{dr_i} \quad (\text{eq. 3})$$

The total potential energy of system is defined by intramolecular and intermolecular interactions (eq. 4).

$$V = E_{bonded} + E_{non-bonded} \quad (\text{eq. 4})$$

where; $E_{bonded} = E_{bond-stretch} + E_{angles-bend} + E_{torsion-angle}$ (eq. 5)

$$E_{bonded} = \sum_{bonds} K_b (r - r_0)^2 + \sum_{angles} K_\theta (\theta - \theta_0)^2 + \sum_{torsion} K_\phi (\phi - \delta)^2 \quad (\text{eq. 6})$$

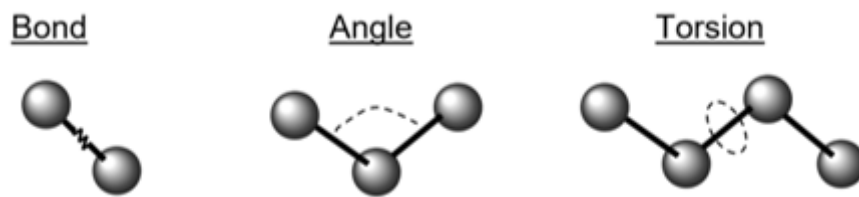


Figure 14. Typical intramolecular interactions

The potential energy derived from bonded and non-bonded term where the bonded term consists of three terms of atomic motion (i) the bond interaction between two atomic ($E_{bond-stretch}$), (ii) the angle between two connected bonds ($E_{angles-bend}$) and (iii) the torsion angle ($E_{torsion-angle}$) (Fig. 14). For the non-bonded term, it can be contributed by two functions (see also eq. 7) (i) the van der Waals interaction is obtained from Lennard-Jones potential in eq. 8 while (ii) Coulomb potential is applied for electrostatic interaction (eq. 9).

$$V_{non-bonded} = E_{van\ der\ Waals} + E_{electrostatic} \quad (\text{eq. 7})$$

where;
$$V_{van\ der\ Waals} = \sum \left(\frac{A_{ij}}{r_{ij}^{12}} - \frac{B_{ij}}{r_{ij}^6} \right) \quad (\text{eq. 8})$$

$$V_{electrostatic} = \sum \frac{q_i q_j}{4\pi} \quad (\text{eq. 9})$$

Binding free energy

The total free energy (ΔG) of a system is calculated from its enthalpy term (ΔH) and the entropy term with constant temperature ($T\Delta S$) (eq. 10).

$$\Delta G = \Delta H - T\Delta S \quad (\text{eq. 10})$$

In ΔH term is sum of molecular mechanics energy of complex (ΔE_{MM}) in the gas phase and term of solvation free energy (ΔG_{sol}). (Eq. 11) can be rewritten as:

$$\Delta H = (\Delta E_{MM} + \Delta G_{sol}) - T\Delta S \quad (\text{eq. 11})$$

ΔE_{MM} is derived from the summation of bonded and non-bonded interactions while ΔG_{sol} is calculated from both polar and non-polar terms (eq. 12). The Poisson Boltzmann (PB) equation in (eq. 13) or the generalized Born (GB) in (eq. 14) are presumed as a polar term while the non-polar term is assumed to the surface accessible surface area (SASA) in eq. 15.

$$\Delta G_{sol} = \Delta G_{PB(GB)} + \Delta G_{SASA} \quad (\text{eq. 12})$$

$$\nabla\{\varepsilon(r)\nabla\phi(r)\} - \varepsilon(r)K(r^2)\sinh[\phi(r)] = -4\pi\rho(r) \quad (\text{eq. 13})$$

$$G_{elec} = \sum \frac{q_i q_j}{4\pi\varepsilon_0 r} - \frac{1}{2} \left(1 - \frac{1}{\varepsilon}\right) \sum_i \sum_j \frac{q_i q_j}{\sqrt{r^2 + a_i a_j \exp\left(-\frac{r^2}{4a_i a_j}\right)}} \quad a_i; \text{Born radius} \quad (\text{eq. 14})$$

$$\Delta G_{SASA} = \gamma SASA + \beta \quad \gamma = 0.00542 \text{ kcal mol}^{-1} \text{ \AA}^2 \quad (\text{eq. 15})$$

$$\beta = 0.92 \text{ kcal mol}^{-1}$$

2.3 Quantitative structure-activity relationship (QSAR)

QSAR is a method that attempts to correlate structural, chemical and pharmacological activities in a quantitative manner for a series of compounds. The activities and properties are connected by mathematical functions, f :

$$\text{Biological activity} = f(\text{physiochemical and/or structural properties})$$

the biological activity can express the experiment values; IC_{50} , ED_{50} , % inhibition

QSAR is a mathematical method being widely applied in drug discovery and design. There are several publications of chalcones as anticancer using QSAR techniques [167-169]. The understanding of the relationship between chemical structures and pharmacological effects leads to some important information about the molecular mechanisms of the inhibition activities [170].

2.3.1 Molecular descriptor [171]

Molecular descriptors are at the core of QSAR modeling and there are many different types of descriptors depending on the dimensionality of the used QSAR. For example, in 1D-QSAR, the molecule can be considered as a one-dimensional molecular representation (e.g. functional groups, rings, bonds, substituents etc.). 2D molecular descriptor are defined to be numerical properties that can be calculated from the connection table representation of a molecule (e.g., elements, formal charges and bonds, but not atomic coordinates). For the 3D-descriptor, the properties that could calculated from the 3D structure of the molecules.

2.3.2 Regression Analysis for QSAR studies

There are many statistical model-building methods. The most commonly used regression-based approaches follow;

2.3.2.1 Multiple Linear Regression (MLR)

MLR is a statistical technique that uses several explanatory variables to predict the relationship between the dependent variable and multiple independent variables. This method is a very popular technique used in QSAR

because of its simplicity, transparency, reproducibility, and easy interpretability [172]. The MLR equation is as follows;

$$Y = a + b_1X_1 + b_2X_2 + b_3X_3 + \dots + b_NX_N \quad (\text{eq. 16})$$

where Y is dependent variable, $X_1, X_2, X_3, \dots, X_N$ are descriptes dependent variables with their regression coefficients $b_1, b_2, b_3, \dots, b_N$, and a is a constant term of the model.

For a statistically reliable model, the number of observations (number of molecules) and number of descriptors should have a ratio of at least 1:5 [173]. This method uses a stepping multiple linear algorithm to generate a model that may be carried out with either a fixed number of steps or an automatically determined end point. The stepping algorithms may give regression equations that use different variables. The statistical significance of the models should to be checked carefully.

2.3.2.2 Partial Least Squares (PLS)

PLS investigation is an extension of the multiple linear regression method also widely used in QSAR. PLS has many advantages, including the ability to robustly handle more descriptor variables than compounds, nonorthogonal descriptors and multiple biological results, while providing more predictive accuracy and a much lower risk of chance correlation [174]. Predictions from PLS models tend to be more accurate than from MLR because PLS can construct predictive models when factors are many and highly collinear by employed cross validation technique [175].

2.3.3 Evaluation of the Models [176]

A developed QSAR model can be accepted by following this criterion.

2.3.3.1 Coefficient of determination (r^2) (≥ 0.7) can define as follows:

$$r^2 = 1 - \frac{\sum (Y_{obs} - Y_{cal})^2}{\sum (Y_{obs} - \bar{Y}_{obs})^2} \quad (\text{eq. 17})$$

where; Y_{obs} stands for the observed response value

Y_{cal} is a model-derived calculated response.

\bar{Y}_{obs} is the average of the observe response values.

2.3.3.2 Standard error of estimate (SEE) For a good model, this value should be smaller, and this is defined as follows:

$$SEE = \sqrt{\frac{\sum (Y_{obs} - Y_{cal})^2}{N - p - 1}} \quad (\text{eq. 18})$$

where; N is number of molecules

p is number of predictor variable used in the model

2.3.3.3 Variance ratio (F) for statistical significance of the model should be high. The variance ratio can be defined as follows:

$$F = \frac{\frac{\sum (Y_{cal} - \bar{Y})^2}{p}}{\frac{\sum (Y_{obs} - Y_{cal})^2}{N - p - 1}} \quad (\text{eq. 19})$$

2.4 ADMET properties of a drug molecule

The success of a drug is determined not only by good efficacy, but also acceptable ADME and toxicity [177]. Pharmacokinetics is the way that body acts on the drug once it is administered. It is the measure of the rate (kinetics) of Absorption, Distribution, Metabolism, Excretion (ADME) and Toxicity. The prediction of the ADMET properties has become one of the most important issues to assess the effects

or risks of these compounds on the human body [178]. When a drug is administered, it should cross the membranes of cells to reach its target. The lipophilicity of the molecule is a measure of the ability of a compound to dissolve in fats, oils, lipids, and non-polar solvents. The lipophilicity is measured from the partition coefficient that is calculated by the following equation 20. The value of $\log P$ is generally in the range 1-5 [166].

$$P = \frac{[Drug]_{octanol}}{[Drug]_{aqueous}} \quad (\text{eq. 20})$$

Another parameter for the prediction of absorption is the polar surface area (PSA) defined as the sum of the surfaces of polar atoms in a molecule. It has been used for predicting intestinal absorption [179] and blood-brain barrier [180]. After the drug absorption, the drug distribution have to be considered. Normally, distribution of drugs is often measured as a volume of distribution. Volume of distribution (V_D) means how extensively drug is distributed to the rest of the body compared to the plasma. It is defined by the ratio of the amount of drug in total body to the concentration of drug in plasma following the equation 21.

$$V_D = \frac{\text{Total amount of drug in body}}{\text{Conc. of drug in plasma}} \quad (\text{eq. 21})$$

There are many physicochemical factors influencing drug distribution not only the volume of distribution, but also physicochemical properties, protein binding and physiologic barriers.

The metabolism of drugs play an important role in both of pharmacodynamic and pharmacokinetic properties [181]. As metabolism occurs, the initial compound is converted to new compounds called metabolites. The metabolism is carried out in the liver by e.g. redox enzymes, termed cytochrome P450 enzymes. Drug metabolism can be divided into two phases; phase I and II metabolism [182]. For phase I, the drug will change the chemical structure by the oxidation, reduction and hydrolysis reaction,

while in phase II drug conversion involves the conjugation reaction between drug and substances in the body such as glucuronic acid, sulfate and glycine. After metabolism process, the drug and their metabolite were eliminated from the body through the kidney. There are three sites are drug excretion occurs (Fig. 15). Firstly, the kidney is the important sites where metabolites are excreted through urine. Second, some of the metabolites are eliminated by the liver in the bile and passes through to the gut until they are finally excreted along with waste products or feces. The last way of excretion is through the lungs (e.g. anesthetic gases) [183].

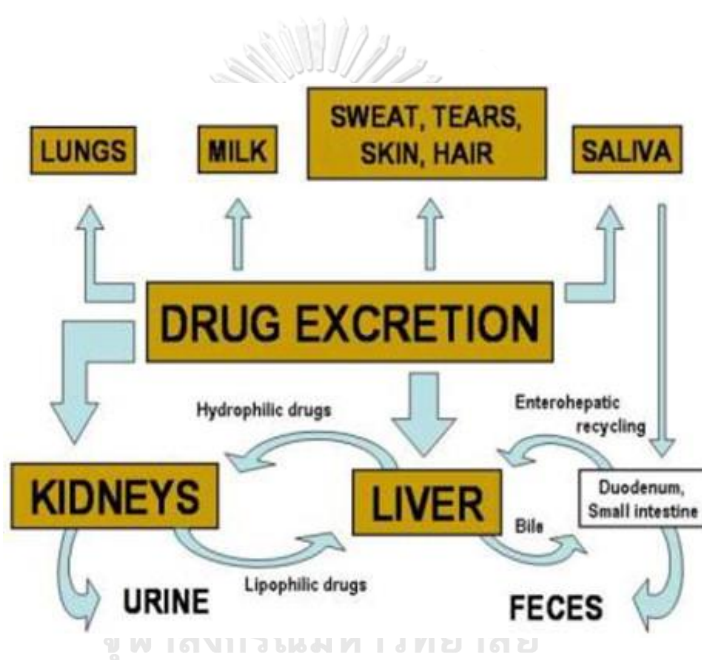


Figure 15. The drug excretion's routes [183]

The toxicity of the drug is also a very important descriptor for the drug prediction. Computational chemists try to predict the ADME-Tox qualities of compounds through methods like QSPR or QSAR. Normally, drug-likeness of a compound is a combination of molecular properties and structure features which determines whether a molecule is similar to available known drugs. In addition, the Lipinski's rule-of-five [184] helps to evaluate drug likeness of any chemical compound with certain pharmacological and biological activity that would likely to be considered as orally active drug. Note that, the properties, such as molecular mass <

500 Da, ClogP < 5, number of hydrogen bond donors < 5, the sum of nitrogen and oxygen atoms < 10 together constitutes the rule of five.

2.5 ADP-Glo Kinase assay

The ADP-Glo™ Kinase Assay is a luminescent ADP detection assay which measures kinase activity by monitoring ADP producing during kinase reaction. The ADP-Glo™ Kinase Assay is a universal assay that can be used to monitor the activity of virtually any ADP-generating enzymes (e.g., kinase or ATPase). Because of its high sensitivity, it is suitable for monitoring enzyme activities at very early substrate conversions requiring very low amount of enzymes [185]. The assay is performed in two steps; first, the ADP Glo reagent is added into reaction to terminate the kinase reaction and deplete the remaining ATP. The Kinase Detection Reagent is added to convert ADP to ATP and then the newly synthesized ATP is measured using a luciferase/luciferin reaction in second step (Fig. 16). The luminescent signal generated is proportional to ADP concentration produced and is correlated with the kinase reaction.

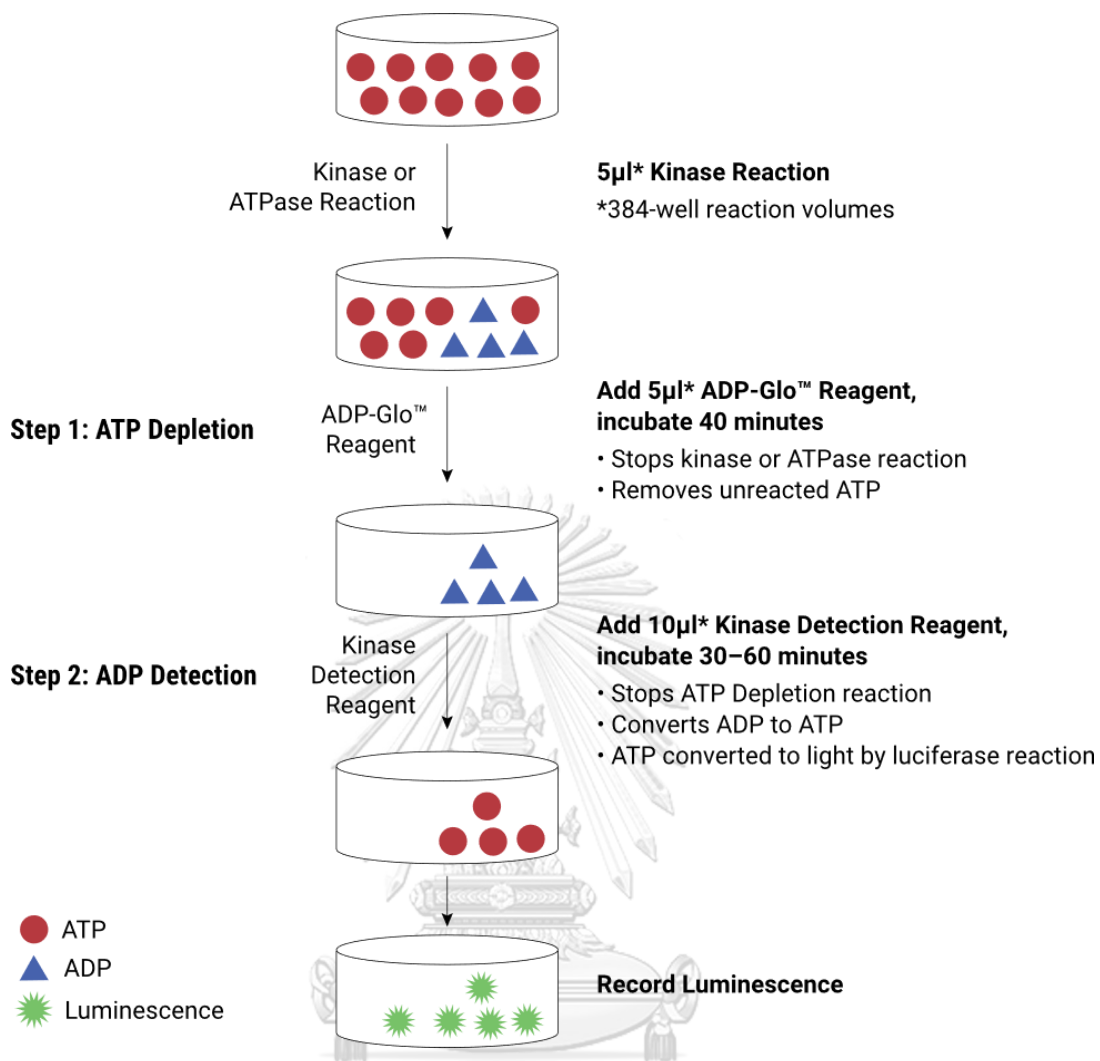


Figure 16. Principle of the ADP-Glo™ Kinase Assay.

CHAPTER III

MATERIALS AND METHODS

3.1 Equipment

Analytical balance	PB303-S, Mettler Toledo, Switzerland.
Autopipette	Gilson, Germany
Centrifuge	Hermle refrigerate centrifuge model Z383K, Hermle Labortechnik GmbH, Germany.
Heat box	D1100, Labnet, USA
Incubator	Accuplus, Thailand
Microplate reader	TECAN, Austria
Nano drop UV/visible spectrophotometer ND-1000	Nanodrop Technologies, USA
pH meter	Seven Easy pH meter, Mettler Toledo, USA
SDS-PAGE electrophoresis	Bio-RAD CA, USA
UV detector	ECONO UV monitor, Bio-Rad, USA
Vortex	Model G-560E, Scientific Industries USA.

3.2 Chemicals

Acrylamide	Bio Basic, Canada
Agar	Merck, Germany
ADP-Glo™ Kinase Assay kit	Promega (Madison, USA)

Adenosine triphosphate (ATP)	Fermentus, USA
Bovine serum albumin (BSA)	Sigma, USA
Chalcone	Synthesis from Center of Excellence in Natural Products Chemistry, Department of Chemistry, Faculty of Science, Chulalongkorn University.
Coomassie brilliant blue R-250	Bio Basic, Canada
Dimethyl sulfoxide (DMSO)	Merck, Germany
Dulbecco's modified eagle's medium (DMEM)	Life Technologies (CA, USA)
Ethylenediaminetetraacetic acid (EDTA)	Merck, Germany
fetal bovine serum (FBS)	Life Technologies (CA, USA)
Isopropyl β -D-1-thiogalactopyranoside (IPTG)	Fermentus, USA
Magnesium chloride (MgCl ₂)	Ajax Finechem, Australia
Methanol	Ajax Finechem, Australia
penicillin- streptomycin (Pen-Strep)	Life Technologies (CA, USA)
phosphate buffered saline (PBS)	Sigma-Aldrich (Darmstadt, Germany)
Plasmid pET28b-hTopoII α -ATPase	Gifted from Dr. Nonlawat Boonyalai
Salvicine	Chemfaces (Wuhan, P.R. China)
Sodium chloride	J.T. Baker, Malaysia
Sodium dodecyl sulfate (SDS)	Sigma-Aldrich (Darmstadt, Germany)
Thiazolyl blue (MTT)	Sigma-Aldrich (Darmstadt, Germany)

Trypsin	Life Technologies (CA, USA)
Tris (hydroxymethyl) aminomethane	Research organic, USA
Triton X-100	USB, USA
Tween 20	USB, USA
Yeast extract powder	Himedia, India

3.3 Cancer cell lines, Enzyme and Bacterial strains

Epidermoid carcinoma cell lines (A431; CRL-1555), Human lung adenocarcinoma cell lines (A549; CCL-185), Homo sapiens cervix adenocarcinoma cell lines (HeLa; CCL-2), urinary bladder carcinoma cell lines, (HT1376; CRL-1472), Human breast adenocarcinoma cell lines (MCF-7; HTB-22): American Type Cell Culture Collection (ATCC)

<i>E. coli</i> BL21 (DE3)	Novagen, Germany
Plasmid pET28b-hTopoII α -ATPase	Gifted from Dr. Nonlawat Boonyalai
EGFR expression plasmid pcDNA6A-EGFR ICD (645-1186)	Gifted from Mien-Chie Hung (Addgene plasmid # 42667)

Part I Computational approach

3.4 Topoisomerase II (hTopoII α)

3.4.1 Molecular docking of hTopoII α

Due to the possibility of the inhibition of two motifs of the hTopoII α (ATP binding site in the ATPase domain and the etoposide binding pocket in the hTopoII α /DNA complex), the predicting mode of the inhibitory activity of chalcones on both sites was studied by molecular docking using the CDOCKER module of Accelrys Discovery Studio 3.0 (Accelrys, Inc.) as previously reported [186]. The starting structures of the 47 designed chalcone derivatives (A1; Appendix) were built by the GaussView program [187], while those of salvicine and etoposide were taken from the ZINC database [188]. To validate the docking method, the co-crystallized ligands were initially docked into the binding pocket with 100 independent runs, i.e., docking of AMP-PNP into the ATP binding site of the hTopoII α ATPase domain (1ZXM.pdb), and etoposide into its binding pocket of the hTopoII α /DNA complex (3QX3.pdb). The position of docked ligands did not differ significantly from the crystallized conformation ligands (RMSD = 0.80 Å for AMP-PNP and 0.44 Å for etoposide) and so the 47 chalcones were then separately docked into both sites, while salvicine (used as the reference compound at the ATPase domain) was only docked into the ATP binding site. The chalcones with predicted interaction energies towards hTopoII α that were more favorable than those of the known inhibitors were synthesized and their *in vitro* cytotoxicity against the three cancer cell lines was tested (section 3.6.3).

3.4.2 MD simulation of hTopoII α

All-atom MD simulations under a periodic boundary condition were performed on the most potent chalcone selected from the *in vitro* cytotoxicity study (section 3.6.3) in complex with hTopoII α in aqueous solution, following the previously reported MD study on the binding of mansonone G to hTopoII α [186]. The partial charges of the ligand were prepared according to standard procedures [189-191]. The ligand was optimized with *ab initio* calculation using the HF/6-31G* method in the Gaussian09 program [192]. The electrostatic potential (ESP) charges of

the ligand were calculated using the same level of theory, and then the restrained ESP (RESP) charges were obtained by the charge fitting procedure using the antechamber module in the AMBER 14 package program [193]. The general AMBER force field (GAFF) [194] and AMBER ff03 force field [195] were applied for the ligand and protein, respectively. The protonation states of all ionizable amino acids were determined using PROPKA 3.1 [196]. The complex was solvated by TIP3P water molecules [197] within 12 Å around the system surface. Chloride ions were introduced to neutralize the total positive charge of the chalcone/hTopoII α complex.

To remove the bad contacts and steric hindrance, the added hydrogen atoms were minimized with 1000 steps of steepest descents (SD) followed by 2000 steps of conjugated gradients (CG) using the SANDER module in AMBER 14. The water molecules and ions were then minimized with 500 steps of SD followed by 500 steps of CG, while a 500 kcal/mol Å² force constant was used to restrain hTopoII α . The whole system was then fully minimized with 1000 steps of SD and CG. All covalent bonds involving hydrogen atoms were constrained by the SHAKE algorithm [198]. The long-range electrostatic interactions were calculated according to the Particle Mesh Ewald (PME) approach [199] with a cutoff distance of 12 Å for non-bonded interactions.

The system was heated to 310 K for 100 ps and then simulated at the same temperature for 80 ns in the NPT ensemble using a time step of 2 fs. The MD trajectories in the production phase were taken for analysis in terms of the per-residue decomposition free energy and intermolecular hydrogen bonds (H-bonds) between the ligand and hTopoII α using the MM/PBSA.py and cpptraj modules, respectively. The percentage of H-bond occupation was calculated using the two criteria of: (i) the distance between proton donor (HD) and acceptor (HA) atoms ≤ 3.5 Å, and (ii) the angle of HD-H...HA $> 120^\circ$.

3.5 Epidermal Growth factor receptor tyrosine kinase domain (EGFR-TK)

3.5.1 MD simulation of EGFR-TK

We employed the homology modeling to generate the full structure of tyrosine kinase from the crystal structure of EGFR-TK domain (pdb code: 1M17) as template using swiss model program. From *in vitro* studies, the screened chalcones

were then docked into the ATP binding site of EGFR-TK model using the CDOCKER module in according to the standard procedures [200, 201]. The docked chalcone/EGFR-TK complex with lowest interaction energy was selected as the initial structure for performing MD simulation. The partial charges of each ligand were prepared as follows. The geometry of ligand was optimized with *ab initio* calculation using HF/6-31G* method in Gaussian09 program [202]. Its electrostatic potential (ESP) charges were evaluated using the same level of theory, and then the restrained electrostatic potential (RESP) charges were retrieved by the charge fitting procedure using the antechamber module in AMBER 16 [203]. The ligand and protein were treated by the general AMBER force field (GAFF) [194] and AMBER ff14SB force field [204], respectively. The protonation states of Asp, Glu, Lys, Arg and His were assigned using PROPKA 3.0 [205]. The complex was solvated by TIP3P water molecules within 12 Å around the system surface and chloride ions were randomly added for system neutralization. All missing hydrogen atoms were added and then minimized with 1000 steps of steepest descents (SD) and 2000 steps of conjugated gradients (CG) using the SANDER module in AMBER 16 to reduce the bad contacts and steric hindrance. The water molecules and ions were then minimized with 2500 steps of SD followed by 2500 steps of CG, while protein backbone was restrained with force constant of 10.0, 5.0 and 1.0 kcal/mol·Å, respectively. Finally, the whole system was fully minimized with 2500 steps of SD and CG. All covalent bonds involving hydrogen atoms were constrained by SHAKE algorithm [206]. The long-range electrostatic interactions were calculated by the Particle Mesh Ewald (PME) approach [199], while a cutoff distance of 12 Å was applied for non-bonded interactions. Each system was heated to 310 K for 200 ps and equilibrated at the same temperature for 200 ps with backbone restraints by force 10 kcal/mol·Å. After that, 1 ns simulation was performed by decreasing restraint weights on protein from 10.0 to 5.0 kcal/mol·Å and then the simulation without any restraint was conducted till 500 ns. The MD trajectories from the last 100-ns simulation were taken for analysis in terms of root mean square deviation, per-residue decomposition free energy, number of hydrogen bonding between ligand and EGFR-TK, time-dependent distance between the centers of mass of the hydrophobic residues L718 and G796 and water accessibility as solvent-accessible surface area (SASA).

Part II Experimental methods

3.6 Topoisomerase II (hTopoII α)

3.6.1 Synthesis of chalcone derivatives

The three selected chalcones (**3c**, **3d** and **3f**) were synthesized by Claisen-Schmidt condensation with some modifications between selected acetophenones and benzaldehydes under a basic condition, according to the procedures described by Cabrera [207]. The target products were purified by column chromatography and their structures were elucidated by NMR spectroscopy.

3.6.2 Cell culture and sample preparation

Stock cultures of HT-1376, HeLa and MCF-7 cell lines were grown in T-75 flasks in complete medium (CM; DMEM, 10% (v/v) FBS and 1% (v/v) Pen-Strep) at 37 °C under 5% (v/v) CO₂. They were subcultured once a week, for HeLa and MCF-7 cells at a 1:100 ratio and for HT-1376 at 1:20 ratio by washing with PBS and then the cells were detached with trypsin. The 10⁻¹ M stock solution of each respective chalcone derivative was prepared in 100% DMSO.

3.6.3 Cytotoxicity assay

The cytotoxicity of the chalcones and salvicine was measured according to a published method [208] with some modifications. The cell viabilities of three cancer cell lines (HT-1376, HeLa and MCF-7) exposed to the screened chalcone derivatives were evaluated by the MTT assay. The cell suspension (100 μ L) was seeded into 96-well plates at a density of 2×10^6 cells/well and then incubated for 24 h under normal culture conditions before the addition of the respective test compound at various concentrations (100, 50, 25, 12.5 and 0 (control) μ M) and incubated for another 24 h. Then, 10 μ L of fresh MTT solution (5 mg/mL) was added to each well and incubated at 37 °C for 2 h, before the reaction was stopped by adding 100 μ L of DMSO. The absorbance was measured at 570 nm with correction for background at 690 nm using a microplate spectrophotometer system (Infinite M200 micro-plate reader, Tecan). The amount of the colored product is assumed to be

directly proportional to the number of viable cells. Each experiment was performed in triplicate and repeated three times. The percentage cell viability in each compound was calculated relative to the control, and the IC_{50} values were determined in comparison with untreated controls using the Table Curve 2D program version 5.01.

3.6.4 Expression and enrichment of the recombinant human

Topoisomerase II α ATPase domain

Expression and enrichment of the hTopoII α ATPase domain was modified from that reported [209]. The expression plasmid pET28b-hTopoII α -ATPase was transformed into *Escherichia coli* BL21 (DE3) cells and a transformant colony was selected for large-scale protein expression and grown at 37 °C to an optical density at 600 nm of ~0.6 in LB broth (2 L) containing 50 μ g/mL kanamycin. Protein expression was then induced by adding 0.5 mM IPTG at 30 °C for 5 h. The cells were harvested by centrifugation at 6000x g, 4 °C and resuspended in lysis buffer (50 mM Tris-Cl pH.8, 0.5 M NaCl, 5 mM imidazole, 0.5% (v/v) TritonX-100, 1 mM PMSF) and lysed by sonication. After clarification by centrifugation (as above) the supernatant was harvested, and the rhTopoII α -ATPase enriched for using HisTrap Chelating HP and Resource S column chromatography, eluting in exchange buffer (50 mM Tris pH.7.5, 50 mM NaCl, 5% (v/v) glycerol, 50 mM KCl, 5 mM MgCl₂) from a PD-10 desalting column. The enriched protein was analyzed by 12% sodium dodecyl sulphate-polyacrylamide gel electrophoresis (SDS-PAGE) and stained by Coomassie blue.

3.6.5 ATPase assay

The inhibitory activities of salvicine and chalcone 3d were determined by measuring the ATPase activity of rhTopoII α -ATPase using the ADP-Glo™ Kinase Assay. Briefly, 8 μ L of buffer (40 mM Tris-HCl pH 7.5, 20 mM MgCl₂, 0.1 mg/mL BSA) was added to each well of a 384-well plate (Promega, solid white) with 5 μ L of enzymes (10 ng/ μ L) and 2 μ L of the test compound at different concentrations. The reaction was initiated by the addition of 5 μ L of 12.5 μ M ATP, allowed to proceed for 1 h at room temperature and then stopped by the addition of 5 μ L of ADP-Glo™

Reagent and incubating at room temperature for 40 min. Next, 10 μL of Detection Reagent was added and incubated for 30 min prior to the addition of luciferase and luciferin to detect the ATP by measuring the luminescence of each well with a microplate spectrophotometer system (Synergy HTX Multi-Mode reader, BioTek). All assays were performed in triplicate. The percentage relative inhibition of salvicine and 3d was calculated as shown in Eq. (1);

$$\% \text{ Relative inhibition} = \frac{[(\text{positive}-\text{negative})-(\text{sample}-\text{negative})] \times 100}{(\text{positive}-\text{negative})} \quad (\text{eq. 22})$$

where negative and positive are the luminescence without and with the enzyme activity, respectively, and sample is luminescence with the test compounds. Finally, the IC_{50} curve was determined by GraphPad Prism version 6.

3.7 Epidermal Growth Factor Receptor tyrosine kinase domain (EGFR-TK)

3.7.1 Cell culture and cell viability assay (MTT assay)

The cytotoxicity activities of the series chalcones derivatives against A431 and A549 were evaluated by using the MTT (3-(4,5-dimethyl-2-thiazolyl)-2,5-diphenyl-2H-tetrazolium bromide) reduction assay. The A431, A549, and HEF were grown with DMEM supplemented with 10% (v/v) fetal bovine serum, 100 U/mL penicillin, and 100 U/mL streptomycin and were routinely cultured at 37 °C in a 5% CO_2 , 95% air humidified incubator. For preliminary screening, the 100 μL of A431 (5000 cells/well), A549 (5000 cells/well), and HEF (7000 cells/well) were seeded into 96-well microplates and incubated for 37 °C for overnight. After cell attachment, fresh complete media containing test compounds and erlotinib (positive control) were replaced at equivalent concentration (100 μM) and continually incubated for 72 hours. At the end of incubation time, the cells were replenished with complete media containing 0.5 mg/mL MTT solution and incubated for 3 hours. After formazan crystal forming, the 50 μL of DMSO was added for solubilization. The reaction was measured at 570 nm measurement wavelength and 630 nm reference wavelength by

using microplate reader (Infinite M200 micro-plate reader, Tecan). After screening, the hits which reduced cell viability lower than 50% were selected for IC₅₀ determining. Survival rate and IC₅₀ were analyzed by using GraphPad Prism version 6.0. Each experiment was performed in triplicate and repeated three times. Note that the cytotoxicity of 47 chalcone derivatives against human embryonic fibroblast cells was also tested by the same method.

3.7.2 Purification of intracellular domain of EGFR transfected HeLa cell

EGFR expression plasmid, pcDNA6A-EGFR ICD (645-1186) was a gift from Mien-Chie Hung (Addgene plasmid # 42667) [210]. The plasmid transfected using DharmaFECT reagent according to manufacturer's instruction. HeLa cells were used as expression host. After 24h transfection, transfected HeLa cells were selected by using BlasticidinS-HCl (Invitrogen) for one month. The cells were cultured in five T75 cm² for protein extraction. After 90% confluence, the cells were harvested and extracted by using RIPA buffer. ICD-EGFR was then purified with anion-exchange column (GigaCap Q) (Tosoh Bioscience, Japan) using AKTA Primer Plus FPLC with buffer A (50 mM Tris-HCl, pH 8.0, 50 mM NaCl, 1 mM Mecraptoethanol, 5 mM MgCl₂, 1 mM EDTA, and 5% Glycerol) for equilibration and buffer B (50 mM Tris-HCl, pH8.0, 1 M NaCl, 1 mM Mecraptoethanol, 5 mM MgCl₂, 1 mM EDTA, and 5% Glycerol) for elution fraction. EGFR protein was carried out and determined with 12% SDS-PAGE. Protein concentration was calculated by absorbance at 280 nm, using $\epsilon(280) = 52,370 \text{ M}^{-1} \text{ cm}^{-1}$ for EGFR.

3.7.3 Tyrosine kinase inhibition assay

Screening the inhibitory activities of erlotinib and potent chalcones (% cell viability less than 10 μM) from cytotoxicity values (**1c**, **2a**, **3e**, **4e**, and **4t**) were determined by measuring tyrosine kinase activity using ADP-Glo™ Kinase Assay. The 8 μl of buffer (40 mM Tris-HCl pH 7.5, 20 mM MgCl₂, 0.1 mg/ml BSA) was added to 384-well plate (Promega, solid white). The 5 μl of 2 ng/ μl of enzymes and 1 μM of inhibitors and erlotinib were then added to each well. Then, 10 μl of mixture of

5 μM ATP and 2.5 μM poly(glu·tyr) was added into the reaction mixture and incubated 1 hours at room temperature prior to the addition of the 5 μl of ADP-Glo reagent and then incubated further for 40 min. Then, 10 μl kinase detection reagent was used to converse ADP to ATP and incubated at room temperature for 30 min before measuring. The ATP was detected by measuring luminescence using a microplate spectrophotometer system (Synergy HTX Multi-Mode reader, BioTek). All assays were performed in triplicate. The percentage relative inhibition of erlotinib and chalcones was calculated.

Part III QSAR and ADMET

3.8 Quantitative structure–activity relationship

The data set of 22 molecules used to predict the relationship between the structure of compounds and their antiproliferation activity on A431 cancer cell lines was extracted from the testing cytotoxicity part [211]. The activity data has been given as IC_{50} values, the all data were converted to negative logarithmic concentration in moles (pIC_{50}) as dependent variables. (Table11). The Chemical structures of the dataset were sketched and optimized by using the Gaussian09 program with M06-2X/6-31G (d,p) method. In an effort to the relationship between the activity and structural feature of chalcone was explained by using QSAR. The chosen of descriptors in QSAR studies are the important step to achieve the model with high correlation and prediction ability [212]. There are many parameters were used in field of QSAR study. They can be classified into three classes: hydrophobic, steric and electronic properties. In this study, the 9 parameters were calculated by Material studio 7.0 package for each molecule. The hydrophobic parameter of drug is widely presented by partition coefficient (AlogP and AlogP98) while the Molecular refractivity, Molecular flexibility and rotatable bond were used as steric parameters. The electronic properties of molecules may effect to receptor-ligand binding. The HOMO, LUMO, hydrogen-bonding were the parameter used to describe electronic effects.

Multiple linear regression (MLR) is one of the best linear statistic methods used in QSAR investigations in which the investigated property is represented as a

linear function of calculated descriptors [213]. The MLR models were built and the QSAR equations with stepwise selection and removal of variables were established to select the set of descriptors that were most related to the anticancer activity (pIC_{50}) [214]. The leave-one out cross-validation procedure was used to validate the model.

In term of the statistic value used in this study is regression coefficient (R), square correlation coefficient (R^2), Fischer's value (F) and significance level (p) < 0.005 for select the best regression performance.

3.9 ADME and toxicity prediction

The physicochemical and pharmacokinetic properties as well as the toxicity of the screened chalcones were investigated by ADMET prediction (Absorption, distribution, metabolism, excretion, and toxicity) using the online SwissADME web program (www.swissadme.ch/) [215], Molinspiration cheminformatics (<http://www.molinspiration.com/>) web program [216] and Osiris prediction tool on DataWarrior program [217].

CHAPTER IV

RESULTS AND DISCUSSION

Part I Computational screening of chalcones acting against topoisomerase II α and their cytotoxicity towards cancer cell lines

4.1 Molecular docking studies

To investigate the most favorable binding site of the 47 designed chalcones, each compound was separately docked into the ATP binding site in the ATPase domain of hTopoII α and the etoposide binding pocket in the hTopoII α /DNA complex. The predicted interaction energies of all chalcones at both sites were plotted and compared with those of salvicine and etoposide (Fig. 17). The interaction energies of the chalcones ranged from -45.6 to -32.4 kcal/mol in the etoposide binding pocket and from -60.0 to -37.5 kcal/mol in the ATP binding site. This suggested that all the chalcone derivatives specifically interacted with the ATPase domain rather than with the hTopoII α /DNA complex.

Among all 47 chalcones, the group 3 compounds (**3c**, **3d** and **3f**) showed high interaction energies with the hTopoII α ATPase domain (-61.1, -60.7 and -59.3 kcal/mol), which were better than that of salvicine (-58.7 kcal/mol) at the hTopoII α ATPase domain. However, none of the tested chalcones were stronger than etoposide binding in the hTopoII α /DNA complex (-72.4 kcal/mol). Additionally, the mode of action of these three compounds was likely comparable with salvicine in the ATP binding pocket (Fig. 18). The important residues that contributed to ligand stabilization via van der Waals (vdW) and H-bond interactions are summarized in Table 8. There are at least four conserved residues between each chalcone and salvicine. The obtained results were similar to the docking study of 4-ethoxycarbonylmethyl-1-(piperidin-4-ylcarbonyl)-thiosemicarbazidehydrochloride, and naphthoquinone-containing compounds, which specifically targeted the ATPase domain. Since **3c**, **3d** and **3f** may be effective as ATP competitors at the ATP binding site of the hTopoII α ATPase domain, these three compounds were synthesized and their in vitro cytotoxicity towards three cancer cell lines was then tested.

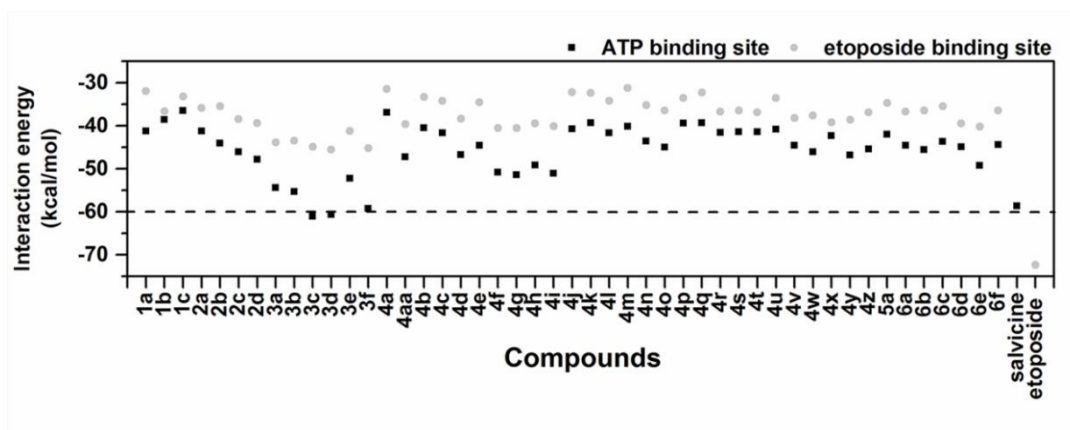


Figure 17. CDOCKER interaction energies (kcal/mol) of the designed chalcone derivatives binding at two different sites relative to the known hTopoII α inhibitors, salvicine and etoposide.

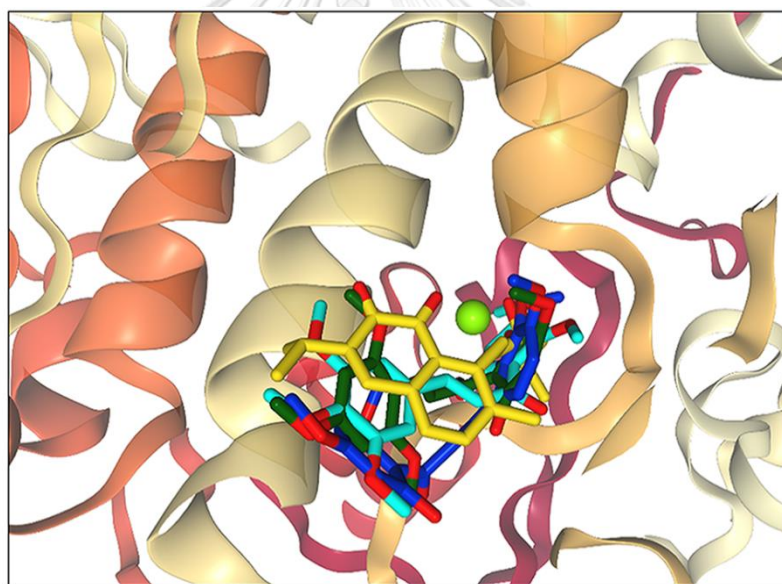
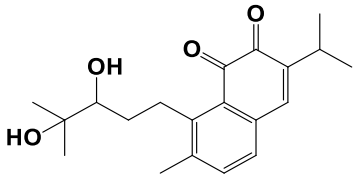
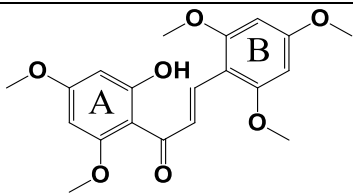
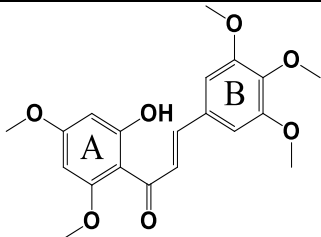
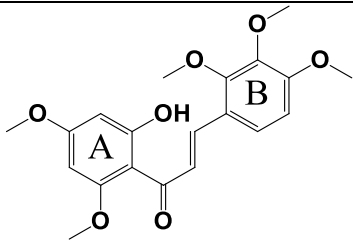


Figure 18. Superimposed structures of the three most active chalcones **3c** (green), **3d** (cyan) and **3f** (blue) from the docking study with that of salvicine in the ATP-binding pocket of the hTopoII α ATPase domain. Figure created by NGL viewer (<http://nglviewer.org/ngl/>).

Table 8 Contact residues of the hTopoII α ATPase domain for the binding of salvicine and three chalcones (**3c**, **3d** and **3f**). The residues in bold format stabilize the ligand binding via H-bond interaction, while the conserved residues between each chalcone and salvicine are shown in underlined format.

Compound	Structure	Contact residues
Salvicine		N91 , S148, S149, R162, G164, A167 and K168
3c		<u>N91</u> , R98, <u>G164</u> , G166 <u>A167</u> and <u>K168</u>
3d		<u>N91</u> , D94, T147, <u>S148</u> , <u>S149</u> , N150, <u>G164</u> , <u>G166</u> and <u>K168</u>
3f		<u>N91</u> , R98, <u>S148</u> , <u>S149</u> , N150, <u>G164</u> , <u>A167</u> and <u>K168</u>

4.2 Cytotoxicity towards cancer cell lines

After screening the potent chalcones for inhibition of hTopoII α by molecular docking, the three compounds that exhibited better interaction energies than salvicine (**3c**, **3d** and **3f**) were selected for synthesis to test their cytotoxicity on the HT-1376, HeLa and MCF-7 cancer-derived cell lines using the MTT assay. The derived IC₅₀ values of the three chalcone derivatives and salvicine on the three cancer cell lines are

summarized in Table 9. All three screened chalcones showed a higher cytotoxicity to all three cell lines than salvicine, with **3d** being the most cytotoxic with an IC₅₀ value of 10.8 ± 1.1 , 3.2 ± 2.2 and 21.1 ± 6.3 μM against the HT-1376, HeLa and MCF-7 cell lines, respectively. The IC₅₀ of salvicine in a lung cancer cell line (A549) was previously reported to be 18.66 μM [218]. The diversity of the cytotoxicity of these three chalcones could suggest that the position of the methoxy group on the B ring of the chalcones affected the cytotoxicity. The methoxy groups substituted at the R₂, R₃ and R₄ positions were found to be most important in terms of anti-cancer activities. Moreover, the different IC₅₀ values of the chalcone derivatives in each cancer cell line may reflect the different expression levels of hTopoII α and proliferation rates between those cell lines [219-222]. Cells containing a high concentration of hTopoII α are more sensitive to hTopoII α -inhibiting drugs than cells containing a lower concentration of hTopoII α . Thus, these chalcones might inhibit HeLa cells better than MCF-7 and HT-1376 cells because of the higher hTopoII α levels typically expressed in cervical cancer cells than in breast and urinary bladder cancer cells [223]. Considering the data from the *in silico* molecular docking and the *in vitro* cytotoxicity against cancer cell lines, it is possible that **3d** tends to inhibit the hTopoII α ATPase domain in a somewhat similar manner as salvicine. However, to gain additional information about the inhibition of hTopoII α at the ATPase domain by salvicine and **3d**, their *in vitro* inhibitory activity against the ATPase activity of rhTopoII α was evaluated.

Table 9. *In vitro* IC₅₀ values of the three chalcone compounds and salvicine against the HT-1376, HeLa and MCF-7 cancer-derived cell lines and the *rhTopoII α* ATPase domain.

Compound	IC ₅₀ value (μ M) against:			IC ₅₀ against <i>rhTopoIIα</i> ATPase domain (nM)
	HT-1376	HeLa	MCF-7	
3c	46.1 \pm 4.2	30.9 \pm 1.3	38.6 \pm 1.4	N/T
3d	10.8 \pm 1.1	3.2 \pm 2.2	21.1 \pm 6.3	7.5 \pm 4.2
3f	92.0 \pm 1.8	21.2 \pm 8.7	72.1 \pm 3.8	N/T
Salvicine	106.5 \pm 4.7	70.1 \pm 4.5	> 200	326.5 \pm 6.6

* *N/T*: non-tested

4.3 Inhibition of the hTopoII α ATPase domain

In order to assess the inhibition of ATPase activity by salvicine and **3d**, the *rhTopoII α* ATPase domain was expressed from the pET28b-expression vector and enriched by following a previously reported protocol [209] for use in the ATPase enzymatic activity assay. The *rhTopoII α* ATPase domain was enriched to apparent homogeneity, with the 45 kDa ATPase domain evident as a single band following SDS-PAGE resolution and Coomassie blue staining (Fig. 19A). The ATPase inhibitory activity of different concentrations of salvicine and **3d** was then comparatively studied using a commercial kit (ADP-Glo™ Kinase Assay, see also in material). The obtained IC₅₀ curves of salvicine and **3d** are shown in Fig. 19B and 19C, respectively, and listed in Table 9. The chalcone **3d** showed an ATPase inhibitory activity with an IC₅₀ value (7.5 nM) that was some 43.5-fold lower than that for salvicine (326.5 nM). To investigate the binding and interaction of **3d** against hTopoII α at the ATPase domain a detailed investigation of the **3d**/hTopoII α complex in aqueous solution was then performed *in silico* using MD simulations.

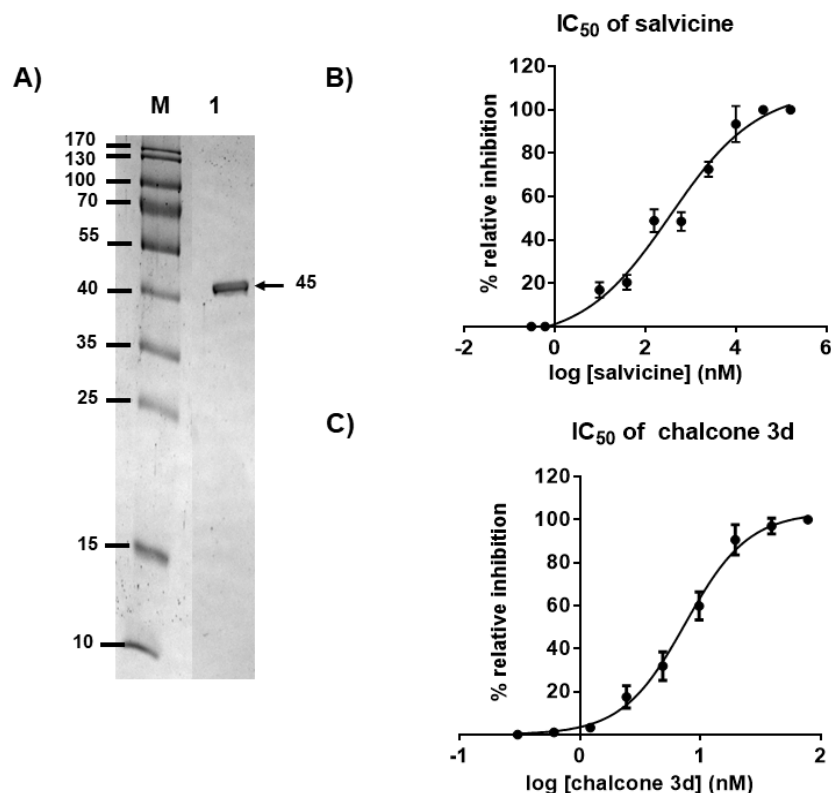


Figure 19. (A) SDS-PAGE gel analysis of the enriched rhTopoII α ATPase domain. Lane M: molecular weight marker of standard protein; Lane 1: enriched rhTopoII α ATPase domain (45 kDa). (B, C) The IC₅₀ curves of (B) salvicine and (C) 3d against the ATPase activity of rhTopoII α . Data are shown as the mean \pm 1 SD, derived from three independent experiments.

4.4 MD simulations

All-atom MD simulations were performed on the docked **3d**/hTopoII α complex with three different velocities for 80 ns to understand the structure and dynamics of **3d** at the ATP binding site of the hTopoII α ATPase domain. Since the **3d** binding patterns and interactions with hTopoII α obtained from three different simulations were similar, the results presented here are taken from one representative simulation. The root mean square displacement (RMSD) plot in Fig. A2 showed that the **3d**/hTopoII α complexes had reached equilibrium by 50 ns. Herein, the snapshots taken from the last 10-ns were extracted for analysis in terms of the binding pattern and ligand-protein interactions as follows.

In order to elucidate the hTopoII α ATPase residues important for **3d** inhibition at the ATP binding site, the per-residue decomposition free energy ($\Delta G_{\text{residue}}$) was

evaluated by the MM/PBSA approach using the 100 snapshots over the last 10-ns simulation. The results are given in Fig. 20A, where the binding orientation of **3d** inside the ATP-binding pocket with the contour energy of residue contribution is drawn in Fig. 20B. The fingerprint in Fig. 20A showed only residues 50–250 in chain A, while the rest of protein (chain A residues 29–49 and 251–405 plus all chain B residues) had no interaction with the ligand. The negative and positive $\Delta G_{\text{residue}}$ values represented the degrees of stabilization and destabilization for ligand binding, respectively.

From Fig. 21A, 10 residues preferentially stabilized **3d** with an energy contribution lower than -1.0 kcal/mol: E87, D94, R98, I125, I141, S148, S149, G164, Y165 and K168. This implies that these residues probably play a crucial role in **3d** binding to the ATPase domain. The free energy contributions of each key residue, decomposed to backbone and side chain as well as electrostatic ($E_{\text{ele}} + G_{\text{polar}}$) and vdW ($E_{\text{vdw}} + G_{\text{nonpolar}}$) terms, are plotted in Fig. 21. Most of the important residues support the **3d** binding via the vdW energy contribution, while E87, D94 and K168 residues likely presented the electrostatic contribution. The strongest energy stabilization for **3d** (-3.8 kcal/mol) came from the K168 residue. In contrast, it has been reported that the K168 was not interfere with salvicine binding and even destabilized some mansonone G compounds in the ATP binding pocket [186]. However, the observed binding patterns of **3d** in this work are somewhat similar with salvicine (E87, I125 and I141) and mansonone G (D94, I125, I141 and G164) in our previous work [186].

The results also demonstrated that the **3d** binding energy is mainly contributed from the side chains of the key residues (E87, D94, R98, I125, I141, S148, S149, G164, Y165 and K168), except for the S148, S149, G164 and Y165 residues where the ligand-protein interactions substantially come from their backbone contributions. The information was well supported by the formation of two strong H-bonds between the carbonyl group of **3d** and the backbone nitrogen of S149 (92%) as well as the 3-methoxy group on its A-ring and the backbone nitrogen of G164 (80%), (see intermolecular H-bonds between **3d** and hTopoII α residues in Fig. 22).

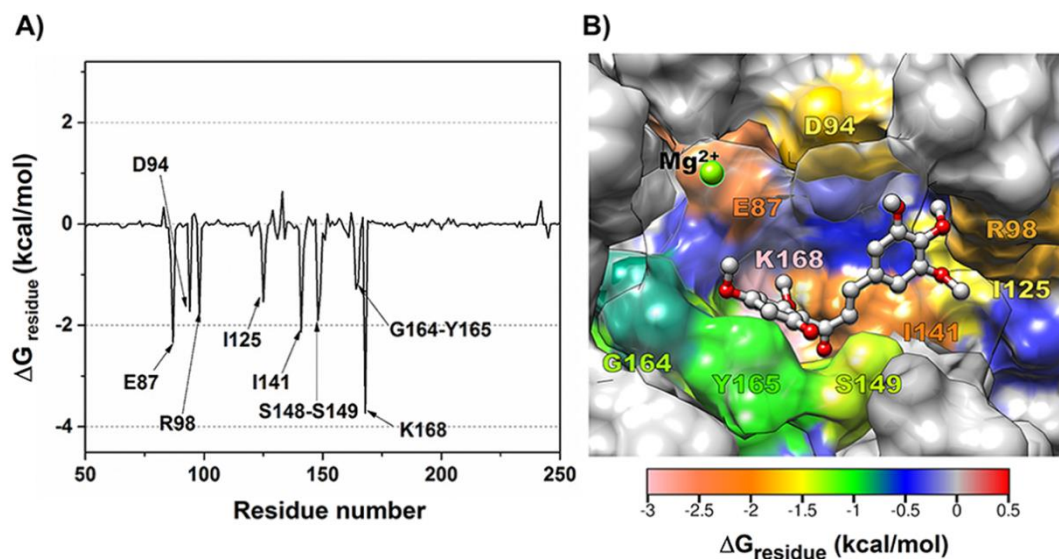


Figure 20. (A) Per-residue decomposition free energy of 3d/hTopoII α complex and (B) the binding orientation of 3d inside the ATP-binding pocket of ATPase domain, drawn from the last MD snapshot.

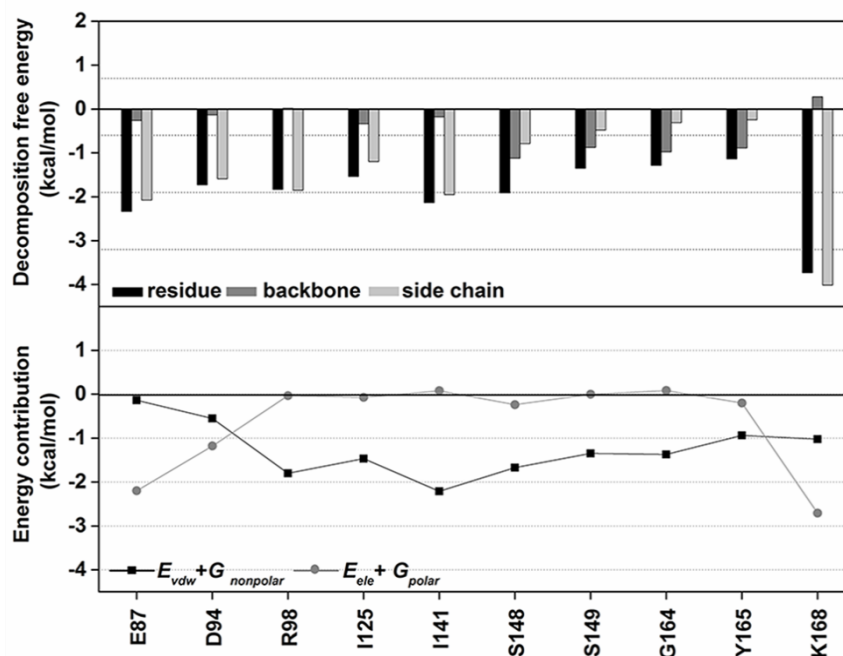


Figure 21. (Top) Per-residue decomposition free energy of the 10 key residues (black) and their contribution from backbone (dark grey) and side chain (light grey). (Bottom) The vdW ($E_{\text{vdW}} + G_{\text{nonpolar}}$) and electrostatic ($E_{\text{ele}} + G_{\text{polar}}$) energy contributions.

(Eele + Gpolar) energy contributions are given in black and grey lines, respectively.

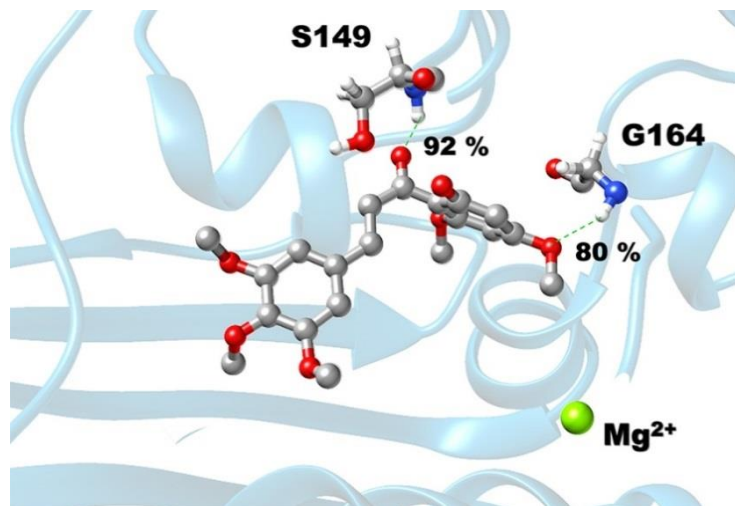


Figure 22. Hydrogen bond formation between chalcone **3d** and the two residues in the ATP binding pocket of hTopoII α ATPase domain, where the percentage of H-bond occupation is also given.

Part II Biological evaluation and molecular dynamics simulation of chalcone derivatives as EGFR-tyrosine kinase inhibitors

4.5 Cytotoxicity effect against A431 and A549 cell lines

The 47 synthesized chalcone compounds (1a-6e) from our previous study [41] and the approved anticancer drug (erlotinib) as EGFR-TK inhibitor were evaluated for anticancer activity against human epidermoid carcinoma (A431) and human lung adenocarcinoma (A549) cell lines using the (3-(4,5-dimethylthiazole-2-yl)-2,5-diphenyltetrazolium bromide) tetrazolium (MTT) assay. From the preliminary results, 100 μ M of all chalcone derivatives and erlotinib were tested. The percentage survival rate of two cancer cells is shown in Fig. 23. The results revealed that some chalcone derivatives exhibited promising cytotoxic effects against both cancer cells with a resulting cell viability of less than 50 % (red bar). The series of chalcone derivatives seem to inhibit A431 better than A549. The difference in inhibition of the chalcones in both cancer cell lines may reflect the different expression levels of EGFR [224, 225]. A431 has a high level of EGFR expression and is therefore more sensitive to EGFR-inhibiting agents than A549 which has a lower level of EGFR expression.

Moreover, the KRAS mutation found in A549 cell lines is able to alter the downstream signaling pathway of EGFR. Importantly, the KRAS mutation is linked to the primary resistance to target EGFR tyrosine kinase inhibitor [226]. Therefore, the inhibition of EGFR may not be able to completely inhibit the proliferation of cancer cell line. After preliminary screening, the 32 compounds that demonstrated a 50% reduction in cell viability were selected for evaluating the half maximal inhibitory concentration (IC_{50}) values. The derived IC_{50} values of the focused chalcones and erlotinib on two cancer cell lines are summarized in Table 10. All 32 chalcones showed moderate to good anticancer activity with IC_{50} in the range of 5.01–55.02 μ M against A431, whereas they displayed moderate to poor activity on A549 cell lines. The five compounds which exhibited the highest level of cytotoxicity were **4t**, **1c**, **2a**, **4e** and **3e** with IC_{50} values of 5.01 ± 3.48 , 8.04 ± 1.21 , 9.89 ± 4.91 , 10.02 ± 5.76 , 10.53 ± 7.39 μ M against A431 cell lines, respectively. The IC_{50} of erlotinib on A431 and A549 were 0.62 ± 0.11 and 18.82 ± 2.44 μ M. By considering the data from the in vitro screening of cytotoxicity against cancer cell lines, it is possible that chalcone derivatives tend to inhibit the high level of EGFR expression in A431. The obtained result was in good agreement with previous studies in which the cytotoxicity of Ec-LDP-hBD1 to EGFR highly expressed A431 cells was more potent than that to EGFR low-expressed human lung carcinoma A549 and H460 [129]. It is a worth noting that this series of chalcone show non-toxicity on human embryonic fibroblast cells (Fig. A3). However, to gain additional information about the inhibition of EGFR at the tyrosine kinase domain by the five potent chalcones, their in vitro inhibitory activity against the kinase activity of EGFR was evaluated and compare with erlotinib.

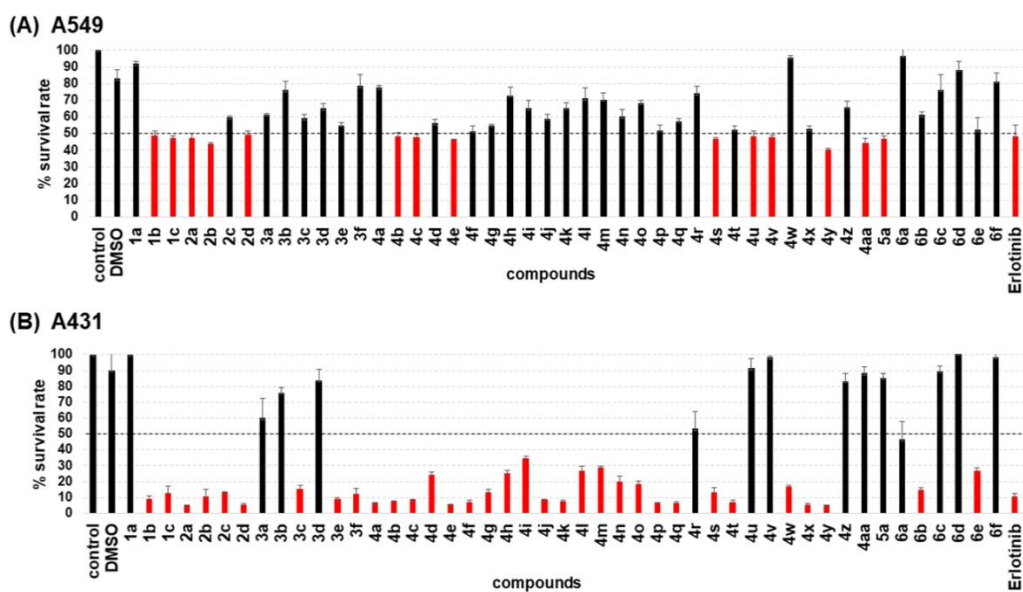


Figure 23. Percent survival rate of the 47 chalcones and erlotinib against (A) human lung adenocarcinoma cell lines (A549) and (B) human epidermoid carcinoma cell lines (A431)

Table 10. IC₅₀ values of potent chalcones against two cancer cell lines A431 and A549 compared to erlotinib

Compounds	IC ₅₀ (μM)	
	A431	A549
1b	33.98 ± 7.37	50.91 ± 3.83
1c	8.04 ± 1.21	25.44 ± 1.16
2a	9.89 ± 4.91	20.18 ± 1.89
2b	29.46 ± 3.50	69.35 ± 7.58
2c	24.61 ± 5.98	>100
2d	26.6 ± 6.89	25.44 ± 1.74
3c	20.67 ± 9.80	>100
3e	10.53 ± 7.39	>100
3f	18.92 ± 11.05	>100
4a	38.93 ± 5.20	>100
4b	25.04 ± 8.74	44.12 ± 9.40
4c	26.85 ± 5.48	20.18 ± 1.89

Compounds	IC ₅₀ (μM)	
	A431	A549
4d	25.13 ± 4.30	>100
4e	10.02 ± 5.76	44.12 ± 5.25
4f	38.8 ± 1.60	>100
4g	21.77 ± 5.32	>100
4h	48.76 ± 3.61	>100
4j	24.01 ± 2.56	>100
4k	14.93 ± 7.56	>100
4l	29.08 ± 4.06	>100
4m	55.02 ± 6.7	>100
4n	22.03 ± 5.25	>100
4o	21.73 ± 6.76	>100
4p	37.49 ± 4.00	>100
4q	25.94 ± 3.80	>100
4s	39.53 ± 7.39	25.44 ± 2.24
4t	5.01 ± 3.48	>100
4u	>100	>100
4v	>100	>100
4w	24.18 ± 4.89	>100
4x	41.53 ± 6.60	>100
4y	41.53 ± 2.04	49.42 ± 7.90
4aa	>100	74.40 ± 6.54
5a	>100	>100
6b	33.43 ± 3.09	>100
6e	39.99 ± 3.94	>100
Erlotinib	0.62 ± 0.11	18.82 ± 2.44

4.6 Inhibition of rEGFR tyrosine kinase activity by chalcones

In order to assess the inhibition of EGFR-TK activity by erlotinib the five potent chalcones (**1c**, **2a**, **3e**, **4e**, and **4t**), the EGFR-TK was expressed by mammalian

expression which retains fully kinase activity [210]. The *r*EGFR tyrosine kinase domain was enhanced to apparent homogeneity, with the 45 kDa kinase domain apparent as a main band following SDS-PAGE resolution and Coomassie blue staining (Fig. 24A). The kinase inhibitory activity of 1 μ M of the five potent chalcones and erlotinib was then comparatively studied using a commercial kit (ADP-Glo™ Kinase Assay, see also in material). Their obtained relative inhibition is plotted in Fig. 24B. The three chalcones **1c**, **2a** and **3e** showed a relative inhibition of EGFR-TK more than 50%, while the other two compounds **4e** and **4t** seem to be less affected to this enzyme. Interestingly, the chalcone **2a** being the most kinase inhibitory activity with a 76.20 % that was slightly higher than erlotinib (75.10 %). To investigate the detailed binding and interaction of these three potent chalcones **1c**, **2a** and **3e** against EGFR-TK domain, the ligand-protein complexes were then studied using MD simulations in aqueous solution.

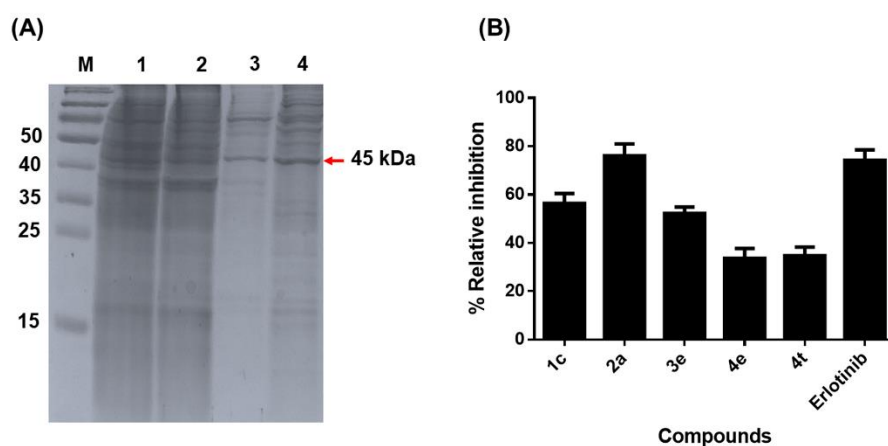


Figure 24. (A) Representative SDS-PAGE gel analysis of the enrichment of the EGFR-TK ICD, loading 5 μ g protein per track. Lane M: molecular weight marker of standard protein; Lane 1: supernatant, Lane 2: Flow through, Lane 3: 10% of buffer B, Lane 4: 45 kDa of EGFR-TK domain (B) The relative EGFR-TKI activity (%) of the five potent chalcone derivatives and erlotinib at 1 μ M, as assayed using the ADP-glo kinase assay.

4.7 Molecular binding and interaction of potent chalcones

The 500-ns MD simulations were performed in triplicate on each complex of the focused chalcones (**1c**, **2a** and **3e**) binding with EGFR-TK domain at the ATP binding site. Since the chalcone binding pattern and intermolecular interactions with EGFR-TK obtained from the three independent simulations were relatively similar, the results presented here are taken from one representative simulation. To find the key residues of EGFR-TK for chalcone binding, the per-residue decomposition free energy ($\Delta G_{\text{residue}}$) based on MM/GBSA method was applied on the 100 snapshots over the last 100-ns simulation. Among 695-1,018 residues of EGFR-TK, only the results of the residues 695-870 are plotted in Fig. 25A, where the ligand binding orientation inside the ATP-binding pocket of EGFR-TK with the contour energy of residue contribution is illustrated in Fig. 25B. Note that the negative and positive $\Delta G_{\text{residue}}$ values indicated the stabilization and destabilization energies for ligand binding, respectively. In addition, the number of the hydrogen bond profile of three chalcones was computed over the simulation period (see also, Fig. 26). From Fig. 25B, all potent chalcones **1c**, **2a** and **3e** shared a similar orientation in the EGFR-TK ATP binding site, in which the aryl moiety deeply inserted into and the carbonyl oxygen pointed toward the binding pocket in a correspondence to the computational study on the other chalcone analogs [227]. These three compounds were preferentially stabilized by the 7 residues with an energy contribution ≤ -0.5 kcal/mol (Fig. 25A): L718, V726, A743, L792, M793, G796, and L844. The residue T854 (-0.78 kcal/mol) additionally contributed for the **3e** binding in compensation with a destabilization by E762 (0.70 kcal/mol). This implies that these residues play a significant role in **1c**, **2a** and **3e** binding to the tyrosine kinase domain. Some chalcone binding residues observed in this work such as L718, A743, L792, M793, G796 and L844 are also found in a major interacting for co-crystallized erlotinib in 1M17 structure [228, 229]. Among the three considered chalcones, **2a** can form the strongest hydrogen bond interactions with enzyme target (as shown in Fig. 27). According to the results, there are three to four hydrogen bonds with the residues M793, T790 and T854 detected along the simulation time. The two hydrogen bonds formed with the hinge region residue M793 was also found in **1c** and **3e**. The obtained information could explain how importance of M793 which provided the relatively high stabilization for our

focused chalcones. This hydrogen bond formation with M793 was reported as a main interaction in erlotinib analogues and gefitinib in complex with wild type and mutant strains [230-232]. Ahmed M. *et al.*, also suggested that M793 plays a significant role in interacting with their screened compounds and erlotinib [233].

To identify the structural change of ATP binding pocket affected by a complexation with chalcones, the distance between the centers of mass of the two hydrophobic residues (L718 and G796, Fig. 27B) was calculated upon simulation time. The distance plot in Fig. 27 showed that in comparison to the apo system (~ 4.0 to ~ 14.0 Å) the three complexes resulted in a shorter distance and maintained at a lower fluctuation of ~ 7.0 to ~ 9.0 Å, indicating the induced-fitted mechanism in chalcone binding to EGFR-TK. This result was well supported by the lower water accessibility into the ATP binding site (Fig. 28) for all three complexes (1c: ~ 400 - 1200 Å²; 2a: ~ 800 - 1500 Å²; and 3e ~ 700 - 1500 Å²) relative to that of apo form (~ 1300 - 2000 Å²). Based on all above data, such three chalcones could be served as new candidates for anti-cancer drug development against EGFR.

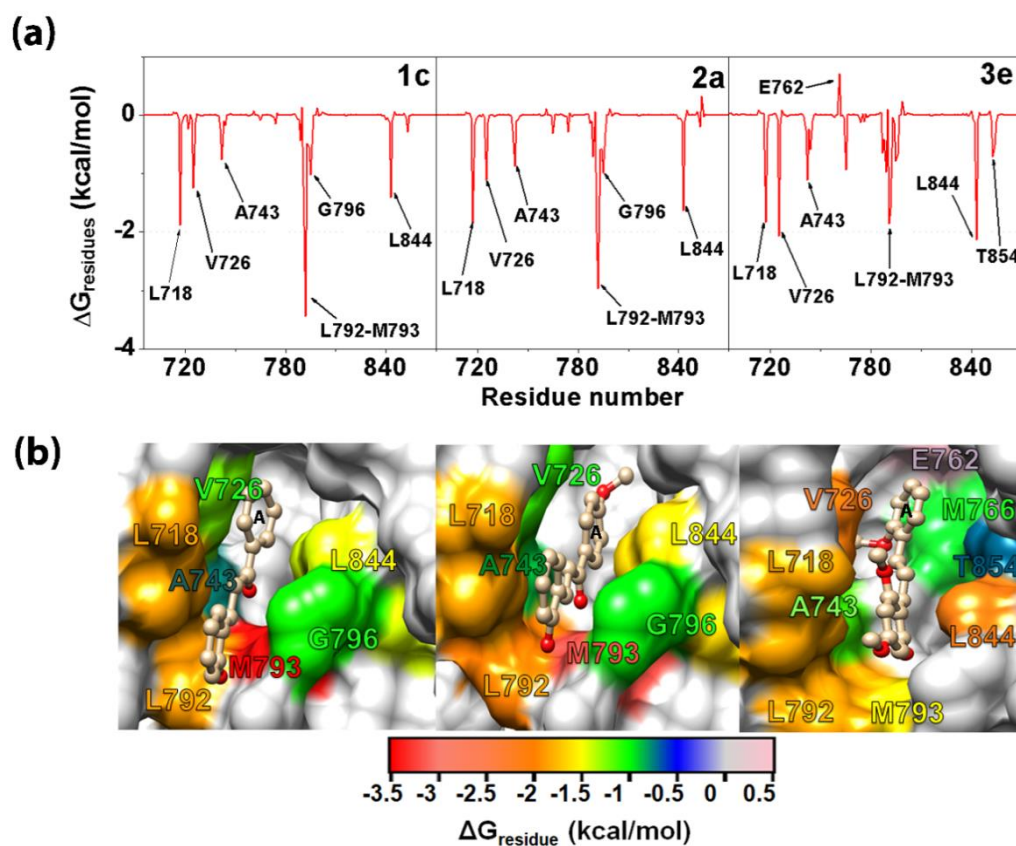


Figure 25. (A) Per-residue decomposition free energy of three chalcone/EGFR-TK complexes and (B) their binding orientation inside the ATP-binding pocket of tyrosine kinase domain drawn from the last MD snapshot, where the energy contour of residue contribution for ligand binding was shaded.

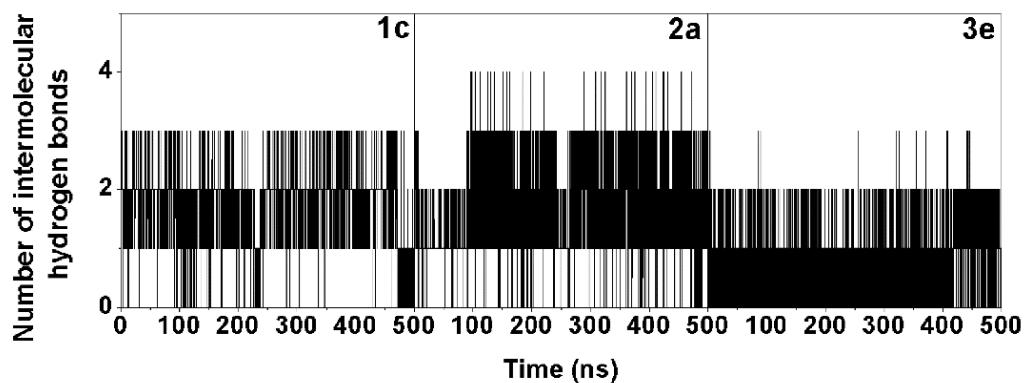


Figure 26. Time evolution of the number of intermolecular hydrogen bonds formed between the EGFR-TK residues and the three screened chalcones.

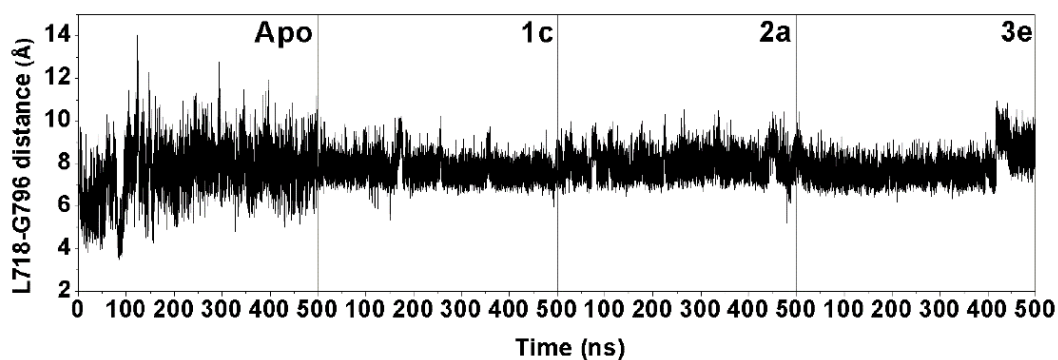


Figure 27. Time-dependent distance between the centers of mass of the residues L718 and G796 for apo and complex forms over the 500 ns of the trajectory.

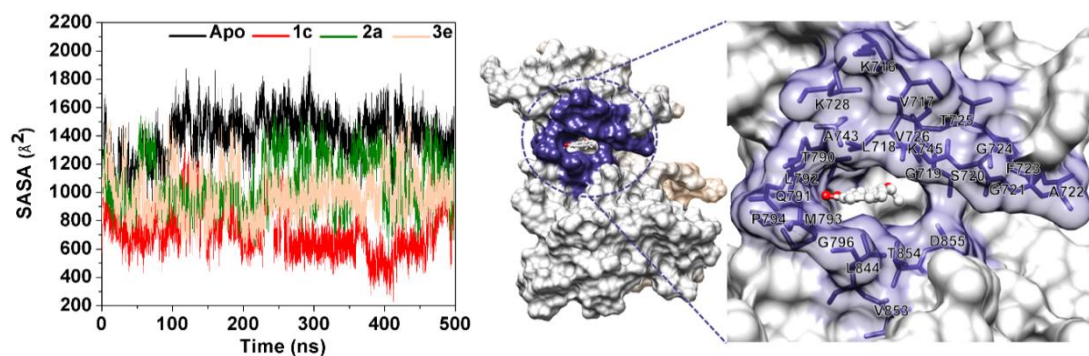


Figure 28. Solvent-accessible surface area (SASA, Å²) of apo form and three chalcones complexes along the 500-ns simulation where the amino acids within a 7-Å sphere of chalcone used for SASA calculations are also shown in the right-hand side.

Part III Quantitative structure–activity relationship and ADMET

4.8 Quantitative structure–activity predicted for skin cancer cell lines

Classical 2D-QSAR studies require the calculation of molecular descriptors and the construction of mathematical models. In this study, the physicochemical properties related to anticancer activity were calculated from Material studio program. The model was computed by multiple linear regression analysis using stepwise procedure. In order to access the predictive ability, the compounds were classified into two groups (i) training set (90 %) and (ii) test set (10 %). The 9 parameters from Material studio were calculated show in table 11. The correlation matrix of activity and all properties based on the correlation coefficients it shows that all properties did not complete significantly. Therefore, all properties were used to fit the equation (see also, table 12). For the $-\log\text{IC}_{50}$ (pIC_{50}), three parameters (LUMO, AlogP and number of hydrogen bond acceptor) were presented in the model I as shown in the table 13 with the r^2 of 0.664. This model has r^2 lower than 0.8, hence it is not an acceptable model. The developing model was done by deleting one outlier (**4m**). After removing the outlier, model II with improved $r^2 = 0.75$ was founded. However, this is also model has not acceptable as seen from the statistic values. After three outliers (**4m**, **2d**, **3e**) were deleted, the model IV (fig. 29) was observed with a good QSAR value of $r^2 = 0.937$. The equation of model IV is as follows;

$$Y = - 0.026 * \text{Hydrogen bond acceptor} - 0.105 * \text{AlogP} + 0.018 * (\text{Hydrogen bond acceptor} * \text{AlogP}) + 4.842$$

A residual value of training and test set obtained from Equation (IV) for A431 cancer cell lines are shown in the table 14. It can be seen that the experimental and the predicted pIC_{50} values show the lowest residual. It indicated that compound in the training set is not an outlier for the response fitting.

Table 11. Calculated properties of chalcone derivatives using the Material studio software.

Comp.	pIC₅₀	HOMO	LUMO	Rotatable bonds	H-bond donor	H-bond acceptor	AlogP	AlogP98	MR	MF
2b	4.530	-8.919	-0.651	6.000	1.000	3.000	4.252	2.494	76.169	6.114
2c	4.610	-8.825	-0.608	5.000	0.000	3.000	3.295	4.970	79.879	4.821
2d	4.580	-9.090	-0.622	6.000	0.000	2.000	6.801	4.897	92.674	6.763
3c	4.680	-8.906	-0.717	10.000	1.000	7.000	1.315	-1.004	101.044	9.411
3e	4.980	-8.760	-0.335	8.000	1.000	5.000	2.940	0.894	88.388	7.757
3f	4.720	-8.824	-0.528	10.000	1.000	7.000	1.959	-0.222	100.613	9.411
4a	4.410	-9.192	-0.901	5.000	1.000	2.000	5.077	3.328	69.651	5.299
4b	4.600	-9.136	-0.933	6.000	1.000	3.000	4.369	2.567	75.994	6.114
4c	4.570	-8.935	-0.867	5.000	1.000	3.000	3.263	5.394	75.109	4.233
4d	4.600	-8.739	-0.752	7.000	1.000	4.000	3.535	1.615	82.371	6.934
4g	4.660	-9.196	-1.037	8.000	1.000	5.000	3.316	1.383	88.296	7.757
4j	4.620	-9.217	-0.991	5.000	2.000	3.000	3.232	5.819	70.340	3.671
4l	4.540	-9.027	-0.899	6.000	2.000	3.000	4.019	2.091	71.320	5.460
4m	4.259	-9.214	-0.983	5.000	2.000	3.000	3.232	5.169	70.340	3.671

Comp.	pIC ₅₀	HOMO	LUMO	Rotatable bonds	H-bond donor	H-bond acceptor	AlogP	AlogP98	MR	MF
4n	4.660	-9.160	-0.805	7.000	2.000	4.000	3.356	1.336	77.564	6.272
4o	4.660	-8.752	-0.943	6.000	2.000	4.000	2.979	4.673	76.804	4.423
4w	4.620	-8.210	-0.697	3.000	2.000	2.000	2.793	4.719	72.737	4.454
4x	4.380	-9.152	-0.898	6.000	1.000	2.000	5.804	4.036	78.800	6.154
4y	4.380	-9.139	-0.887	7.000	1.000	2.000	6.530	4.744	87.950	7.014

*** RT: Rotatable bonds, MR; Molecular refractivity, MF: Molecular flexibility



Table 12. Correlation matrix of anticancer activity against A431 for 9 properties. High correlations ($\geq \pm 0.8$) are labelled in gray cells.

	pIC ₅₀	HOMO	LUMO	Rotatable e bonds	H-bond donor	H-bond acceptor	AlogP	AlogP98	MR	MF
pIC ₅₀	1.000									
HOMO	0.439	1.000								
LUMO	0.612	0.533	1.000							
Rotatable bonds	0.438	-0.137	0.317	1.000						
H-donor	-0.090	0.072	-0.442	-0.227	1.000					
H-acceptor	0.609	0.141	0.335	0.857	-0.006	1.000				
AlogP	-0.524	-0.434	-0.191	-0.315	-0.351	-0.747	1.000			
AlogP98	-0.509	-0.075	-0.376	-0.832	0.066	-0.802	0.453	1.000		
MR	0.438	0.095	0.511	0.845	-0.513	0.688	-0.157	-0.601	1.000	
MF	0.430	0.017	0.465	0.910	-0.411	0.701	-0.136	-0.842	0.896	1.000

*** RT: Rotatable bonds, MR; Molecular refractivity, MF: Molecular flexibility

Table 13. Regression Statistic for the QSAR Models I-IV

Model	MLR equation	R	R ²	F
Model I	$Y = 0.087 * (\text{LUMO} * \text{AlogP}) - 0.024 * (\text{Hydrogen bond acceptor} * \text{AlogP}) + 4.560$	0.815	0.664	15.845
Model II	$Y = 0.312 * \text{LUMO} - 0.061 * \text{AlogP} + 0.018 * (\text{Hydrogen bonds acceptor} * \text{AlogP}) + 4.856$	0.867	0.752	14.159
Model III	$Y = - 0.126 * \text{AlogP} + 0.067 * (\text{LUMO} * \text{Hydrogen bond acceptor}) + 0.032 * (\text{Hydrogen bond acceptor} * \text{AlogP}) + 4.862$	0.92	0.84	24.465
Model IV	$Y = - 0.026 * \text{Hydrogen bond acceptor} - 0.105 * \text{AlogP} + 0.018 * (\text{Hydrogen bond acceptor} * \text{AlogP}) + 4.842$	0.968	0.937	60.145

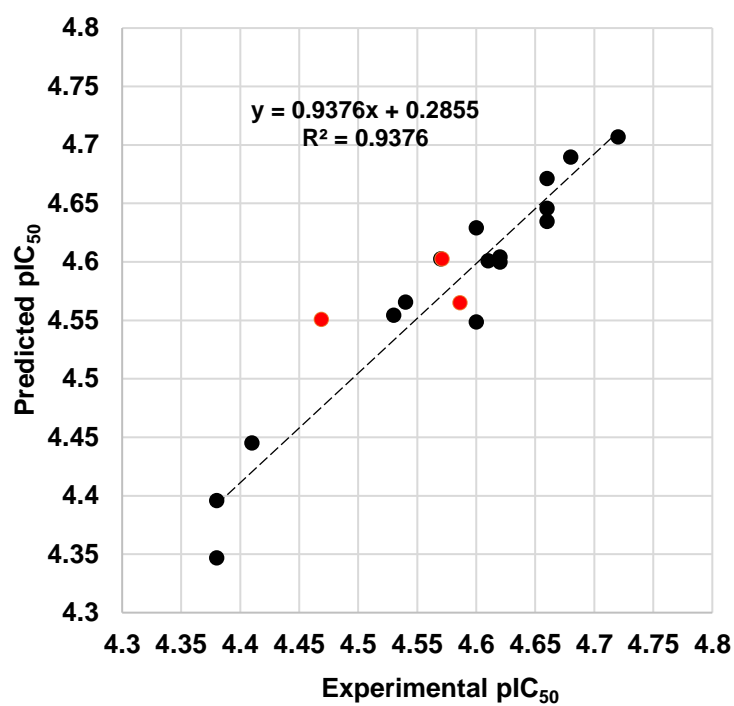


Figure 29. Plot of multiple linear regression analysis which indicates linear relationship between experimental and predicted logIC₅₀ with $r^2 = 0.93$ for human skin cancer cell lines.

Table 14. Residual values of training and test set obtained from Equation (IV) for A431 cancer cell lines.

Training set			
Structures	Exp. pIC₅₀	Pred. pIC₅₀	residual
2b	4.530	4.554	-0.024
2c	4.610	4.600	0.009
2d	4.580	outlier	
3c	4.680	4.689	-0.009
3e	4.980	outlier	
3f	4.720	4.706	0.013
4a	4.410	4.445	-0.035
4b	4.600	4.548	0.051
4c	4.570	4.602	-0.032
4d	4.600	4.629	-0.029
4g	4.660	4.671	-0.011
4j	4.620	4.604	0.016
4l	4.540	4.565	-0.025
4m	4.359	outlier	
4n	4.660	4.634	0.025
4o	4.660	4.645	0.014
4w	4.620	4.599	0.020
4x	4.380	4.395	-0.015
4y	4.380	4.346	0.033
Test set			
4q	4.586	4.564	0.021
4c	4.571	4.602	-0.031
1b	4.468	4.550	-0.081

4.9 Physicochemical properties of potent chalcones

The physicochemical and pharmacokinetic properties as well as the toxicity of the six focused chalcones were investigated by ADMET prediction (Absorption, distribution, metabolism, excretion, and toxicity) using the online SwissADME web program (www.swissadme.ch/) [50] Molinspiration cheminformatics (<http://www.molinspiration.com/>) web program [51] and Osiris prediction tool on DataWarrior program [52]. Their toxicity risk (mutagenicity, tumorigenicity, irritation and reproduction), physicochemical (molecular weight, cLogP, total polar surface area, solubility), drug likeness and pharmacokinetic (GI absorption, BBB permeant, P-gp substrate and Cytochrome P450 inhibitor) properties are summarized in Table 15 and 16. From toxicity prediction, all investigated compounds had no risk of mutagenicity, tumorigenicity, irritating effects and reproductive effects. For the physicochemical properties, they showed a moderate solubility, while erlotinib was poorly soluble. Thus, erlotinib requires high doses in order to reach therapeutic plasma concentrations after oral administration. The pharmacokinetic profiles suggested that all compounds can pass through the blood brain barrier except **3c**, **3d** and **3f**. By considering the drug likeness, the six potent chalcones could likely be used as an orally active drug for human in near future

Table 15. Toxicity, ADME, drug likeness and pharmacokinetics of three potent chalcones and salvicine against Topoisomerase II.

		3c	3d	3f	salvicine
Toxicity risks	Mutation ^a	+++	+++	+++	+++
	Tumor ^a	+++	+++	+++	+++
	irritant ^a	+++	+++	+++	+++
	Reproduction effective ^a	+++	+++	+++	+++
Physicochemical properties	Molecular weight (g/mol) ^b	374.38	374.38	374.38	330.42
	cLOGP ^b	3.10	3.10	3.10	2.97
	TPSA (Å ²) ^b	83.45	83.45	83.45	74.60
	Solubility class ^c	Moderately soluble	Moderately soluble	Moderately soluble	Moderately soluble
Drug likeness	Lipinski's rule of five ^c	Yes	Yes	Yes	Yes
	Ghose ^c	Yes	Yes	Yes	Yes
	Veber ^c	Yes	Yes	Yes	Yes
	Egan ^c	Yes	Yes	Yes	Yes
	Muegge ^c	Yes	Yes	Yes	Yes
Pharmacokinetic	Gastro Intestinal absorption (%) ^c	High	High	High	High
	Blood-brain barrier permeant ^c	No	No	No	Yes
	P-gp substrate ^c	No	No	No	No
	CYP1A2	No	No	No	No

	3c	3d	3f	salvicine
inhibitor ^c				
CYP2C19 inhibitor ^c	No	No	No	Yes
CYP2C9 inhibitor ^c	Yes	Yes	Yes	No
CYP2D6 inhibitor ^c	No	No	No	No
CYP3A4 inhibitor ^c	Yes	Yes	Yes	No

^aPredicted properties taken from Osiris on Dataworrier program; +++, not toxic; ++ low toxic; - high toxic. ^bPredicted properties taken from Molinspiration cheminformatics. ^cDrug likeness and pharmacokinetic obtained from SwissADME.



Table 16. Toxicity, ADME, drug likeness and pharmacokinetics of three potent chalcones and erlotinib against EGFR.

		1c	2a	3e	Erlotinib
Toxicity risks	Mutation ^a	+++	+++	+++	+++
	Tumor ^a	+++	+++	+++	+++
	irritant ^a	+++	+++	+++	+++
	Reproduction effective ^a	+++	+++	+++	+++
Physicochemical properties	Molecular weight (g/mol) ^b	224.25	254.28	314.33	393.44
	cLOGP ^b	2.96	2.88	2.75	2.79
	TPSA (Å ²) ^b	37.30	46.53	65.00	74.73
	Solubility class ^c	Moderately soluble	Moderately soluble	Moderately soluble	Poorly soluble
Drug likeness	Lipinski's rule of five ^c	Yes	Yes	Yes	Yes
	Ghose ^c	Yes	Yes	Yes	Yes
	Veber ^c	Yes	Yes	Yes	Yes
	Egan ^c	Yes	Yes	Yes	Yes
	Muegge ^c	Yes	Yes	Yes	Yes
Pharmacokinetic	Gastro Intestinal absorption (%) ^c	High	High	High	High
	Blood-brain barrier permeant ^c	Yes	Yes	Yes	Yes
	P-gp substrate ^c	No	No	No	No
	CYP1A2	No	Yes	Yes	Yes

	1c	2a	3e	Erlotinib
inhibitor ^c				
CYP2C19 inhibitor ^c	Yes	Yes	Yes	Yes
CYP2C9 inhibitor ^c	Yes	Yes	Yes	Yes
CYP2D6 inhibitor ^c	No	No	No	Yes
CYP3A4 inhibitor ^c	No	Yes	Yes	Yes

^aPredicted properties taken from Osiris on Dataworrier program; +++, not toxic; ++ low toxic; - high toxic. ^bPredicted properties taken from Molinspiration cheminformatics. ^cDrug likeness and pharmacokinetic obtained from SwissADME.



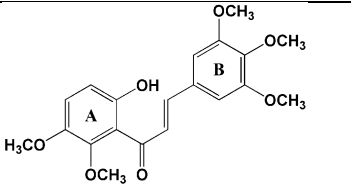
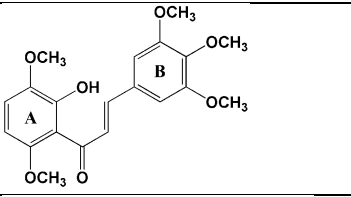
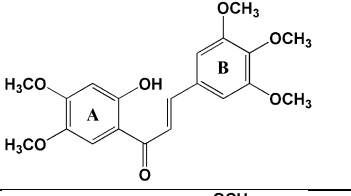
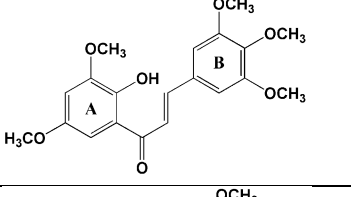
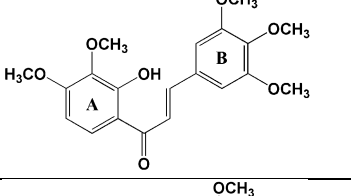
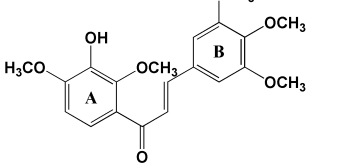
Part IV Design new compounds for topoisomerase II α and EGFR-TK inhibitor

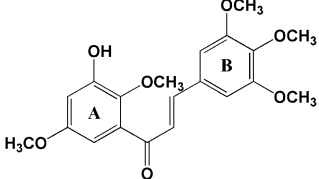
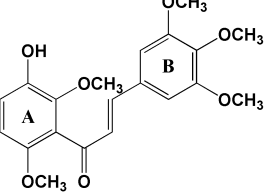
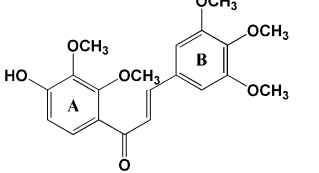
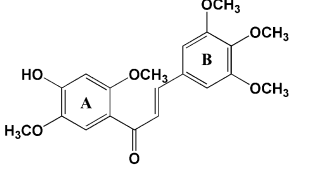
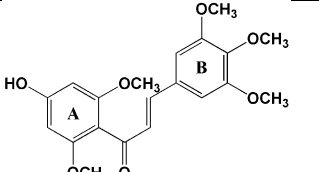
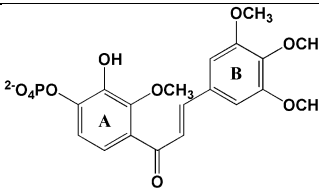

4.10 Topoisomerase

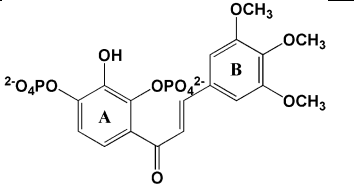
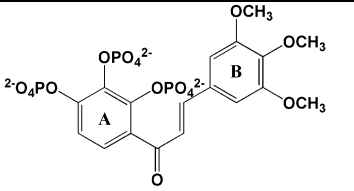
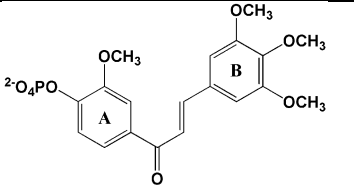
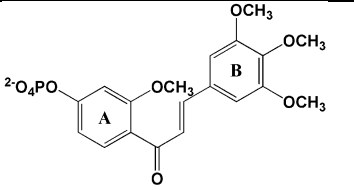
4.10.1 Design the new compound for topoisomerase II α inhibitors

The idea of biostructure-based drug design is to utilize the information from the properties of the binding site of the target and the binding pattern of the ligand inside the binding pocket from the MD simulation to design compounds. Based on the binding pattern and their interaction of **3d** into ATPase binding site of topoisomerase II, the 16 new analogs of chalcone were designed. Firstly, the compound 1 to 11 were changed position of substituted functional group on A ring and then docking into ATPase binding site (Table. 17). From the all compounds, compound 6 exhibited the lowest interaction energy with -62.65 kcal/mol and show good result in drug likeness criteria. Then, the compound 6 was used as a template to design the compound 12 to 16 by change the functional group on the position 4, 5 and 6 of A ring while the position of substitute on B ring are remained. As the binding pattern from Docking and MD results, most of the interactions inside binding pocket are the positive charges, so then, the negative charge functional group should be design on the compounds. Compound 12, the phosphate group is added to the position 4 on A ring instead the methoxy group. It makes the strong interaction energy (-99.88) than compound 6 (-62.65) almost two times. Although, this compound showed the strong interaction with this protein but in term of drug-likeness is not pass the criteria of Veber, Egan and Muegge. After that, the compound 13 and 14 were designed by adding the 2 and 3 phosphates groups, respectively. It was found that they give the lowest interaction energy (-121.72 and -126.79) but they could not be a drug due to the higher of polarity. To reduce the polarity of the molecule the compound 15 and 16 were designed and observed the interaction energy and the drug likeness properties. Compound 16 exhibited a good both in term of interaction energy and drug likeness.

Table 17. Design of new compounds from **3d** scaffold with CDOCKER interaction energy (kcal/mol) inhibit topoisomerase II α .

Comp.	Structure	CDOCKER interaction energy (kcal/mol)	Drug likeness
1		-58.47	Yes
2		-60.45	Yes
3		-58.74	Yes
4		-60.87	Yes
5		-60.38	Yes
6		-62.65	Yes

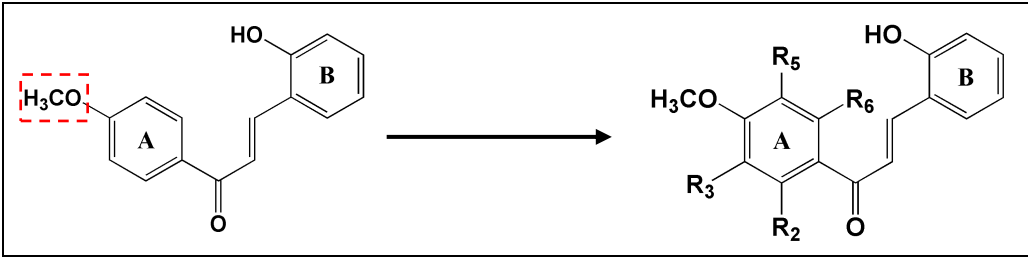
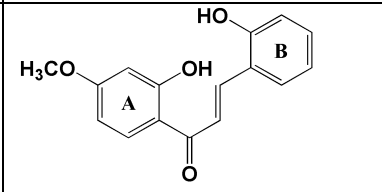
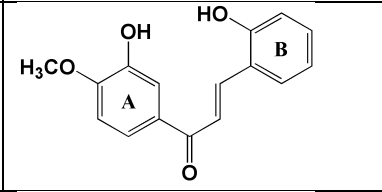
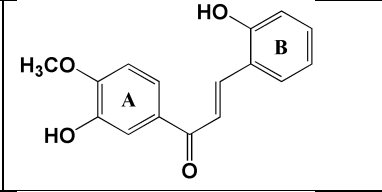
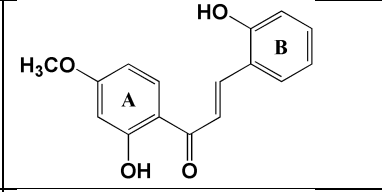
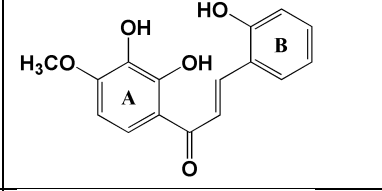
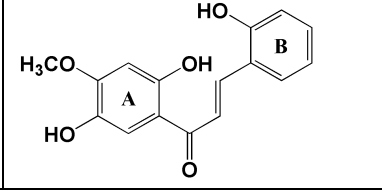
Comp.	Structure	CDOCKER interaction energy (kcal/mol)	Drug likeness
7		-60.32	Yes
8		-59.48	Yes
9		-62.23	Yes
10		-60.12	Yes
11		-60.48	Yes
12		-99.88	No
			

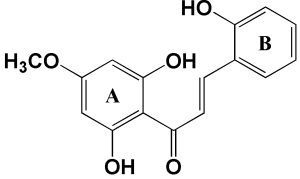
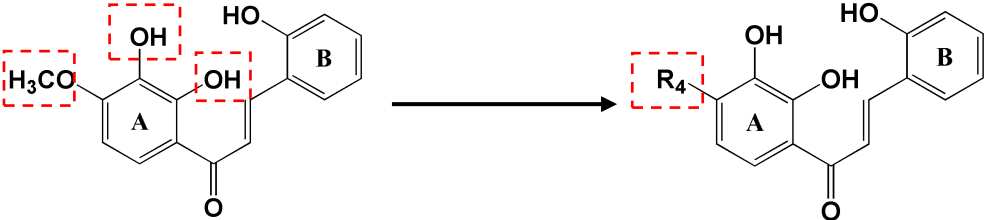
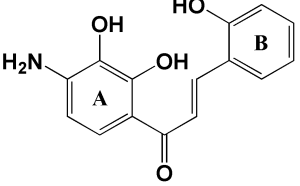
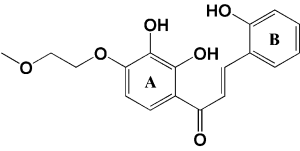
Comp.	Structure	CDOCKER interaction energy (kcal/mol)	Drug likeness
13		-121.72	No
14		-126.79	No
15		-92.84	Yes
16		-97.36	Yes

4.11 Design the new compound for EGFR-TK inhibitors

To develop new therapeutic candidates from the compound **2a**, which is a potent chalcone showing highest inhibition in EGFR-TK, 9 chalcones analog of **2a** were designed (Table. 18). Based on the MD simulation results, the most important amino acid residues that interact with **2a** were non-polar groups, so then we could afford some suggestions on the structural modification of the new designed compounds to enhance the activities. Firstly, it should contain polar substituents at the A ring. The mono-hydroxy group was added to each position on A ring. (compounds 1 to 4). The addition of a hydroxy group on the A ring influences the binding of ligand inside the pocket, it was observed that the interaction energy of compound 1 to 4 is lower than **2a** (-37.20 kcal/mol). Then, the dihydroxy groups were investigated with regard to their interaction energy (compound 5-7). We found that compound 5 showed the lowest interaction energy with substitution of OH groups at 5 and 6 position on the A ring. After that, compound 5 was used as a template to design compounds 8 and 9 by changing the functional groups on the positions 5 and 6 of the A ring while the position of substitution on the B ring remained. NH₂ was substituted at position 4 on the A ring instead of OCH₃. It was found that NH₂ has an effect on ligand binding as documented of the higher interaction energy (-39.48 kcal/mol). The aliphatic chain on erlotinib was used to modify our molecule (compound 9) by substituting that chain at position 4. This substituent affects the ligand binding, it makes the ligand fit well into the binding pocket with an interaction energy of -49.36 kcal/mol.

Table 18. Design of the new compounds from **2a** scaffold with CDOCKER interaction energy (kcal/mol) inhibiting EGFR-TK.

Comp.	Structure	CDOCKER interaction energy (kcal/mol)	Predicted pIC ₅₀ from QSAR	Drug likeness
				
1		-40.01	4.668	Yes
2		-41.37	4.659	Yes
3		-41.21	4.645	Yes
4		-41.43	4.703	Yes
5		-42.04	4.700	Yes
6		-38.30	4.705	Yes

7		-41.49	4.777	Yes
				
8		-39.48	4.763	Yes
9		-49.36	4.732	Yes

CHAPTER V

CONCLUSION

5.1 Computational screening of chalcones acting against topoisomerase II α and their cytotoxicity towards cancer cell lines

A series of 47 designed chalcones were screened *in silico* as potent anti-cancer agents by computational methods. Molecular docking of the chalcone derivatives relative to salvicine, a known inhibitor of hTopoII at the ATPase domain, suggested that the ATP-binding site of hTopoII α ATPase domain serves as the target site for the considered chalcones. The three most active chalcones (**3c**, **3d** and **3f**) had interaction energies towards the ATPase domain that were stronger than that of salvicine. Compound **3d**, containing 2,4-dimethoxy and 6-hydroxy groups on A ring and 3',4',5'-trimethoxy on the B ring, showed the highest *in vitro* cytotoxicity against the HT-1376, HeLa and MCF-7 cancer cell lines. Moreover, **3d** inhibited the *rh*TopoII α ATPase activity *in vitro* with an IC₅₀ value some 43.5-fold lower than that for salvicine. From 80-ns MD simulations of the **3d**/hTopoII α complex, the key residues responsible for **3d** binding via vdW and electrostatic interactions were E87, D94, R98, I125, I141, S148, S149, G164, Y165 and K168. The residue K168 exhibited the strongest energy stabilization for **3d**, while residues S149 and G164 formed two strong H-bond interactions with the carbonyl and 3-methoxy groups of **3d**. In summary, the *in silico* and *in vitro* results suggested that **3d** can serve as a lead compound for further anti-cancer drug development.

5.2 Biological evaluation and molecular dynamics simulation of chalcone derivatives as EGFR-tyrosine kinase inhibitors

A series of the 47 synthesized chalcones were *in vitro* tested for the cytotoxicity by MTT assay with the A431 and A549 cancer cell lines compared with erlotinib, a known inhibitor of EGFR-TK. All chalcones seemed to be more active to A431 over A549 cancer cells. The five most active chalcones (**1c**, **2a**, **3e**, **4e** and **4t**) showed the highest *in vitro* cytotoxicity against the A431 cancer cell lines. Among these five chalcones, the **1c**, **2a** and **3e** inhibited the tyrosine kinase activity more than 50%. Then, the three chalcone derivatives in complex with EGFR-TK were selected to study the inhibition mechanism in molecular level by all-atom MD simulations in

aqueous solution. From MD results, it was found that the key residues responsible for chalcone binding are L718, V276, A743, L972, M973, G976, and L844 while **3e** was additionally stabilized by T854 in compensation of the E762 destabilization. The hinge region residue M793 exhibited the strongest energy stabilization through hydrogen bonding as found for the other known EGFR-TK inhibitors. In summary, the *in silico* and *in vitro* results suggested that three chalcone derivatives (**1c**, **2a** and **3e**) can be served as lead compounds for further anti-cancer drug development.

5.3 QSAR model

The quantitative structure-activity relationships of chalcone derivatives were investigated by 2D-QSAR. The inhibition concentration (IC_{50}) of a series synthesized chalcones against A431 cancer cell lines were used. The M06-2X/6-31G (d,p) method in Gaussian09 program was justified to be a suitable method for structural optimization. In comparison among all models, model IV produced a statistically coherent model with a good predictive value $r^2 = 0.968$. An analysis of QSAR indicated that the AlogP the chalcone structure plays an important role for the A431 activity. Compounds that shows a low value of AlogP, the IC_{50} values are high. In addition, the H-bond acceptor number resulted in a negative coefficient at the same time it participant in a positive coefficient of the combined two properties. Therefore, the appropriate number of hydrogen bond acceptor should be 3 to 5. In order to improve a better QSAR model, more chalcone compounds with anticancer activity are needed. Moreover, the biological activity should be displayed in a good distribution because the data analysis works better when the biological activity shows good distribution. The compounds should have a broad activity range.

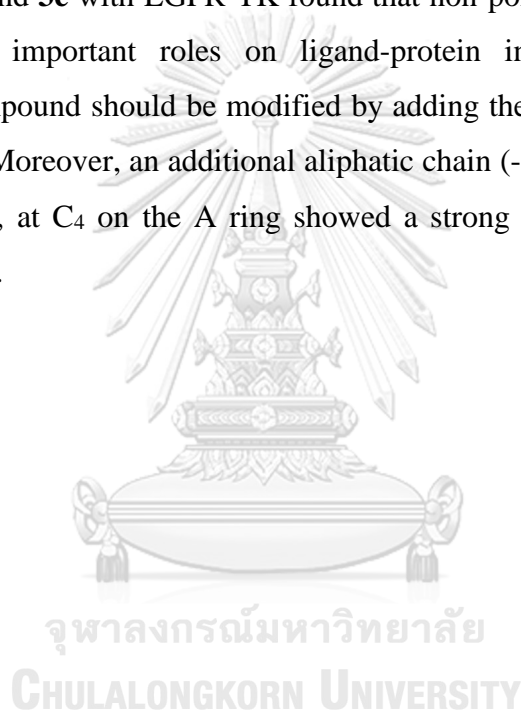
5.4 Physic properties of potent chalcones

In silico ADMET evaluation was perform on six potent chalcone derivatives that inhibit topoisomerase $II\alpha$ and EGFR-TK in comparison to known standards. The results showed that all compounds presented a good profile for pharmacokinetic and low toxicity risk. In this way, it is expected that these compounds may be proper lead candidates for development of anticancer drugs.

5.5 Design of the new compounds

Using the information obtained from all investigations in this study, we could suggest on the structural modifications of chalcone derivatives to enhance the biological activities to inhibit topoisomerase II α and EGFR-TK as follows.

For Topoisomerase II α , the inhibitors should contain negative or charged substituents such as phosphate at the C₄ on the A ring to improve the strong interaction between ligand and protein because the key amino acid residues that play an important role to bind with **3d** have positive charges. The investigation on binding pattern of **1c**, **2a** and **3e** with EGFR-TK found that non-polar amino acid residues are crucially playing important roles on ligand-protein interaction. Therefore, the designed new compound should be modified by adding the polar group at the C₅ and C₆ on the A ring. Moreover, an additional aliphatic chain (-OCH₂CH₂OCH₃), which is a part of erlotinib, at C₄ on the A ring showed a strong binding affinity of ligand-protein interaction.



REFERENCES

1. Australia, C.C., Understanding Complementary Therapies. Cancer Council Australia.
2. Mortality, G.B.D. and C. Causes of Death, Global, regional, and national life expectancy, all-cause mortality, and cause-specific mortality for 249 causes of death, 1980-2015: a systematic analysis for the Global Burden of Disease Study 2015. *Lancet* (London, England), 2016. **388**(10053): p. 1459-1544.
3. Organization, W.H. WHO cancer. 2017; Available from: <http://www.who.int/mediacentre/factsheets/fs297/en/>.
4. Siegel, R.L., K.D. Miller, and A. Jemal, Cancer statistics, 2018. *CA: A Cancer Journal for Clinicians*, 2018. **68**(1): p. 7-30.
5. Ferlay, J.S., I.; Ervik, M.; Dikshit, R.; Eser, S.; Mathers, C.; Rebelo, M.; Parkin, D.M.; Forman, D.; and F. Bray. Globocan 2012 Cancer Incidence and Mortality Worldwide. [cited 2016 26 January]; Available from: <http://globocan.iarc.fr/>.
6. Virani, S., *et al.*, National and Subnational Population-Based Incidence of Cancer in Thailand: Assessing Cancers with the Highest Burdens. *Cancers*, 2017. **9**(8): p. 108.
7. Precision Medicine in Cancer Treatment. April 29, 2015]; Available from: <https://www.cancer.gov/about-cancer/treatment/types/surgery>.
8. Baskar, R., *et al.*, Cancer and radiation therapy: current advances and future directions. *International journal of medical sciences*, 2012. **9**(3): p. 193-199.
9. Chabner, B.A. and T.G. Roberts Jr, Chemotherapy and the war on cancer. *Nature Reviews Cancer*, 2005. **5**: p. 65.
10. Huang, C.-Y., *et al.*, A review on the effects of current chemotherapy drugs and natural agents in treating non-small cell lung cancer. *BioMedicine*, 2017. **7**(4): p. 23.
11. Harrold, J.M. and R.S. Parker, Clinically relevant cancer chemotherapy dose scheduling via mixed-integer optimization. *Computers & Chemical Engineering*, 2009. **33**(12): p. 2042-2054.
12. Itik, M., M.U. Salamci, and S.P. Banks, Optimal control of drug therapy in cancer treatment. *Nonlinear Analysis: Theory, Methods & Applications*, 2009. **71**(12): p. e1473-e1486.
13. Malhotra, V. and M.C. Perry, Classical Chemotherapy: *Mechanisms, Toxicities and the Therapeutic Window*. *Cancer Biology & Therapy*, 2003. **2**: p. 1-3.
14. Chen, Y., *et al.*, Collateral damage in cancer chemotherapy: oxidative stress in nontargeted tissues. *Molecular interventions*, 2007. **7**(3): p. 147.
15. Grochow, L.B., Busulfan disposition: the role of therapeutic monitoring in bone marrow transplantation induction regimens. *Seminars in oncology*, 1993. **20**: p. 18-25; quiz 26.
16. Wu, Y.-L., *et al.*, Afatinib versus cisplatin plus gemcitabine for first-line treatment of Asian patients with advanced non-small-cell lung cancer harbouring EGFR mutations (LUX-Lung 6): an open-label, randomised phase 3 trial. *The lancet oncology*, 2014. **15**(2): p. 213-222.
17. Kelsen, D., *et al.*, Cisplatin, vindesine, and bleomycin chemotherapy of local-regional and advanced esophageal carcinoma. *The American journal of medicine*, 1983. **75**(4): p. 645-652.

18. Kosaka, Y., *et al.*, Phase III placebo-controlled, double-blind, randomized trial of pegfilgrastim to reduce the risk of febrile neutropenia in breast cancer patients receiving docetaxel/cyclophosphamide chemotherapy. *Supportive Care in Cancer*, 2015. **23**(4): p. 1137-1143.
19. Barlogie, B., *et al.*, High-dose melphalan with autologous bone marrow transplantation for multiple myeloma. *Blood*, 1986. **67**(5): p. 1298-1301.
20. Shirota, Y., *et al.*, ERCC1 and thymidylate synthase mRNA levels predict survival for colorectal cancer patients receiving combination oxaliplatin and fluorouracil chemotherapy. *Journal of Clinical Oncology*, 2001. **19**(23): p. 4298-4304.
21. Mittal, A., *et al.*, Efficacy of gemcitabine conjugated and miRNA-205 complexed micelles for treatment of advanced pancreatic cancer. *Biomaterials*, 2014. **35**(25): p. 7077-7087.
22. Xian, C.J., *et al.*, Cellular mechanisms for methotrexate chemotherapy-induced bone growth defects. *Bone*, 2007. **41**(5): p. 842-850.
23. Holmboe, L., *et al.*, High dose methotrexate chemotherapy: pharmacokinetics, folate and toxicity in osteosarcoma patients. *British journal of clinical pharmacology*, 2012. **73**(1): p. 106-114.
24. Ajani, J.A., Optimizing docetaxel chemotherapy in patients with cancer of the gastric and gastroesophageal junction: evolution of the docetaxel, cisplatin, and 5-fluorouracil regimen. *Cancer*, 2008. **113**(5): p. 945-955.
25. Shi, S., *et al.*, Dual drugs (microRNA-34a and paclitaxel)-loaded functional solid lipid nanoparticles for synergistic cancer cell suppression. *Journal of controlled release*, 2014. **194**: p. 228-237.
26. of Trialists, I.C., International phase III trial assessing neoadjuvant cisplatin, methotrexate, and vinblastine chemotherapy for muscle-invasive bladder cancer: long-term results of the BA06 30894 trial. *Journal of Clinical Oncology*, 2011. **29**(16): p. 2171.
27. van den Bent, M.J., *et al.*, Adjuvant procarbazine, lomustine, and vincristine chemotherapy in newly diagnosed anaplastic oligodendroglioma: long-term follow-up of EORTC brain tumor group study 26951. *Journal of clinical oncology*, 2012. **31**(3): p. 344-350.
28. Liu, C., *et al.*, The microRNA miR-34a inhibits prostate cancer stem cells and metastasis by directly repressing CD44. *Nature medicine*, 2011. **17**(2): p. 211.
29. Buzdar, A.U., *et al.*, Significantly higher pathologic complete remission rate after neoadjuvant therapy with trastuzumab, paclitaxel, and epirubicin chemotherapy: results of a randomized trial in human epidermal growth factor receptor 2-positive operable breast cancer. *Journal of clinical oncology*, 2005. **23**(16): p. 3676-3685.
30. Wilson, K. and A. Paterson, First-line mitoxantrone chemotherapy for advanced breast cancer. *Cancer treatment reports*, 1986. **70**(8): p. 1021-1022.
31. Houghton, P.J., *et al.*, Efficacy of topoisomerase I inhibitors, topotecan and irinotecan, administered at low dose levels in protracted schedules to mice bearing xenografts of human tumors. *Cancer chemotherapy and pharmacology*, 1995. **36**(5): p. 393-403.
32. Nitiss, J.L., Targeting DNA topoisomerase II in cancer chemotherapy. *Nature Reviews Cancer*, 2009. **9**(5): p. 338.

33. Kantarjian, H.M., *et al.*, Phase I study of topotecan, a new topoisomerase I inhibitor, in patients with refractory or relapsed acute leukemia. *Blood*, 1993. **81**(5): p. 1146-1151.
34. Mathijssen, R.H., *et al.*, Pharmacology of topoisomerase I inhibitors irinotecan (CPT-11) and topotecan. *Current cancer drug targets*, 2002. **2**(2): p. 103-123.
35. Verschraegen, C.F., *et al.*, Phase II study of irinotecan in prior chemotherapy-treated squamous cell carcinoma of the cervix. *Journal of clinical oncology*, 1997. **15**(2): p. 625-631.
36. Chabot, G.G., Clinical pharmacokinetics of irinotecan. *Clinical pharmacokinetics*, 1997. **33**(4): p. 245-259.
37. Bailly, C., Contemporary challenges in the design of topoisomerase II inhibitors for cancer chemotherapy. *Chemical reviews*, 2012. **112**(7): p. 3611-3640.
38. Hu, C.-X., *et al.*, Salvicine functions as novel topoisomerase II poison by binding to ATP pocket. *Molecular pharmacology*, 2006.
39. MENG, L.h. and J. Ding, Salvicine, a novel topoisomerase II inhibitor, exerts its potent anticancer activity by ROS generation 1. *Acta Pharmacologica Sinica*, 2007. **28**(9): p. 1460-1465.
40. Kesharwani, R.K., *et al.*, Computational study of curcumin analogues by targeting DNA topoisomerase II: a structure-based drug designing approach. *Network Modeling Analysis in Health Informatics and Bioinformatics*, 2018. **7**(1): p. 15.
41. Sangpheak, K., *et al.*, Computational screening of chalcones acting against topoisomerase II α and their cytotoxicity towards cancer cell lines. *Journal of enzyme inhibition and medicinal chemistry*, 2019. **34**(1): p. 134-143.
42. Goto, K., *et al.*, Combined chemotherapy with cisplatin, etoposide, and irinotecan versus topotecan alone as second-line treatment for patients with sensitive relapsed small-cell lung cancer (JCOG0605): a multicentre, open-label, randomised phase 3 trial. *The Lancet Oncology*, 2016. **17**(8): p. 1147-1157.
43. Koh, A., *et al.*, The skeletal impact of the chemotherapeutic agent etoposide. *Osteoporosis International*, 2017. **28**(8): p. 2321-2333.
44. Dezhenkova, L.G., V.B. Tsvetkov, and A. Shtil, Topoisomerase I and II inhibitors: chemical structure, mechanisms of action and role in cancer chemotherapy. *Russian Chemical Reviews*, 2014. **83**(1): p. 82.
45. Kaur, P., V. Kaur, and S. Kaur, DNA Topoisomerase II: promising target for anticancer drugs, in *Multi-Targeted Approach to Treatment of Cancer*. 2015, Springer. p. 323-338.
46. Zhou, C., *et al.*, Final overall survival results from a randomised, phase III study of erlotinib versus chemotherapy as first-line treatment of EGFR mutation-positive advanced non-small-cell lung cancer (OPTIMAL, CTONG-0802). *Annals of Oncology*, 2015. **26**(9): p. 1877-1883.
47. Wu, Y.-L., *et al.*, First-line erlotinib versus gemcitabine/cisplatin in patients with advanced EGFR mutation-positive non-small-cell lung cancer: analyses from the phase III, randomized, open-label, ENSURE study. *Annals of oncology*, 2015. **26**(9): p. 1883-1889.
48. Seto, T., *et al.*, Erlotinib alone or with bevacizumab as first-line therapy in patients with advanced non-squamous non-small-cell lung cancer harbouring EGFR mutations (JO25567): an open-label, randomised, multicentre, phase 2

- study. *The lancet oncology*, 2014. **15**(11): p. 1236-1244.
49. Venook, A.P., *et al.*, CALGB/SWOG 80405: Phase III trial of irinotecan/5-FU/leucovorin (FOLFIRI) or oxaliplatin/5-FU/leucovorin (mFOLFOX6) with bevacizumab (BV) or cetuximab (CET) for patients (pts) with KRAS wild-type (wt) untreated metastatic adenocarcinoma of the colon or rectum (MCRC). 2014, American Society of Clinical Oncology.
 50. Burotto, M., *et al.*, Gefitinib and erlotinib in metastatic non-small cell lung cancer: a meta-analysis of toxicity and efficacy of randomized clinical trials. *The oncologist*, 2015. **20**(4): p. 400-410.
 51. Ramalingam, S.S., *et al.*, A randomized, phase III study (FLAURA) of AZD9291, a novel EGFR-TKI, versus gefitinib or erlotinib in treatment-naïve patients with advanced non-small cell lung cancer and an EGFR-TKI-sensitizing mutation. 2015, American Society of Clinical Oncology.
 52. Drake, C.G., E.J. Lipson, and J.R. Brahmer, Breathing new life into immunotherapy: review of melanoma, lung and kidney cancer. *Nature reviews Clinical oncology*, 2014. **11**(1): p. 24.
 53. Understanding Immunotherapy [cited 2017 1 June 2017]; Available from: <https://www.cancervic.org.au/cancer-information/treatments/treatments-types/immunotherapy#side-effects>.
 54. Institute, C.R. Cancer Immunology Research. [cited 2018 August 24, 2018]; Available from: <https://www.cancerresearch.org/immunotherapy/what-is-immunotherapy>.
 55. Gerber, D.E., Targeted therapies: a new generation of cancer treatments. *American family physician*, 2008. **77**(3).
 56. Finley, R.S., Overview of targeted therapies for cancer. *American journal of health-system pharmacy*, 2003. **60**(suppl 9): p. S4-S10.
 57. Ke, X. and L. Shen, Molecular targeted therapy of cancer: The progress and future prospect. *Frontiers in Laboratory Medicine*, 2017. **1**(2): p. 69-75.
 58. Padma, V.V., *An overview of targeted cancer therapy*. *BioMedicine*, 2015. **5**(4).
 59. Hojjat-Farsangi, M., Small-molecule inhibitors of the receptor tyrosine kinases: promising tools for targeted cancer therapies. *International journal of molecular sciences*, 2014. **15**(8): p. 13768-13801.
 60. Press, O.W., *et al.*, Monoclonal antibody 1F5 (anti-CD20) serotherapy of human B cell lymphomas. *Blood*, 1987. **69**(2): p. 584-591.
 61. Reff, M.E., *et al.*, Depletion of B cells in vivo by a chimeric mouse human monoclonal antibody to CD20. *Blood*, 1994. **83**(2): p. 435-445.
 62. Maloney, D., *et al.*, Phase I clinical trial using escalating single-dose infusion of chimeric anti-CD20 monoclonal antibody (IDEC-C2B8) in patients with recurrent B-cell lymphoma. *Blood*, 1994. **84**(8): p. 2457-2466.
 63. Hudziak, R.M., *et al.*, p185HER2 monoclonal antibody has antiproliferative effects in vitro and sensitizes human breast tumor cells to tumor necrosis factor. *Molecular and cellular biology*, 1989. **9**(3): p. 1165-1172.
 64. Carter, P., *et al.*, Humanization of an anti-p185HER2 antibody for human cancer therapy. *Proceedings of the National Academy of Sciences*, 1992. **89**(10): p. 4285-4289.
 65. Naito, K., *et al.*, Calicheamicin-conjugated humanized anti-CD33 monoclonal antibody (gemtuzumab zogamicin, CMA-676) shows cytotoxic effect on CD33-

- positive leukemia cell lines, but is inactive on P-glycoprotein-expressing sublines. *Leukemia*, 2000. **14**(8): p. 1436.
66. Boghaert, E.R., *et al.*, Tumoricidal effect of calicheamicin immuno-conjugates using a passive targeting strategy. *International journal of oncology*, 2006. **28**(3): p. 675-684.
 67. Lozanski, G., *et al.*, Alemtuzumab is an effective therapy for chronic lymphocytic leukemia with p53 mutations and deletions. *Blood*, 2004. **103**(9): p. 3278-3281.
 68. Kaufman, D., *et al.*, Alemtuzumab induction and prednisone-free maintenance immunotherapy in simultaneous pancreas-kidney transplantation comparison with rabbit antithymocyte globulin induction—long-term results. *American journal of transplantation*, 2006. **6**(2): p. 331-339.
 69. Chinn, P.C., *et al.*, Preclinical evaluation of 90Y-labeled anti-CD20 monoclonal antibody for treatment of non-Hodgkin's lymphoma. *International journal of oncology*, 1999. **15**(5): p. 1017-1042.
 70. Kaminski, M.S., *et al.*, Iodine-131-anti-B1 radioimmunotherapy for B-cell lymphoma. *Journal of Clinical Oncology*, 1996. **14**(7): p. 1974-1981.
 71. Vose, J.M., *et al.*, Multicenter phase II study of iodine-131 tositumomab for chemotherapy-relapsed/refractory low-grade and transformed low-grade B-cell non-Hodgkin's lymphomas. *Journal of clinical oncology*, 2000. **18**(6): p. 1316-1323.
 72. Liu, S.Y., *et al.*, Follow-up of relapsed B-cell lymphoma patients treated with iodine-131-labeled anti-CD20 antibody and autologous stem-cell rescue. *Journal of Clinical Oncology*, 1998. **16**(10): p. 3270-3278.
 73. Huang, S.-M., J.M. Bock, and P.M. Harari, Epidermal growth factor receptor blockade with C225 modulates proliferation, apoptosis, and radiosensitivity in squamous cell carcinomas of the head and neck. *Cancer research*, 1999. **59**(8): p. 1935-1940.
 74. Baselga, J., *et al.*, Phase I studies of anti-epidermal growth factor receptor chimeric antibody C225 alone and in combination with cisplatin. *Journal of Clinical Oncology*, 2000. **18**(4): p. 904-904.
 75. Jimeno, A., *et al.*, Epidermal growth factor receptor dynamics influences response to epidermal growth factor receptor targeted agents. *Cancer research*, 2005. **65**(8): p. 3003-3010.
 76. Willett, C.G., *et al.*, Direct evidence that the VEGF-specific antibody bevacizumab has antivasular effects in human rectal cancer. *Nature medicine*, 2004. **10**(2): p. 145.
 77. Seo, Y.H., Dual inhibitors against topoisomerases and histone deacetylases. *Journal of cancer prevention*, 2015. **20**(2): p. 85.
 78. Kato, S. and A. Kikuchi, DNA topoisomerase: the key enzyme that regulates DNA super structure. *Nagoya journal of medical science*, 1998. **61**: p. 11-26.
 79. Pommier, Y., *et al.*, Roles of eukaryotic topoisomerases in transcription, replication and genomic stability. *Nature reviews Molecular cell biology*, 2016. **17**(11): p. 703.
 80. Wang, J.C., DNA topoisomerases. *Annual review of biochemistry*, 1996. **65**(1): p. 635-692.
 81. Hande, K.R., Topoisomerase II inhibitors. *Update on cancer therapeutics*, 2008.

- 3(1): p. 13-26.
82. Heck, M. and W.C. Earnshaw, Topoisomerase II: A specific marker for cell proliferation. *J Cell Biol*, 1986. **103**(6 Pt 2): p. 2569-2581.
 83. Wendorff, T.J., et al., The Structure of DNA-Bound Human Topoisomerase II Alpha: Conformational Mechanisms for Coordinating Inter-Subunit Interactions with DNA Cleavage. *Journal of molecular biology*, 2012. **424**(3-4): p. 109-124.
 84. Robinson, M.J., *et al.*, Effects of quinolone derivatives on eukaryotic topoisomerase II. A novel mechanism for enhancement of enzyme-mediated DNA cleavage. *Journal of Biological Chemistry*, 1991. **266**(22): p. 14585-14592.
 85. Classen, S., S. Olland, and J.M. Berger, Structure of the topoisomerase II ATPase region and its mechanism of inhibition by the chemotherapeutic agent ICRF-187. *Proceedings of the National Academy of Sciences*, 2003. **100**(19): p. 10629-10634.
 86. Wu, T., Y. Wang, and Y. Yuan, Antiviral activity of topoisomerase II catalytic inhibitors against Epstein–Barr virus. *Antiviral Research*, 2014. **107**: p. 95-101.
 87. Cai, Y.-J., *et al.*, Salvicine triggers DNA double-strand breaks and apoptosis by GSH-depletion-driven H₂O₂ generation and topoisomerase II inhibition. *Free Radical Biology and Medicine*, 2008. **45**(5): p. 627-635.
 88. Pastor, N., *et al.*, The DNA topoisomerase II catalytic inhibitor merbarone is genotoxic and induces endoreduplication. *Mutation Research/Fundamental and Molecular Mechanisms of Mutagenesis*, 2012. **738–739**: p. 45-51.
 89. Baviskar, A.T., *et al.*, Switch in Site of Inhibition: A Strategy for Structure-Based Discovery of Human Topoisomerase II α Catalytic Inhibitors. *ACS Medicinal Chemistry Letters*, 2015. **6**(4): p. 481-485.
 90. Fortune, J.M. and N. Osheroff, Merbarone inhibits the catalytic activity of human topoisomerase II α by blocking DNA cleavage. *Journal of Biological Chemistry*, 1998. **273**(28): p. 17643-17650.
 91. Meng, L.-h., J.-s. Zhang, and J. Ding, Salvicine, a novel DNA topoisomerase II inhibitor, exerting its effects by trapping enzyme-DNA cleavage complexes. *Abbreviations: ADM, adriamycin; VP16, etoposide; Topo, topoisomerase; kDNA, knetoplast DNA; HCPT, hydrocamptothecin; SC, supercoiled form; RLX, relaxed form; LNR, linear form; and NC, nicked form. Biochemical Pharmacology*, 2001. **62**(6): p. 733-741.
 92. Kesharwani, R.K. and K. Misra, Prediction of binding site for curcuminoids at human topoisomerase II α protein; an in silico approach. *Current Science*, 2011: p. 1060-1065.
 93. DING, J., Salvicine, a novel topoisomerase II inhibitor, exerts its potent anticancer activity by ROS generation. *Acta Pharmacologica Sinica*, 2007. **28**(9): p. 1460-1465.
 94. Hu, C.-X., *et al.*, Salvicine functions as novel topoisomerase II poison by binding to ATP pocket. *Molecular pharmacology*, 2006. **70**(5): p. 1593-1601.
 95. Schmidt, B.H., N. Osheroff, and J.M. Berger, Structure of a topoisomerase II–DNA–nucleotide complex reveals a new control mechanism for ATPase activity. *Nature structural & molecular biology*, 2012. **19**(11): p. 1147.
 96. Laponogov, I., *et al.*, Structure of an ‘open’ clamp type II topoisomerase-DNA complex provides a mechanism for DNA capture and transport. *Nucleic acids*

- research, 2013. **41**(21): p. 9911-9923.
97. Grochow, L.B., *et al.*, Pharmacokinetics and pharmacodynamics of topotecan in patients with advanced cancer. *Drug Metabolism and Disposition*, 1992. **20**(5): p. 706.
 98. Kollmannsberger, C., *et al.*, Topotecan – A Novel Topoisomerase I Inhibitor: Pharmacology and Clinical Experience. *Oncology*, 1999. **56**(1): p. 1-12.
 99. Herben, V.M.M., W.W. ten Bokkel Huinink, and J.H. Beijnen, Clinical Pharmacokinetics of Topotecan. *Clinical Pharmacokinetics*, 1996. **31**(2): p. 85-102.
 100. Creemers, G., *et al.*, Topotecan, an active drug in the second-line treatment of epithelial ovarian cancer: results of a large European phase II study. *Journal of Clinical oncology*, 1996. **14**(12): p. 3056-3061.
 101. Jonker, J.W., *et al.*, Role of breast cancer resistance protein in the bioavailability and fetal penetration of topotecan. *Journal of the National Cancer Institute*, 2000. **92**(20): p. 1651-1656.
 102. Xu, Y. and M.A. Villalona-Calero, Irinotecan: mechanisms of tumor resistance and novel strategies for modulating its activity. *Annals of Oncology*, 2002. **13**(12): p. 1841-1851.
 103. Ron, H.J.M., *et al.*, Pharmacology of Topoisomerase I Inhibitors Irinotecan (CPT-11) and Topotecan. *Current Cancer Drug Targets*, 2002. **2**(2): p. 103-123.
 104. Saltz, L.B., *et al.*, Irinotecan plus fluorouracil and leucovorin for metastatic colorectal cancer. *New England Journal of Medicine*, 2000. **343**(13): p. 905-914.
 105. Noda, K., *et al.*, Irinotecan plus cisplatin compared with etoposide plus cisplatin for extensive small-cell lung cancer. *New England Journal of Medicine*, 2002. **346**(2): p. 85-91.
 106. Montecucco, A., F. Zanetta, and G. Biamonti, Molecular mechanisms of etoposide. *EXCLI journal*, 2015. **14**: p. 95-108.
 107. Hande, K., Etoposide: four decades of development of a topoisomerase II inhibitor. *European journal of cancer*, 1998. **34**(10): p. 1514-1521.
 108. Johnson, D.H., *et al.*, Current status of etoposide in the management of small cell lung cancer. *Cancer*, 1991. **67**(S1): p. 231-244.
 109. Aisner, J. and E.J. Lee, Etoposide. Current and future status. *Cancer*, 1991. **67**(S1): p. 215-219.
 110. Sledge Jr, G.W., Etoposide in the management of metastatic breast cancer. *Cancer*, 1991. **67**(S1): p. 266-270.
 111. Del Bino, G. and Z. Darzynkiewicz, Camptothecin, teniposide, or 4'-(9-acridinylamino)-3-methanesulfon-m-anisidide, but not mitoxantrone or doxorubicin, induces degradation of nuclear DNA in the S phase of HL-60 cells. *Cancer research*, 1991. **51**(4): p. 1165-1169.
 112. Hande, K.R., Etoposide: four decades of development of a topoisomerase II inhibitor. *European Journal of Cancer*, 1998. **34**(10): p. 1514-1521.
 113. Piccart-Gebhart, M.J., *et al.*, Taxanes alone or in combination with anthracyclines as first-line therapy of patients with metastatic breast cancer. 2008.
 114. Minotti, G., *et al.*, Anthracyclines: molecular advances and pharmacologic developments in antitumor activity and cardiotoxicity. *Pharmacological reviews*, 2004. **56**(2): p. 185-229.

115. Speth, P.A.J., Q.G.C.M. van Hoesel, and C. Haanen, Clinical Pharmacokinetics of Doxorubicin. *Clinical Pharmacokinetics*, 1988. **15**(1): p. 15-31.
116. von der Maase, H., *et al.*, Gemcitabine and cisplatin versus methotrexate, vinblastine, doxorubicin, and cisplatin in advanced or metastatic bladder cancer: results of a large, randomized, multinational, multicenter, phase III study. *Journal of clinical oncology*, 2000. **18**(17): p. 3068-3077.
117. Liu, X.-Y., S. Pestka, and Y.-F. Shi, *Recent advances in cancer research and therapy*. 2012: Elsevier.
118. Miao, Z.H., *et al.*, Characterization of salvicine-resistant lung adenocarcinoma A549/SAL cell line. *International journal of cancer*, 2004. **110**(5): p. 627-632.
119. Deng, F., *et al.*, Synthesis and antitumor activity of novel salvicine analogues. *Chinese Chemical Letters*, 2011. **22**(1): p. 25-28.
120. Hynes, N.E. and H.A. Lane, ERBB receptors and cancer: the complexity of targeted inhibitors. *Nat Rev Cancer*, 2005. **5**(5): p. 341-354.
121. Olayioye, M.A., *et al.*, The ErbB signaling network: receptor heterodimerization in development and cancer. *EMBO J.*, 2000. **19**(13): p. 3159-3167.
122. Woodburn, J., *The epidermal growth factor receptor and its inhibition in cancer therapy*. *Pharmacology & therapeutics*, 1999. **82**(2): p. 241-250.
123. Ogiso, H., *et al.*, Crystal structure of the complex of human epidermal growth factor and receptor extracellular domains. *Cell*, 2002. **110**(6): p. 775-787.
124. Woodburn, J.R., *The Epidermal Growth Factor Receptor and Its Inhibition in Cancer Therapy*. *Pharmacol. Ther.*, 1999. **82**(2-3): p. 241-250.
125. Harari, P.M. and S.-M. Huang. Epidermal growth factor receptor modulation of radiation response: preclinical and clinical development. in *Seminars in radiation oncology*. 2002. Elsevier.
126. Okita, R., *et al.*, PD-L1 overexpression is partially regulated by EGFR/HER2 signaling and associated with poor prognosis in patients with non-small-cell lung cancer. *Cancer Immunology, Immunotherapy*, 2017. **66**(7): p. 865-876.
127. Forcella, M., *et al.*, Non-small cell lung cancer (NSCLC), EGFR downstream pathway activation and TKI targeted therapies sensitivity: Effect of the plasma membrane-associated NEU3. *PloS one*, 2017. **12**(10): p. e0187289.
128. Doyle, H.A., *et al.*, Epidermal growth factor receptor peptide vaccination induces cross-reactive immunity to human EGFR, HER2, and HER3. *Cancer Immunology, Immunotherapy*, 2018: p. 1-11.
129. Liu, W.-J., *et al.*, EGFR-targeting, β -defensin-tailored fusion protein exhibits high therapeutic efficacy against EGFR-expressed human carcinoma via mitochondria-mediated apoptosis. *Acta Pharmacologica Sinica*, 2018: p. 1.
130. Yewale, C., *et al.*, Epidermal growth factor receptor targeting in cancer: a review of trends and strategies. *Biomaterials*, 2013. **34**(34): p. 8690-8707.
131. Slovin, S.F., *et al.*, Anti—Epidermal Growth Factor Receptor Monoclonal Antibody Cetuximab Plus Doxorubicin in the Treatment of Metastatic Castration-Resistant Prostate Cancer. *Clin. Genitourinary Cancer*, 2009. **7**(3): p. E77-E82.
132. Green, M.R., *Targeting Targeted Therapy*. *N Engl J Med*, 2004. **350**(21): p. 2191-2193.
133. Maemondo, M., *et al.*, Gefitinib or chemotherapy for non—small-cell lung cancer with mutated EGFR. *New England Journal of Medicine*, 2010. **362**(25): p. 2380-

- 2388.
134. Ganjoo, K.N. and H. Wakelee, Review of erlotinib in the treatment of advanced non-small cell lung cancer. *Biologics: targets & therapy*, 2007. **1**(4): p. 335.
 135. Geyer, C.E., *et al.*, Lapatinib plus capecitabine for HER2-positive advanced breast cancer. *New England Journal of Medicine*, 2006. **355**(26): p. 2733-2743.
 136. Li, D., *et al.*, BIBW2992, an irreversible EGFR/HER2 inhibitor highly effective in preclinical lung cancer models. *Oncogene*, 2008. **27**(34): p. 4702.
 137. Kalous, O., *et al.*, Dacomitinib (PF-00299804), an irreversible Pan-HER inhibitor, inhibits proliferation of HER2-amplified breast cancer cell lines resistant to trastuzumab and lapatinib. *Molecular cancer therapeutics*, 2012.
 138. Ferguson, K.M., Structure-based view of epidermal growth factor receptor regulation. *Annu. Rev. Biophys.*, 2008. **37**: p. 353-373.
 139. Eitsuka, T., *et al.*, Synergistic anticancer effect of tocotrienol combined with chemotherapeutic agents or dietary components: a review. *International journal of molecular sciences*, 2016. **17**(10): p. 1605.
 140. Abu, N., *et al.*, The flavokawains: uprising medicinal chalcones. *Cancer Cell International*, 2013. **13**(1): p. 102.
 141. Haraguchi, H., *et al.*, Antioxidative and superoxide scavenging activities of retrochalcones in *Glycyrrhiza inflata*. *Bioorganic & medicinal chemistry*, 1998. **6**(3): p. 339-347.
 142. Akihisa, T., *et al.*, Chalcones, coumarins, and flavanones from the exudate of *Angelica keiskei* and their chemopreventive effects. *Cancer Letters*, 2003. **201**(2): p. 133-137.
 143. Chopra, P.G., Chalcones: A brief review. *International Journal of Research in Engineering and Applied Sciences*, 2016. **6**(5): p. 173-185.
 144. Won, S.-J., *et al.*, Synthetic chalcones as potential anti-inflammatory and cancer chemopreventive agents. *European journal of medicinal chemistry*, 2005. **40**(1): p. 103-112.
 145. Nowakowska, Z., A review of anti-infective and anti-inflammatory chalcones. *European journal of medicinal chemistry*, 2007. **42**(2): p. 125-137.
 146. Mahapatra, D.K., S.K. Bharti, and V. Asati, Anti-cancer chalcones: Structural and molecular target perspectives. *European Journal of Medicinal Chemistry*, 2015. **98**: p. 69-114.
 147. Potter, G., P. Butler, and E. Wanogho, Substituted chalcones as therapeutic compounds. 2001, Google Patents.
 148. Chauhan, S.S., *et al.*, Synthesis of novel β -carboline based chalcones with high cytotoxic activity against breast cancer cells. *Bioorganic & medicinal chemistry letters*, 2014. **24**(13): p. 2820-2824.
 149. Nakhjavani, M., A. Zarghi, and F. H Shirazi, Cytotoxicity of selected novel chalcone derivatives on human breast, lung and hepatic carcinoma cell lines. *Iranian Journal of Pharmaceutical Research*, 2014. **13**(3): p. 953-958.
 150. Ducki, S., *et al.*, Combretastatin-like chalcones as inhibitors of microtubule polymerisation. Part 2: Structure-based discovery of alpha-aryl chalcones. *Bioorganic & medicinal chemistry*, 2009. **17**(22): p. 7711-7722.
 151. Warmka, J.K., *et al.*, Inhibition of mitogen activated protein kinases increases the sensitivity of A549 lung cancer cells to the cytotoxicity induced by a kava chalcone analog. *Biochemical and biophysical research communications*, 2012.

- 424**(3): p. 488-492.
152. Park, S., et al., Cardamonin suppresses the proliferation of colon cancer cells by promoting β -catenin degradation. *Biological and Pharmaceutical Bulletin*, 2013. **36**(6): p. 1040-1044.
 153. Wei, H., et al., Chalcone derivatives from the fern *Cyclosorus parasiticus* and their anti-proliferative activity. *Food and chemical toxicology*, 2013. **60**: p. 147-152.
 154. Echeverria, C., et al., Structural antitumoral activity relationships of synthetic chalcones. *International journal of molecular sciences*, 2009. **10**(1): p. 221-231.
 155. Vogel, S., et al., Natural and non-natural prenylated chalcones: synthesis, cytotoxicity and anti-oxidative activity. *Bioorganic & medicinal chemistry*, 2008. **16**(8): p. 4286-4293.
 156. Jandial, D.D., et al., Molecular Targeted Approaches to Cancer Therapy and Prevention Using Chalcones. *Current cancer drug targets*, 2014. **14**(2): p. 181-200.
 157. Gaur, R. and L. Mishra, Synthesis and characterization of Ru (II)-DMSO-Cl-chalcone complexes: DNA binding, nuclease, and topoisomerase II inhibitory activity. *Inorganic chemistry*, 2012. **51**(5): p. 3059-3070.
 158. Kim, S.-H., et al., Chalcones, inhibitors for topoisomerase I and cathepsin B and L, as potential anti-cancer agents. *Bioorganic & medicinal chemistry letters*, 2013. **23**(11): p. 3320-3324.
 159. Jeon, K.-H., et al., Synthesis and topoisomerases inhibitory activity of heteroaromatic chalcones. *Bioorganic & medicinal chemistry*, 2016. **24**(22): p. 5921-5928.
 160. Banday, A.H., V.V. Kulkarni, and V.J. Hruby, Design, synthesis, and biological and docking studies of novel epipodophyllotoxin-chalcone hybrids as potential anticancer agents. *MedChemComm*, 2015. **6**(1): p. 94-104.
 161. Chinthala, Y., et al., Synthesis, docking and ADMET studies of novel chalcone triazoles for anti-cancer and anti-diabetic activity. *European journal of medicinal chemistry*, 2015. **93**: p. 564-573.
 162. Ma, Y.-C., et al., Dual Inhibition of Topoisomerase II and Tyrosine Kinases by the Novel Bis-Fluoroquinolone Chalcone-Like Derivative HMNE3 in Human Pancreatic Cancer Cells. *PloS one*, 2016. **11**(10): p. e0162821.
 163. Santos, M.B., et al., Antiproliferative and pro-apoptotic activities of 2'- and 4'-aminochalcones against tumor canine cells. *European Journal of Medicinal Chemistry*, 2017. **138**: p. 884-889.
 164. Wu, G., et al., Detailed analysis of grid-based molecular docking: A case study of CDOCKER—A CHARMM-based MD docking algorithm. *Journal of computational chemistry*, 2003. **24**(13): p. 1549-1562.
 165. Erickson, J.A., et al., Lessons in molecular recognition: the effects of ligand and protein flexibility on molecular docking accuracy. *Journal of medicinal chemistry*, 2004. **47**(1): p. 45-55.
 166. Grover, A., *Drug Design: Principles and Applications*. 2017: Springer.
 167. Dimić, D., A.G. Mercader, and E.A. Castro, Chalcone derivative cytotoxicity activity against MCF-7 human breast cancer cell QSAR study. *Chemometrics and Intelligent Laboratory Systems*, 2015. **146**: p. 378-384.
 168. Gul, H.I., et al., Cytotoxicity, apoptosis, and QSAR studies of phenothiazine

- derived methoxylated chalcones as anticancer drug candidates. *Medicinal Chemistry Research*, 2018. **27**(10): p. 2366-2378.
169. Chen, G., *et al.*, A natural chalcone induces apoptosis in lung cancer cells: 3D-QSAR, docking and an in vivo/vitro assay. *Scientific reports*, 2017. **7**(1): p. 10729.
 170. Doweiko, A.M., QSAR: Dead or alive? *Journal of Computer-Aided Molecular Design*, 2008. **22**(2): p. 81-89.
 171. Cherkasov, A., *et al.*, QSAR modeling: where have you been? Where are you going to? *Journal of medicinal chemistry*, 2014. **57**(12): p. 4977-5010.
 172. Snedecor, G. and W. Cochran, *Statistical Methods* Oxford and IBH publishing co. New Delhi, 1967: p. 593.
 173. Roy, K., S. Kar, and R.N. Das, *Statistical methods in QSAR/QSPR*, in *A primer on QSAR/QSPR modeling*. 2015, Springer. p. 37-59.
 174. Cramer, R.D., *Partial least squares (PLS): its strengths and limitations*. *Perspectives in drug discovery and design*, 1993. **1**(2): p. 269-278.
 175. Stone, M., *Cross-validatory choice and assessment of statistical predictions*. *Journal of the royal statistical society. Series B (Methodological)*, 1974: p. 111-147.
 176. Veerasamy, R., *et al.*, *Validation of QSAR models-strategies and importance*. *International Journal of Drug Design & Discovery*, 2011. **3**: p. 511-519.
 177. Segall, M.D., *et al.*, *Focus on success: using a probabilistic approach to achieve an optimal balance of compound properties in drug discovery*. *Expert opinion on drug metabolism & toxicology*, 2006. **2**(2): p. 325-337.
 178. Cheng, F., *et al.*, *In silico ADMET prediction: recent advances, current challenges and future trends*. *Current topics in medicinal chemistry*, 2013. **13**(11): p. 1273-1289.
 179. Palm, K., *et al.*, *Polar molecular surface properties predict the intestinal absorption of drugs in humans*. *Pharmaceutical research*, 1997. **14**(5): p. 568-571.
 180. Kelder, J., *et al.*, *Polar molecular surface as a dominating determinant for oral absorption and brain penetration of drugs*. *Pharmaceutical research*, 1999. **16**(10): p. 1514-1519.
 181. Testa, B. and J. Mayer, *Molecular toxicology and the medicinal chemist*. *II Farmaco*, 1998. **53**(4): p. 287-291.
 182. Camile, W., *The practice of medicinal chemistry*. Academic Press, San Diego, 2003.
 183. Kapusta, D., *Drug Excretion*, in *xPharm: The Comprehensive Pharmacology Reference*, S.J. Enna and D.B. Bylund, Editors. 2007, Elsevier: New York. p. 1-2.
 184. Lipinski, C.A., *et al.*, *Experimental and computational approaches to estimate solubility and permeability in drug discovery and development settings*. *Advanced drug delivery reviews*, 1997. **23**(1-3): p. 3-25.
 185. Zegzouti, H., *et al.*, *ADP-Glo: a bioluminescent and homogeneous ADP monitoring assay for kinases*. *Assay and drug development technologies*, 2009. **7**(6): p. 560-572.
 186. Mahalaputr, P., *et al.*, *Molecular recognition of naphthoquinone-containing compounds against human DNA topoisomerase II α ATPase domain: A*

- molecular modeling study. *Journal of Molecular Liquids*, 2017. **247**(Supplement C): p. 374-385.
187. Dennington, R.D., T.A. Keith, and J.M. Millam, GaussView 5.0. 8. Gaussian Inc, 2008.
 188. Irwin, J.J., *et al.*, ZINC: A Free Tool to Discover Chemistry for Biology. *Journal of Chemical Information and Modeling*, 2012. **52**(7): p. 1757-1768.
 189. Meeprasert, A., *et al.*, Binding pattern of the long acting neuraminidase inhibitor laninamivir towards influenza A subtypes H5N1 and pandemic H1N1. *Journal of Molecular Graphics and Modelling*, 2012. **38**: p. 148-154.
 190. Meeprasert, A., S. Hannongbua, and T. Rungrotmongkol, Key binding and susceptibility of NS3/4A serine protease inhibitors against hepatitis C virus. *Journal of chemical information and modeling*, 2014. **54**(4): p. 1208-1217.
 191. Kaiyawet, N., T. Rungrotmongkol, and S. Hannongbua, Effect of halogen substitutions on dUMP to stability of thymidylate synthase/dUMP/mTHF ternary complex using molecular dynamics simulation. *Journal of chemical information and modeling*, 2013. **53**(6): p. 1315-1323.
 192. Gaussian09, R.A., I, MJ Frisch, GW Trucks, HB Schlegel, GE Scuseria, MA Robb, JR Cheeseman, G. Scalmani, V. Barone, B. Mennucci, GA Petersson *et al.*, Gaussian. Inc., Wallingford CT, 2009.
 193. Duke, R., *et al.*, *Amber 14*. 2014, University of California: San Francisco, CA
 194. Wang, J., *et al.*, Development and testing of a general amber force field. *Journal of computational chemistry*, 2004. **25**(9): p. 1157-1174.
 195. Duan, Y., *et al.*, A point-charge force field for molecular mechanics simulations of proteins based on condensed-phase quantum mechanical calculations. *J. Comput. Chem.*, 2003. **24**(16): p. 1999-2012.
 196. Olsson, M.H., *et al.*, PROPKA3: consistent treatment of internal and surface residues in empirical p K a predictions. *J. Chem. Theory Comput.*, 2011. **7**(2): p. 525-537.
 197. Jorgensen, W.L., *et al.*, Comparison of simple potential functions for simulating liquid water. *J. Biol. Chem.*, 1983. **79**(2): p. 926-935.
 198. Ryckaert, J.-P., G. Ciccotti, and H.J. Berendsen, Numerical integration of the cartesian equations of motion of a system with constraints: molecular dynamics of n-alkanes. *Journal of Computational Physics*, 1977. **23**(3): p. 327-341.
 199. York, D.M., T.A. Darden, and L.G. Pedersen, The effect of long-range electrostatic interactions in simulations of macromolecular crystals: A comparison of the Ewald and truncated list methods. *The Journal of Chemical Physics*, 1993. **99**(10): p. 8345-8348.
 200. Mahalapbutr, P., *et al.*, Molecular recognition of naphthoquinone-containing compounds against human DNA topoisomerase II α ATPase domain: A molecular modeling study. *Journal of Molecular Liquids*, 2017. **247**: p. 374-385.
 201. Panman, W., *et al.*, Computational screening of fatty acid synthase inhibitors against thioesterase domain. *Journal of Biomolecular Structure and Dynamics*, 2017: p. 1-12.
 202. Frisch, M.J., Trucks, G.W., Schlegel, H.B., Scuseria, G.E., Robb, M.A., Cheeseman, J.R., Scalmani, G., Barone, V., Mennucci, B., Petersson, G.A., Nakatsuji, H., Caricato, M., Li, X., Hratchian, H.P., Izmaylov, A.F., Bloino, J., Zheng, G., Sonnenberg, J.L., Hada, M., Ehara, M., Toyota, K., Fukuda, R.,

- Hasegawa, J., Ishida, M., Nakajima, T., Honda, Y., Kitao, O., Nakai, H., Vreven, T., Montgomery Jr., J.A., Peralta, J.E., Ogliaro, F., Bearpark, M., Heyd, J.J., Brothers, E., Kudin, K.N., Staroverov, V.N., Kobayashi, R., Normand, J., Raghavachari, K., Rendell, A., Burant, J.C., Iyengar, S.S., Tomasi, J., Cossi, M., Rega, N., Millam, J.M., Klene, M., Knox, J.E., Cross, J.B., Bakken, V., Adamo, C., Jaramillo, J., Gomperts, R., Stratmann, R.E., Yazyev, O., Austin, A.J., Cammi, R., Pomelli, C., Ochterski, J.W., Martin, R.L., Morokuma, K., Zakrzewski, V.G., Voth, G.A., Salvador, P., Dannenberg, J.J., Dapprich, S., Daniels, A.D., Farkas, O., Foresman, J.B., Ortiz, J.V., Cioslowski, J. and Fox, D.J., *Gaussian 09*. Gaussian Inc. Wallingford, CT, USA, , 2010.
203. D.A. Case, R.M.B., D.S. Cerutti, T.E. Cheatham, III, T.A. Darden, R.E. Duke, T.J. Giese, H. Gohlke, A.W. Goetz, N. Homeyer, S. Izadi, P. Janowski, J. Kaus, A. Kovalenko, T.S. Lee, S. LeGrand, P. Li, C. Lin, T. Luchko, R. Luo, B. Madej, D. Mermelstein, K.M. Merz, G. Monard, H. Nguyen, H.T. Nguyen, I. Omelyan, A. Onufriev, D.R. Roe, A. Roitberg, C. Sagui, C.L. Simmerling, W.M. Botello-Smith, J. Swails, R.C. Walker, J. Wang, R.M. Wolf, X. Wu, L. Xiao and P.A. Kollman, *AMBER 2016*. University of California San Francisco, 2016.
204. Maier, J.A., *et al.*, ff14SB: Improving the Accuracy of Protein Side Chain and Backbone Parameters from ff99SB. *Journal of Chemical Theory and Computation*, 2015. **11**(8): p. 3696-3713.
205. Olsson, M.H.M., *et al.*, PROPKA3: Consistent Treatment of Internal and Surface Residues in Empirical pKa Predictions. *Journal of Chemical Theory and Computation*, 2011. **7**(2): p. 525-537.
206. Ryckaert, J.-P., G. Ciccotti, and H.J.C. Berendsen, Numerical integration of the cartesian equations of motion of a system with constraints: molecular dynamics of n-alkanes. *Journal of Computational Physics*, 1977. **23**(3): p. 327-341.
207. Cabrera, M., *et al.*, Synthetic chalcones, flavanones, and flavones as antitumoral agents: Biological evaluation and structure–activity relationships. *Bioorganic & Medicinal Chemistry*, 2007. **15**(10): p. 3356-3367.
208. Sangpheak, W., *et al.*, Physical properties and biological activities of hesperetin and naringenin in complex with methylated beta-cyclodextrin. *Beilstein J Org Chem*, 2015. **11**: p. 2763-73.
209. Boonyalai, N., *et al.*, Biophysical and molecular docking studies of naphthoquinone derivatives on the ATPase domain of human topoisomerase II. *Biomedicine & Pharmacotherapy*, 2013. **67**(2): p. 122-128.
210. Hsu, S.-C. and M.-C. Hung, *Characterization of a novel tripartite nuclear localization sequence in the EGFR family*. *Journal of Biological Chemistry*, 2007.
211. Bagul, C., *et al.*, Synthesis and biological evaluation of chalcone-linked pyrazolo [1, 5-a] pyrimidines as potential anticancer agents. *MedChemComm*, 2017. **8**(9): p. 1810-1816.
212. Pourbasheer, E., *et al.*, QSAR study of ACK1 inhibitors by genetic algorithm–multiple linear regression (GA–MLR). *Journal of Saudi Chemical Society*, 2014. **18**(5): p. 681-688.
213. Iman, M., A. Davood, and N. BANAROU EI, QSAR study of chalcone derivatives as anti-Leishmania agents. *Turkish Journal of Chemistry*, 2014. **38**(5): p. 716-724.

214. Davood, A. and M. Iman, Molecular docking and QSAR study on imidazole derivatives as 14/alpha-demethylase inhibitors. *Turkish Journal of Chemistry*, 2013. **37**(1): p. 119-133.
215. Daina, A., O. Michielin, and V. Zoete, SwissADME: a free web tool to evaluate pharmacokinetics, drug-likeness and medicinal chemistry friendliness of small molecules. *Scientific Reports*, 2017. **7**: p. 42717.
216. Nadeem, S., *et al.*, Synthesis, spectral characterization and in vitro antibacterial evaluation and Petra/Osiris/Molinspiration analyses of new Palladium (II) iodide complexes with thioamides. *Alexandria Journal of Medicine*, 2016. **52**(3): p. 279–288.
217. Sander, T., *et al.*, DataWarrior: An Open-Source Program For Chemistry Aware Data Visualization And Analysis. *Journal of Chemical Information and Modeling*, 2015. **55**(2): p. 460-473.
218. Zhang, Y., *et al.*, Anti-angiogenic activity of salvicine. *Pharmaceutical Biology*, 2013. **51**(8): p. 1061-1065.
219. Järvinen, T.A.H., *et al.*, Amplification and Deletion of Topoisomerase II α Associate with ErbB-2 Amplification and Affect Sensitivity to Topoisomerase II Inhibitor Doxorubicin in Breast Cancer. *The American Journal of Pathology*, 2000. **156**(3): p. 839-847.
220. Froelich-Ammon, S.J. and N. Osheroff, Topoisomerase poisons: harnessing the dark side of enzyme mechanism. *Journal of Biological Chemistry*, 1995. **270**(37): p. 21429-21432.
221. Wang, J.C., DNA topoisomerases. *Annual review of biochemistry*, 1985. **54**(1): p. 665-697.
222. Järvinen, T., *et al.*, Expression of topoisomerase II α is associated with rapid cell proliferation, aneuploidy, and c-erbB2 overexpression in breast cancer. *The American journal of pathology*, 1996. **148**(6): p. 2073.
223. McLeod, H.L., *et al.*, Topoisomerase I and II activity in human breast, cervix, lung and colon cancer. *International journal of cancer*, 1994. **59**(5): p. 607-611.
224. Ono, M., *et al.*, Sensitivity to gefitinib (Iressa, ZD1839) in non-small cell lung cancer cell lines correlates with dependence on the epidermal growth factor (EGF) receptor/extracellular signal-regulated kinase 1/2 and EGF receptor/Akt pathway for proliferation. *Molecular cancer therapeutics*, 2004. **3**(4): p. 465-472.
225. Zhang, F., *et al.*, Quantification of epidermal growth factor receptor expression level and binding kinetics on cell surfaces by surface plasmon resonance imaging. *Analytical chemistry*, 2015. **87**(19): p. 9960-9965.
226. Acquaviva, J., *et al.*, Targeting KRAS-mutant non-small cell lung cancer with the Hsp90 inhibitor ganetespib. *Molecular cancer therapeutics*, 2012.
227. Rao, C.M.M.P., *et al.*, Molecular docking based screening of novel designed chalcone series of compounds for their anti-cancer activity targeting EGFR kinase domain. *Bioinformatics*, 2015. **11**(7): p. 322.
228. Sharma, V.K., *et al.*, Structure guided design and binding analysis of EGFR inhibiting analogues of erlotinib and AEE788 using ensemble docking, molecular dynamics and MM-GBSA. *RSC Advances*, 2016. **6**(70): p. 65725-65735.
229. Liu, B., B. Bernard, and J.H. Wu, Impact of EGFR point mutations on the sensitivity to gefitinib: insights from comparative structural analyses and

- molecular dynamics simulations. *Proteins: Structure, Function, and Bioinformatics*, 2006. **65**(2): p. 331-346.
230. Rajith, B., et al., Structural signature of the G719S-T790M double mutation in the EGFR kinase domain and its response to inhibitors. *Scientific reports*, 2014. **4**: p. srep05868.
231. Martínez-Jiménez, F., et al., Rational design of non-resistant targeted cancer therapies. *Scientific reports*, 2017. **7**: p. 46632-46632.
232. Stamos, J., M.X. Sliwkowski, and C. Eigenbrot, Structure of the epidermal growth factor receptor kinase domain alone and in complex with a 4-anilinoquinazoline inhibitor. *Journal of Biological Chemistry*, 2002. **277**(48): p. 46265-46272.
233. Ahmed, M., *et al.*, In silico design: Extended molecular dynamic simulations of a new series of dually acting inhibitors against EGFR and HER2. *Journal of Molecular Graphics and Modelling*, 2013. **44**: p. 220-231.



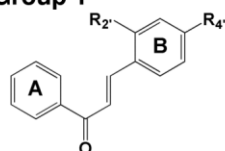
APPENDICES



จุฬาลงกรณ์มหาวิทยาลัย
CHULALONGKORN UNIVERSITY

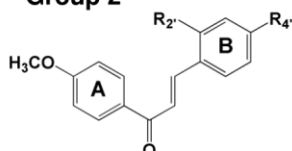
APPENDIX 1: Chemical structure of the 47 designed chalcones from six different groups.

Group 1



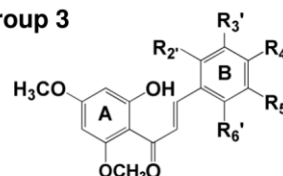
1a; R2' = -H, R4' = -OCH₃,
1b; R2' = -H, R4' = -OH
1c; R2' = -OH, R4' = -H

Group 2



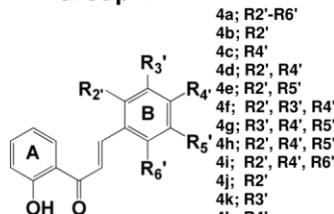
2a; R2' = -OH, R4' = -H
2b; R4' = -OH, R2' = -H
2c; R2' = -OCH₃, R4' = -H
2d; R4' = -C(CH₃)₃, R2' = -H

Group 3



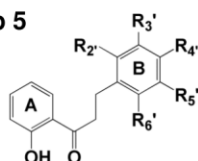
3a; R2', R4' = -OCH₃, R3', R5', R6' = -H
3b; R2', R5' = -OCH₃, R3', R4', R6' = -H
3c; R2', R4', R6' = -OCH₃, R3', R5' = -H
3d; R3', R4', R5' = -OCH₃, R2', R6' = -H
3e; R2' = -OCH₃, R3', R6' = -H
3f; R2', R3', R4' = -OCH₃, R5', R6' = -H

Group 4



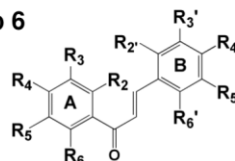
4a; R2'-R6' = -H,
4b; R2' = -OCH₃, R3', R6' = -H
4c; R4' = -OCH₃, R2', R3', R5', R6' = -H
4d; R2', R4' = -OCH₃, R3', R5', R6' = -H
4e; R2', R5' = -OCH₃, R3', R4', R6' = -H
4f; R2', R3', R4' = -OCH₃, R5', R6' = -H
4g; R3', R4', R5' = -OCH₃, R2', R6' = -H
4h; R2', R4', R5' = -OCH₃, R3', R6' = -H
4i; R2', R4', R6' = -OCH₃, R3', R5' = -H
4j; R2' = -OH, R3', R6' = -H
4k; R3' = -OH, R2', R4', R5', R6' = -H
4l; R4' = -OH, R2', R3', R5', R6' = -H
4m; R5' = -OH, R2', R3', R4', R6' = -H
4n; R2' = -OCH₃, R6' = -OH, R3', R4', R5' = -H
4o; R4' = -OCH₃, R2', R3', R6' = -H
4p; R4' = -F, R2', R3', R5', R6' = -H
4q; R4' = -Cl, R2', R3', R5', R6' = -H
4r; R2', R4' = -Cl, R3', R5', R6' = -H
4s; R2', R6' = -Cl, R3', R4', R5' = -H
4t; R3', R4' = -Cl, R2', R5', R6' = -H
4u; R4' = -Br, R2', R3', R5', R6' = -H
4v; R4' = -C(CH₃)₃, R2', R3', R5', R6' = -H
4w; R4' = -(CH₂CH₂)₂NH, R2', R3', R5', R6' = -H
4x; R4' = -CH₂CH₃, R2', R3', R5', R6' = -H
4y; R4' = -(CH₃)₂CHCH₂, R2', R3', R5', R6' = -H
4z; R4' = -C₆H₅, R2', R3', R5', R6' = -H
4aa; R4' = -C₃H₅, R2', R3', R5', R6' = -H

Group 5



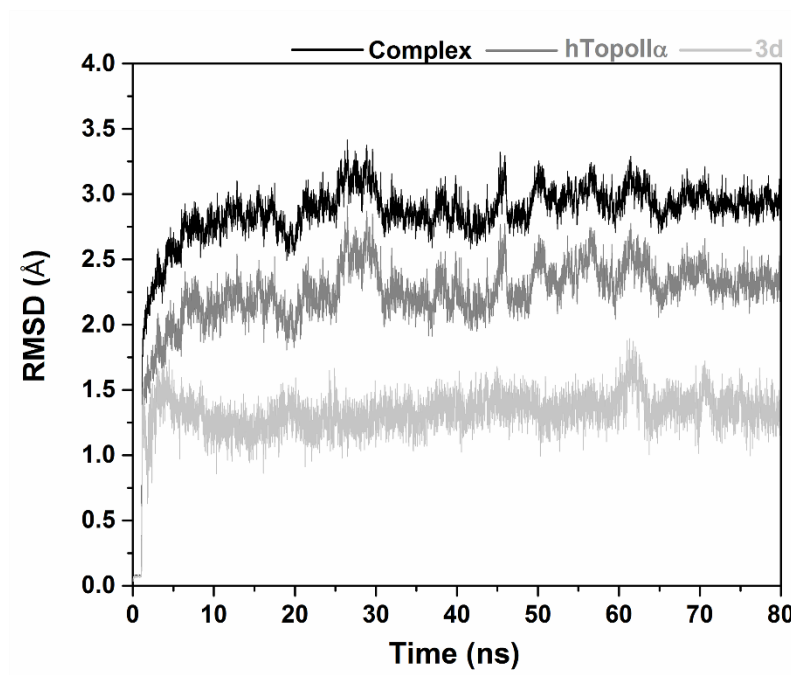
5a; R4' = -OH, R2', R3', R5', R6' = -H

Group 6

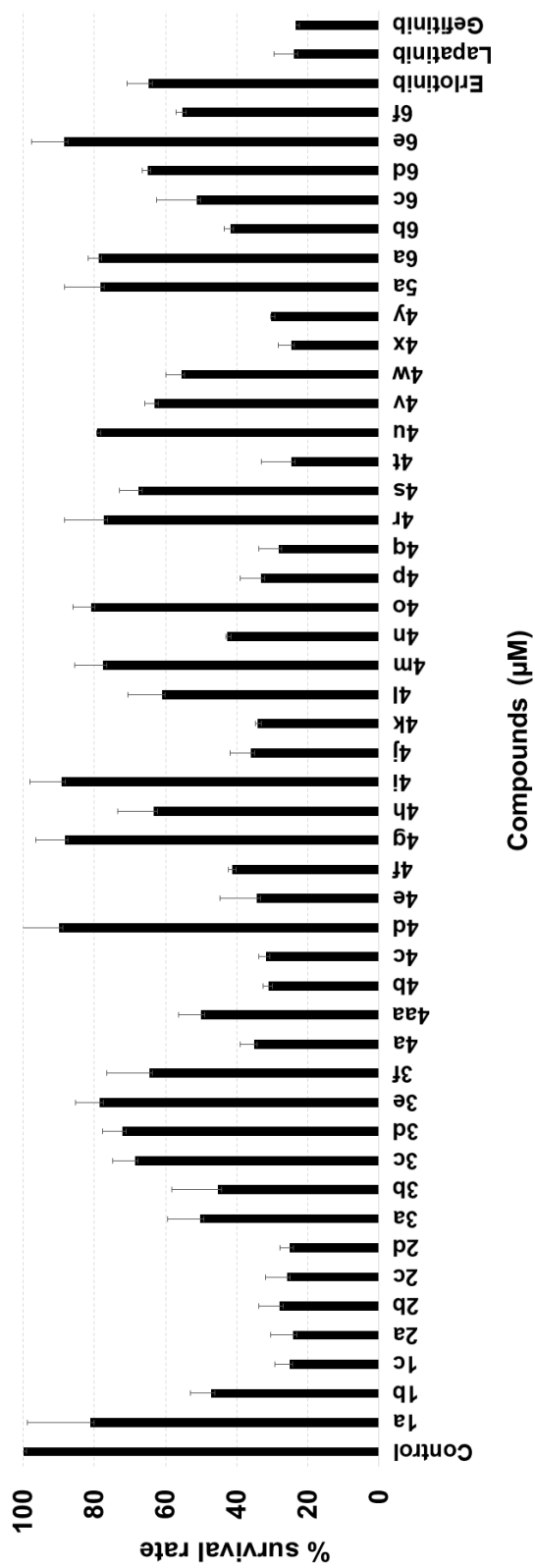


6a; R4, R2, R4' = -OH, R2 = -OCH₃, R4' = -OCH₃
6b; R6 = -OH, R3, R5 = -Br, R4' = -OH
6c; R6 = -OH, R4 = -OCH₃
6d; R2, R6 = -OH, R4' = -OCH₃
6e; R4, R6 = -OH, R4, R2 = -OH
6f; R6 = -OCH₃

APPENDIX 2: RMSD plots during 80 ns MD for the simulated systems of chalcone 3d/hTopoII α



APPENDIX 3: The percent survival rate of the 47 chalcones against human embryonic fibroblast compare with approved anticancer drug



VITA

NAME Kanyani Sangpheak

DATE OF BIRTH 15 June 1990

PLACE OF BIRTH Samutprakarn

INSTITUTIONS ATTENDED Chulalongkorn University

HOME ADDRESS

PUBLICATION

1. Darai, N.; Mahalapbutr, P.; Sangpheak, K.; Rungnim, C.; Wolschann, P.; Kungwan, N.; Rungrotmongkol, T., In silico screening of chalcones against Epstein-Barr virus nuclear antigen 1 protein. *Songklanakar Journal of Science and Technology (SJST)*.(revision)

2. Sangpheak, K.; Tabtimmai, L.; Seetaha, S.; Rungnim, C.; Chavasiri, W.; Wolschann, P.; Choowongkomon, K.; Rungrotmongkol, T., Biological evaluation and molecular dynamics simulation of chalcone derivatives as EGFR-tyrosine kinase inhibitors. *Molecules*. 2019, 24(6), 1092;

3. Sangpheak, K.; Mueller, M.; Darai, N.; Wolschann, P.; Suwattanasophon, C.; Ruga, R.; Chavasiri, W.; Seetaha, S.; Choowongkomon, K.; Kungwan, N.; Rungnim, C.; Rungrotmongkol, T., Computational screening of chalcones acting against topoisomerase II α and their cytotoxicity towards cancer cell lines. *Journal of Enzyme Inhibition and Medicinal Chemistry* 2019, 34 (1), 134-143.

4. Kicuntod, J.; Sangpheak, K.; Mueller, M.; Wolschann, P.; Viernstein, H.; Yanaka, S.; Kato, K.; Chavasiri, W.; Pongsawasdi, P.; Kungwan, N., Theoretical and Experimental Studies on Inclusion Complexes of Pinostrobin and β -Cyclodextrins. *Scientia pharmaceutica* 2018, 86 (1), 5.

AWARD RECEIVED

1. K. Sangpheak, B. Nutho B, P. Chusuth, M. Muller, P. Wolschann, T. Rungrotmogkol. In vitro and in silico studies of chalcone against cancer protein targets, The 13th Thai Summer School of Computational Chemistry Workshop, 2016. (Outstanding award for poster presentation)

2. K. Sangpheak, C. Rungnim, W. Chavasiri, P. Wolschann, M. Muller, T. Rungrotmongkol. In vitro and

in silico studies of chalcone as a new anticancer drug candidate against a cancer target protein.

21th International Annual Symposium on Computational Science and Engineering (ANSCSE 20), Thailand Science Park, Pathum Thani, Thailand, August 3-4th, 2017. (2nd award for oral presentation)



จุฬาลงกรณ์มหาวิทยาลัย
CHULALONGKORN UNIVERSITY